



**Politecnico  
di Torino**

Master's Degree in Mechatronic Engineering

A.Y. 2023/2024

Graduate Session of December 2024

Final Project Work

# **Analysis and control of high efficient electro-hydraulic solutions for the actuation systems of off-road vehicles**

SUPERVISORS:

Prof. Ing. Luigi Mazza

Prof. Ing. Andrea Vacca

CANDIDATE:

Carmine Conte

ID 305309

# INDEX

LIST OF FIGURES .....	V
LIST OF TABLES .....	X
SYMBOLS.....	XII
ABBREVIATIONS.....	XVII
NOMENCLATURE .....	XIX
ABSTRACT .....	XXI
1. INTRODUCTION.....	1
1.1 Working principle .....	1
1.2 Motivation.....	6
1.3 State of the art .....	13
1.4 Research objectives.....	18
1.5 Thesis structure .....	20
2. STUDIED EHA.....	22
2.1 Sizing of the system.....	22
2.1.1 Hydraulic Unit.....	27
2.1.2 Electric Unit .....	29
2.2 Hydraulic architectures .....	34
2.2.1 Open circuit.....	35
2.2.2 Closed circuit .....	36
2.3 Actuation modes .....	37
2.3.1 Four quadrant modes.....	38

2.3.2 Slow/fast sub-modes .....	45
2.4 Control strategies .....	50
2.4.1 Mode selection .....	51
2.4.2 Bypass valve control .....	53
2.4.3 Pump speed control .....	54
2.4.4 Open-circuit variant .....	56
3.    COMPONENTS SIZING AND SELECTION .....	57
3.1 Closed-circuit components .....	57
3.1.1 Electric motor.....	57
3.1.2 Hydraulic pump.....	59
3.1.3 Accumulator sizing and selection .....	62
3.1.4 Valves and filter selection.....	66
3.1.5 Manifold design .....	68
3.2 Open-circuit valves and filter .....	74
4.    SIMULATION MODEL .....	76
4.1 Control logic .....	76
4.2 Thermal-hydraulic model .....	78
4.3 Electric motor model .....	84
4.4 2D mechanical model .....	84
5.    EXPERIMENTAL SETUP .....	87
5.1 Reference vehicle.....	87
5.2 Hydraulic configuration.....	91
5.3 Power electronics.....	97
6.    RESULTS .....	99
6.1 Simulation results .....	99
6.1.1 Open-circuit results .....	99

6.1.2 Closed-circuit results.....	107
6.2 Experimental results .....	117
7. CONCLUSION.....	131
7.1 Summary.....	131
7.2 Future work.....	135
8. BIBLIOGRAPHY.....	137
9. APPENDIX A – VALVES AND FILTER SELECTION ACCORDING TO ACCUMULATOR SIZING FOR THE CLOSED-CIRCUIT EHA .....	142
ACKNOWLEDGMENTS .....	149

# LIST OF FIGURES

Figure 1.1: Hydraulic systems applications: (a) robotics, (b) construction, (c) agriculture and (d) aerospace.....	4
Figure 1.2: ISO schematic of a basic hydraulic system.....	5
Figure 1.3: Power flow of hydraulic systems [%].....	5
Figure 1.4: Annual CO <sub>2</sub> Emissions [7].....	6
Figure 1.5: Average temperature anomaly, Global [8].....	7
Figure 1.6: 2019 U.S Greenhouse Emission [9].....	7
Figure 1.7: Fluid Power Product Sales by Customer Market [10] .....	8
Figure 1.8: Energy consumption for a load-sensing excavator hydraulic system .....	10
Figure 1.9: Open-circuit EHA architecture [16].....	14
Figure 1.10: Closed-circuit EHA architecture [18] .....	14
Figure 1.11: EGM 3D model [20] .....	16
Figure 1.12: IGM 3D model [21] .....	17
Figure 2.1: Working principle of hydraulic actuators .....	23
Figure 2.2: Working principle of a basic EHA drive in resistive modes .....	25
Figure 2.3: Working principle of a basic EHA drive in assistive modes .....	25
Figure 2.4: Four-quadrants representation of the system sizing.....	26
Figure 2.5: SynRM internal structure [31] .....	33
Figure 2.6: Stator and rotor structure of SynRM (left side) and PMSynRM (right side) [32].....	33
Figure 2.7: Open-circuit EHA system schematic .....	35
Figure 2.8: Closed-circuit EHA system schematic.....	36
Figure 2.9: Closed-circuit four-quadrant modes .....	39
Figure 2.10: Closed-circuit resistive extension mode .....	40
Figure 2.11: Closed-circuit assistive extension mode .....	41

Figure 2.12: Closed-circuit resistive retraction mode .....	41
Figure 2.13: Closed-circuit assistive retraction mode .....	42
Figure 2.14: Open-circuit four quadrant modes .....	45
Figure 2.15: Closed-circuit full four-quadrant map .....	46
Figure 2.16: Slow speed resistive extension closed-circuit.....	47
Figure 2.17: Slow-speed assistive extension closed-circuit .....	47
Figure 2.18: Slow-speed resistive retraction closed-circuit .....	48
Figure 2.19: Slow-speed assistive retraction closed-circuit .....	49
Figure 2.20: Fast-speed assistive retraction closed-circuit.....	49
Figure 2.21: Open-circuit full four-quadrant map.....	50
Figure 2.22: Flow chart closed-circuit.....	55
Figure 3.1: 3D model of synchronous reluctance motor .....	58
Figure 3.2: Continuum external gear pump/motor .....	60
Figure 3.3: Circuits for testing pumping mode (a) and motoring mode (b) .....	61
Figure 3.4: Accumulator discharge .....	63
Figure 3.5: Accumulator charge .....	64
Figure 3.6: Polytropic behaviour of the gas inside the accumulator [1] .....	65
Figure 3.7: Closed-circuit manifold schematic .....	69
Figure 3.8: Hydraulic hose sizing nomogram [42].....	70
Figure 4.1: Simulation model in Amesim Simcenter .....	76
Figure 4.2: Simulation signals exchange.....	78
Figure 4.3: Graphical representation of the thermal-hydraulic closed-circuit system in Simcenter Amesim .....	83
Figure 4.4: Graphical representation of the thermal-hydraulic open-circuit system in Simcenter Amesim .....	83
Figure 4.5: 2D mechanical model of boom and bucket in Simcenter Amesim..	85
Figure 4.6: Synchronous 2D mechanical model of the reference vehicle.....	86
Figure 5.1: Reference vehicle CASE TV380 .....	87
Figure 5.2: ISO schematic of the baseline open centre hydraulic circuit .....	88
Figure 5.3: Principle of operation of open centre system [1] .....	90
Figure 5.4: Boom EHA implementation .....	91
Figure 5.5: Bucket EHA implementation.....	92

Figure 5.6: Conceptual architecture of the experimental setup .....	93
Figure 5.7: CASE TV380 implementing closed-circuit EHA.....	94
Figure 5.8: Experimental setup implemented on the skid steer loader.....	95
Figure 5.9: Conceptual schematic of the data acquisition system.....	96
Figure 5.10: Power electronics setup.....	97
Figure 6.1: Simulation model open-circuit.....	100
Figure 6.2: Open-circuit power flow: resistive modes (a), assistive modes (b) .....	101
Figure 6.3: Power maps of open-circuit from simulation.....	102
Figure 6.4: Power flow of open-circuit EHA: 50% actuation velocity command, 50 <i>kN</i> load force .....	103
Figure 6.5: Efficiency maps of the open-circuit EHA electric motor, hydraulic pump and hydraulic system from simulation .....	104
Figure 6.6: HP efficiency map of the open-circuit EHA from simulation .....	104
Figure 6.7: EM efficiency map of the open-circuit EHA from simulation .....	105
Figure 6.8: Power flow of open-circuit EHA: 75% actuation velocity command, 5 <i>kN</i> load force.....	105
Figure 6.9: Hydraulic system efficiency map of the open-circuit EHA from simulation .....	106
Figure 6.10: Efficiency map of the open-circuit EHA from simulation.....	106
Figure 6.11: Simulation model closed-circuit .....	107
Figure 6.12: Closed-circuit power flow: resistive extension (a), assistive extension (b), resistive retraction (c), assistive retraction (d) .....	108
Figure 6.13: Power maps of closed-circuit from simulation .....	108
Figure 6.14: Accumulator power of closed-circuit from simulation.....	109
Figure 6.15: Power flow of closed-circuit EHA: 50% actuation velocity command, 50 <i>kN</i> load force.....	110
Figure 6.16: Efficiency maps of the closed-circuit EHA electric motor, hydraulic pump and hydraulic system from simulation .....	111
Figure 6.17: HP efficiency map of the closed-circuit EHA from simulation...	111
Figure 6.18: EM efficiency map of the closed-circuit EHA from simulation..	112

Figure 6.19: Hydraulic system efficiency map of the closed-circuit EHA from simulation .....	113
Figure 6.20: Efficiency map of the closed-circuit EHA from simulation .....	113
Figure 6.21: Boom cylinder duty cycle .....	114
Figure 6.22: Duty cycle scatter over total efficiency map for the closed-circuit EHA .....	115
Figure 6.23: Closed-circuit losses contribution: 20 kN applied force, 0.13 m/s actuation velocity .....	115
Figure 6.24: Efficiency difference map from simulation .....	116
Figure 6.25: Simulation model of closed-circuit EHA with 2D mechanism ...	120
Figure 6.26: Measured and simulated normalized powers for the empty bucked load condition .....	122
Figure 6.27: Measured and simulated normalized efficiencies for the empty bucked load condition .....	123
Figure 6.28: Measured and simulated total efficiency for the empty bucked load condition .....	124
Figure 6.29: Measured and simulated normalized powers for the 1500 lb load condition .....	124
Figure 6.30: Measured and simulated normalized efficiencies for the 1500 lb load condition .....	125
Figure 6.31: Measured and simulated total efficiency for the 1500 lb load condition .....	126
Figure 6.32: Measured and simulated powers for the 3260 lb load condition	126
Figure 6.33: Measured and simulated normalized efficiencies for the 3260 lb load condition .....	127
Figure 6.34: Measured and simulated total efficiency for the 3260 lb load condition .....	128
Figure 6.35: Measured and simulated EHU normalized efficiency under all load conditions .....	129
Figure 6.36: Measured and simulated hydraulic system normalized efficiency under all load conditions .....	130

Figure 6.37: Measured and simulated EHA total efficiency under all load conditions .....130

# LIST OF TABLES

Table 1.1: Advantages and disadvantages of hydraulic and pneumatic systems .2	
Table 1.2: Construction machinery fuel consumption and hydraulic efficiency [11] .....	9
Table 1.3: Hydraulic architectures energy efficiency increase [14] .....	11
Table 1.4: Comparison between EGM and IGM.....	17
Table 2.1: Positive displacement machines types and characteristics [26] .....	29
Table 2.2: Electric motors types and characteristics [15, 27, 28, 29].....	31
Table 2.3: Mode selection .....	52
Table 2.4: Sub-mode selection .....	52
Table 2.5: EM speed in closed-circuit .....	55
Table 2.6: EM speed and 4/3 DV position in open-circuit.....	56
Table 3.1: Electric motor parameters .....	58
Table 3.2: Hydraulic pump parameters .....	62
Table 3.3: Accumulator properties .....	66
Table 3.4: Valve/filter maximum operating conditions .....	67
Table 3.5: Closed-circuit valves and filter .....	68
Table 3.6: Operating conditions of the manifold ports.....	71
Table 3.7: List of components in the manifold.....	72
Table 3.8: Fluid velocity in the manifold with 22 cc/rev HP .....	73
Table 3.9: Manifold drawing .....	74
Table 3.10: Hydraulic components open-circuit .....	75
Table 4.1: Modelling hydraulic components in simulation.....	82
Table 5.1: CASE TV380 specifications .....	89
Table 5.2: Hardware list of the EHA implementation on skid-steer .....	94
Table 5.3: Electrical hardware list of the data acquisition system .....	96
Table 5.4: Electrical components of the power electronics setup .....	98

Table 6.1: Measured signals from tests .....	118
Table 6.2: Derived signals from measurements .....	119
Table 9.1: Selected components from Sun Hydraulics .....	143
Table 9.2: Selected components from Parker Hannifin.....	143
Table 9.3: Selected components from Bosh Rexroth .....	144
Table 9.4: Selected components from Hydac .....	144
Table 9.5: Accumulator parameters using Sun Hydraulics components.....	145
Table 9.6: Accumulator parameters using Parker Hannifin valves and Hydac filter .....	146
Table 9.7: Accumulator parameters using Bosh Rexroth valves and Hydac filter .....	146
Table 9.8: Final accumulator parameters .....	147
Table 9.9: Pressure drop in Sun Hydraulic components with 22 <i>cc/rev</i> HP..	147
Table 9.10: Final accumulator parameters with 22 <i>cc/rev</i> pump.....	147
Table 9.11: Accumulator size based on components selection and HP volumetric displacement.....	148

# SYMBOLS

$2p$	Number of poles electric motor, [-]
$\alpha$	Proportion of heat generation from the pump to the fluid, [%]
$\gamma$	Polytropic index, [-]
$\Delta\eta_{tot}$	Total efficiency difference between closed- and open-circuit EHA, [-]
$\Delta p, dp$	Pressure difference, [ <i>bar</i> ]
$\Delta p_{cv}$	Check valve pressure drop, [ <i>bar</i> ]
$\Delta p_{cyl}$	Cylinder pressure difference, [ <i>bar</i> ]
$\Delta p_{fl}$	Filter pressure drop, [ <i>bar</i> ]
$\Delta p_{HP}$	Hydraulic pump pressure difference, [ <i>bar</i> ]
$\Delta p_{max}$	Maximum pressure difference, [ <i>bar</i> ]
$\Delta p_{meas}$	Measured pressure difference across BPV, [ <i>bar</i> ]
$\Delta p_{pcv}$	Pilot operated check valve pressure drop, [ <i>bar</i> ]
$\partial T$	Temperature variation, [ $^{\circ}C$ ]
$\Delta V$	Differential volume cylinder, [ <i>L</i> ]
$\eta$	System efficiency, [-]
$\eta_{closed}$	Closed-circuit hydraulic efficiency, [-]
$\eta_{EHU}$	Electro-Hydraulic Unit efficiency, [-]
$\eta_{EM,mot}$	Electric motor efficiency in motor mode, [-]
$\eta_{EM,gen}$	Electric motor efficiency in generator mode, [-]
$\eta_{hm,P}, \eta_{hm,M}$	Pump, motor hydro-mechanical efficiency, [-]
$\eta_{HP,pump}$	Hydraulic pump efficiency in pump mode, [-]
$\eta_{HP,mot}$	Hydraulic pump efficiency in motor mode, [-]
$\eta_{inv}$	Inverter efficiency, [-]

$\eta_{mech}$	Mechanical efficiency, [-]
$\eta_{open}$	Open-circuit hydraulic efficiency, [-]
$\eta_{ref}$	Reference efficiency, [-]
$\eta_{sys}$	System efficiency, [-]
$\eta_{tot,closed}$	Total efficiency closed-circuit EHA, [-]
$\eta_{tot,open}$	Total efficiency open-circuit EHA, [-]
$\eta_{v,P}, \eta_{v,M}$	Pump, motor volumetric efficiency, [-]
$\eta_{vol}$	Volumetric efficiency, [-]
$\lambda$	Area ratio, [-]
$\rho$	Density, [ $kg/m^3$ ]
$\zeta$	Saliency ratio, [-]
$\dot{\phi}_c$	Correction of free convection and radiation, [ $W$ ]
$\Phi_d, \Phi_q$	d-axis, q- axis flux, [ $Wb$ ]
$\Phi_m$	Flux linkage of the PMs, [ $Wb$ ]
$\Omega_0$	Orifice area, [ $mm^2$ ]
$\Omega_{des}$	Desired orifice area, [ $mm^2$ ]
$\omega_e$	Electric motor angular speed, [ $rad/s$ ]
$\Omega_{max}$	Maximum orifice area at $\Delta p_{max}$ , [ $mm^2$ ]
$A$	Sectional area hose, manifold port, [ $m^2$ ]
$A_p, A_r$	Piston, rod side area, [ $m^2$ ]
$B_T$	Isothermal bulk modulus, [ $N/m^2$ ]
$c$	Specific heat capacity of accumulator gas, [ $J/(kg K)$ ]
$C_f$	Orifice coefficient, [-]
$C_{poly}$	Polytropic constant, [-]
$D$	Hose internal diameter, [ $m$ ]
$dh$	Heat exchange, [ $W$ ]
$F$	Load force, [ $N$ ]
$h_{line}$	Equivalent heat exchange coefficient for hoses, fittings, and connections, [ $W/(m^2 \text{ } ^\circ C)$ ]
$i$	Speed command, [-]
$I$	Current, [ $A$ ]

$i_d, i_q$	d-axis, q-axis current, [A]
$I_{peak}$	Peak current electric motor, [ $A_{rms}$ ]
$j$	BPV command, [-]
$J_p$	Pump shaft inertia, [ $kg\ cm^2$ ]
$J_r$	Rotor inertia, [ $kg\ cm^2$ ]
$K_{heat}$	Percentage of heat generated by friction transferred to the fluid, [%]
$k_{th}$	Thermal exchange coefficient, [ $W/m^2/^\circ C$ ]
$k_{visc}$	Viscous friction coefficient, [ $N/(m/s)$ ]
$L$	Hose length, [m]
$L_d, L_q$	d-axis, q-axis inductance, [H]
$M$	Motor weight, [kg]
$m_g$	Accumulator gas mass, [kg]
$n$	Shaft speed [rev/min]
$n_{des}$	Desired rotational speed, [rpm]
$n_{min}, n_{max}$	Minimum, maximum shaft speed [rev/min]
$n_p, n_M$	Pump, motor rotational speed, [rpm]
$p$	Pole pairs of the electric machine, [-]
$p_0$	Accumulator pre-charge pressure, [bar]
$p_1$	Minimum gas pressure accumulator, [bar]
$p_2$	Maximum gas pressure accumulator, [bar]
$p_1, p_2$	Inlet, outlet hydraulic pump pressure, [bar]
$p_A, p_a$	Piston, rod chamber pressure, [bar]
$p_{acc}$	Accumulator pressure, [bar]
$P_{acc}$	Accumulator power, [W]
$p_{atm}$	Atmospheric pressure, [bar]
$p_{crack}$	Cracking pressure, [bar]
$P_{CYL}$	Cylinder mechanical power, [W]
$P_{cyl,hyd}$	Cylinder hydraulic power, [kW]
$p_{drain}$	Drain line pressure, [bar]
$P_e$	Electric power, [W]

$P_{el,in}, P_{el,out}$	Input, output electric power, [W]
$P_{EM}$	Electric motor mechanical power, [kW]
$PF$	Power factor, [-]
$P_{frict}$	Heat power generated by friction, [W]
$P_{HP}$	Hydraulic pump power, [kW]
$P_{inv}$	Inverter power, [kW]
$p_{line}$	Pressure of the low-pressure line, [bar]
$P_{loss}$	Power loss, [W]
$p_{max}$	Maximum load pressure of the system, [bar]
$P_{mech}$	Mechanical power, [W]
$P_{mot}$	Rated power electric motor, [kW]
$P_{out}, P_{in}$	Output, input power, [W]
$P_{peak}$	Peak power electric motor, [kW]
$P_{P,hyd}, P_{M,hyd}$	Pump, motor hydraulic power [W]
$P_{P,mech}, P_{M,mech}$	Pump, motor mechanical power [W]
$p_{P,bore}, p_{P,rod}$	Bore, rod pump pressure, [bar]
$p_{ratio}$	Pilot area ratio, [-]
$P_{ref}$	Reference power, [kW]
$p_{rel}$	Relief pressure, [bar]
$p_{sat}$	Saturation pressure, [bar]
$P_{sys}$	Hydraulic system power, [kW]
$Q$	Volumetric flow rate, [L/min]
$Q_A, Q_a$	Piston, rod flow rate, [L/min]
$Q_{acc}$	Accumulator flow rate, [L/min]
$Q_{Ai}, Q_{ai}$	Piston, rod ideal flow rate, [L/min]
$Q_{bvp}$	Bypass valve flow rate, [L/min]
$Q_{dif}$	Differential flow, [L/min]
$Q_{in}, Q_{out}$	Input, output volumetric flow rate, [L/min]
$Q_{min}, Q_{max}$	Minimum, maximum flow rate, [L/min]
$Q_p$	Pump flow rate, [L/min]
$Q_P, Q_M$	Pump, motor mode volumetric flow rate, [L/min]

$R_s$	Stator resistance of the electric machine, [ $\Omega$ ]
$s$	Cylinder stroke, [ $m$ ]
$T$	Shaft torque, [ $N\ m$ ]
$T_e$	Electric motor torque, [ $Nm$ ]
$T_{ext}, T_{int}$	External, internal temperature, [ $^{\circ}C$ ]
$T_g$	Accumulator gas temperature, [ $K$ ]
$T_p, T_M$	Pump, motor torque, [ $N\ m$ ]
$T_{peak}$	Peak torque electric motor, [ $Nm$ ]
$U$	Inverter power supply, [ $V_{dc}$ ]
$V$	Voltage, [ $V$ ]
$V_0$	Accumulator effective gas volume, [ $L$ ]
$V_1, V_2$	Minimum, maximum gas volume, [ $L$ ]
$V_d$	Volumetric displacement, [ $cm^3/rev$ ]
$V_{ds}, V_{qs}$	d-axis, q-axis voltage, [ $V$ ]
$V_g$	Accumulator gas volume, [ $V$ ]
$V_p, V_r$	Piston, rod side cylinder volume, [ $L$ ]
$V_{rest}$	Accumulator minimum rest volume, [ $L$ ]
$\dot{x}$	Actuator linear velocity, [ $m/s$ ]
$\dot{x}_{des}$	Desired actuator linear velocity, [ $m/s$ ]
$\dot{x}_{ex}, \dot{x}_{re}$	Extension, retraction velocity, [ $m/s$ ]
$\dot{x}_{fluid}$	Fluid velocity, [ $m/s$ ]
$\dot{x}_{max}$	Maximum actuator linear velocity, [ $m/s$ ]
$\dot{x}_{max,ex}, \dot{x}_{max,re}$	Maximum extension, retraction actuator velocity, [ $m/s$ ]
$x_v$	Fractional valve opening, [%]

# ABBREVIATIONS

AC	Alternate Current
BLDC	Brushless DC Motor
BPV	Bypass Valve
BV	Ball Valve
CAN	Controller Area Network
CNH	Chase New Holland
CV	Check Valve
CYL	Hydraulic Cylinder
DAQ	Data Acquisition
DC	Direct Current – Displacement Control
DV	Directional Valve
ECU	Electric Control Unit
EGM	External Gear Machine
EHA	Electro-Hydraulic Actuators
EHU	Electro-Hydraulic Unit
EM	Electric Motor
EU	Electric Unit
FL	Filter
FP	Fixed Displacement Pump
HM	Hydraulic Machine
HP	Hydraulic Pump
ICE	Internal Combustion Engines
IGM	Internal Gear Machine
IM	Induction Machines
ISO	International Organization for Standardization
LS	Load Sensing

MMF	Magneto Motive Force
MPR	Multi-Pressure Rails
NFPA	National Fluid Power Association
NI	National Instruments
PCV	Pilot Operated Check Valve
PMSM	Permanent Magnet Synchronous Motor
PMSynRM	Permanent Magnet Synchronous Reluctance Motors
RV	Relief Valve
SRM	Switched Reluctance Motor
SynRM	Synchronous Reluctance Motor
VM	Variable Speed Motor

# NOMENCLATURE

acc	Accumulator
atm	Atmospheric
crack	Cracking
cyl	Cylinder
des	Desired
dif	Differential
el	Electric
empt	Empty
est	Estimated
ex	Extension
ext	External
frict	Friction
gen	Generator
hm	Hydro-Mechanical
hydr, hyd	Hydraulic
in	Input
int	Internal
inv	Inverter
max	Maximum
mech	Mechanical
meas	Measured
min	Minimum
mot	Motor
out	Output
poly	Polytropic
re	Retraction

ref	Reference
rel	Relief
sat	Saturation
sim	Simulated
sys	System
th	Thermal
tot	Total
visc	Viscous
vol	Volumetric

# ABSTRACT

Transitioning to cleaner technologies, such as electrified systems in off-road vehicles, is crucial for reducing greenhouse gas emissions and promoting sustainable practices. This shift toward electrification is driving advancements in dedicated electrified hydraulic actuation systems.

Traditional centralized fluid power architectures remain popular for their cost-effectiveness, power density, and reliability. However, the increasing demand for lower emissions is raising interest in electro-hydraulic actuators. By adopting individualization strategies, the overall efficiency of hydraulic systems, generally under 30%, can be increased through reduced throttling losses and the ability to recover energy during assistive loads. This capability not only improves transmission efficiency but also leads to lower fuel consumption, making EHAs an appealing alternative for meeting stringent emission regulations.

This study explores two types of EHA architectures: an open-circuit design that connects directly to the tank, and a closed-circuit design where the differential volume of the linear actuator is stored and supplied by an accumulator. The sizing procedure for the electro-hydraulic system is discussed in detail, aiming to maintain the functionality of the baseline hydraulic system while optimizing costs. Both EHA configurations utilize a commercial electro-hydraulic unit that combines a variable-speed electric motor with a fixed-displacement hydraulic pump. A complete speed range across all four-quadrants is achieved without requiring the hydraulic pump to operate at low rotational speeds, ensuring high efficiency throughout the unit's operation. This setup not only provides a cost-effective solution but also operates quietly, making it an attractive option for modern applications.

In developing an effective EHA, careful attention must be paid to the components that ensure optimal performance and efficiency. A systematic approach to sizing various system elements, including the electric motor and hydraulic unit, is essential. The selection of these components follows an established sizing methodology, with particular emphasis on valve and filter selection influenced by the accumulator sizing. Additionally, the design of a manifold to house the cartridge valves and filter is addressed, underscoring its significance within the overall system architecture.

To validate the EHA design, it is critical to predict the system's behavior before engaging in costly experiments and demonstrations. An integrated simulation model is developed using the lumped parameter approach within the Simcenter Amesim environment. This model incorporates the electric system, hydraulic system, and the intended mechanism, facilitating a thorough efficiency analysis.

In the final phase, the closed-circuit EHA system is integrated into a reference vehicle, specifically a Case New Holland TV380 skid steer loader. Implementing the new electro-hydraulic system requires minor modifications to the baseline hydraulic circuit, along with instrumentation of the power electronics to operate the EHU. The conducted experiments focus on the energy-saving potential of the EHA, which shows efficiency up to 70% supporting the potential for commercializing these hydraulic systems in mobile applications.

# 1. INTRODUCTION

Fluid power systems - encompassing hydraulic and pneumatic technologies - play a crucial role in the design and operation of machinery and equipment across diverse industries. These systems harness the properties of fluids under pressure to transmit and control energy. Several are the applications in which these capabilities are employed: from aerospace and automotive engineering to manufacturing and robotics.

Fluid power systems are celebrated for their ability to deliver high force and precision, often in compact and efficient forms. Hydraulic architectures implemented on mechatronic systems are renowned for their robust force transmission and adaptability in heavy-duty applications, while pneumatic systems offer advantages in speed and cleanliness, making them ideal for lighter and faster operations. The evolving landscape in a great variety of engineering fields - material science, electronics, and control systems - are pushing the boundaries of fluid power technologies walking toward system with improved performances in efficiency, reliability and functionality.

## 1.1 WORKING PRINCIPLE

Fluid power can be divided in two main technologies:

- Pneumatics: rely on air or gases under pressure to perform light operations or complex automations.
- Hydraulics: an almost incompressible fluid (water and mineral oil in general) is used to transmit and control energy in heavy fixed and mobile applications.

When designing a fluid power system, it is important to evaluate the required performances from the system and chose the best technology to transmit the

mechanical power. Hence, it is essential to consider the specific advantages and limitations of hydraulic and pneumatic technologies. Table 1.1 summarizes the key benefits and drawbacks of hydraulic and pneumatic systems, providing a clear comparison to help guide decisions based on application requirements.

**Table 1.1: Advantages and disadvantages of hydraulic and pneumatic systems**

	<b>Advantages</b>	<b>Disadvantages</b>
<b>Hydraulics</b>	<ul style="list-style-type: none"> <li>• High force and power density</li> <li>• Precise control and smooth operation</li> <li>• Flexible arrangement</li> <li>• Auto-lubrication</li> <li>• Force multiplication</li> <li>• Fast response time</li> </ul>	<ul style="list-style-type: none"> <li>• Potential for oil leak and environmental concerns</li> <li>• Fluid contamination</li> <li>• Pressure oscillations</li> <li>• Tolerance requirements</li> <li>• Fluid temperature control</li> </ul>
<b>Pneumatics</b>	<ul style="list-style-type: none"> <li>• Availability of air</li> <li>• Environmental friendly</li> <li>• Low initial and maintenance costs</li> <li>• Safer due to lower forces involved</li> <li>• Clean and simple, with no risk of oil leakage</li> </ul>	<ul style="list-style-type: none"> <li>• Limited force capability compared to hydraulics</li> <li>• Low energy conversion efficiency</li> <li>• Less precise control</li> <li>• Corrosion (water and oxygen)</li> <li>• No fine positioning/rigid holding</li> </ul>

From this first comparison it is evident that hydraulic systems are preferred to pneumatic systems in off-road vehicles where high forces are implied.

With respect to competing technologies such as mechanical and electrical drives, hydraulic drives guarantee higher performance in terms of power to weight ratio, controllability and flexibility. However, some drawbacks arise when hydraulics are used for power transmission: energy losses, high influence of temperature, leakages, aging and contamination of working fluid [1].

Being hydraulic fluid power a cornerstone of modern engineering, it provides a reliable and efficient solution to a multitude of applications:

- **Aerospace:** Hydraulic systems are crucial in aircraft for controlling flight surfaces, landing gear, and braking systems. For example, hydraulic actuators manage the movement of flaps and ailerons to ensure stable flight and maneuverability.

- Robotics: Hydraulic systems provide high-force capabilities for tasks requiring precision and strength, such as in industrial robots used for assembly lines and heavy-duty robotic arms that handle large components.
- Industry: Hydraulic presses and lifts are widely used in manufacturing for tasks such as metal forming, stamping, and material handling.
- Mobile Applications: In construction and agriculture, hydraulic systems operate excavators, loaders, bulldozers, harvesters, etc. These systems enable precise control and powerful movements, crucial for earthmoving, digging, and lifting operations.
- Automotive: Fluid power systems are essential for power steering, brakes, automatic transmissions. Hydraulics enhance not only safety and high performances in these applications but also improvements in comfort.

Some examples of hydraulic fluid power applications are shown in Figure 1.1 [2-5].



a) Boston Dynamics' Stretch [2]



b) Compact loader Case TV380 [3]



c) Case IH Magnum 400 [4]



d) Boeing 787 Dreamliner [5]

**Figure 1.1: Hydraulic systems applications: (a) robotics, (b) construction, (c) agriculture and (d) aerospace.**

A basic hydraulic system is shown in Figure 1.2. Starting from the mechanical domain, a combustion engine or an electric motor provides the input power to the hydraulic system. The energy source is the prime mover that drives the hydraulic pump. Safety systems - like a pressure relief valve - and fluid conditioning elements - such as coolers, heaters and filters - can be included in the generator part. Thanks to the hydraulic pump, flow is delivered in the lines based on the shaft angular speed and the volumetric displacement. In the control part one or more valves can deliver the flow to all the actuators in the system regulating their actuation speed (angular or linear). Based on the type of motion actuators are divided in linear (e.g., hydraulic cylinders) and rotary (e.g., hydraulic motors) actuators. Finally, a load is driven thanks to the actuator. This last step gives a new energy conversion from the hydraulic domain to the mechanical domain.

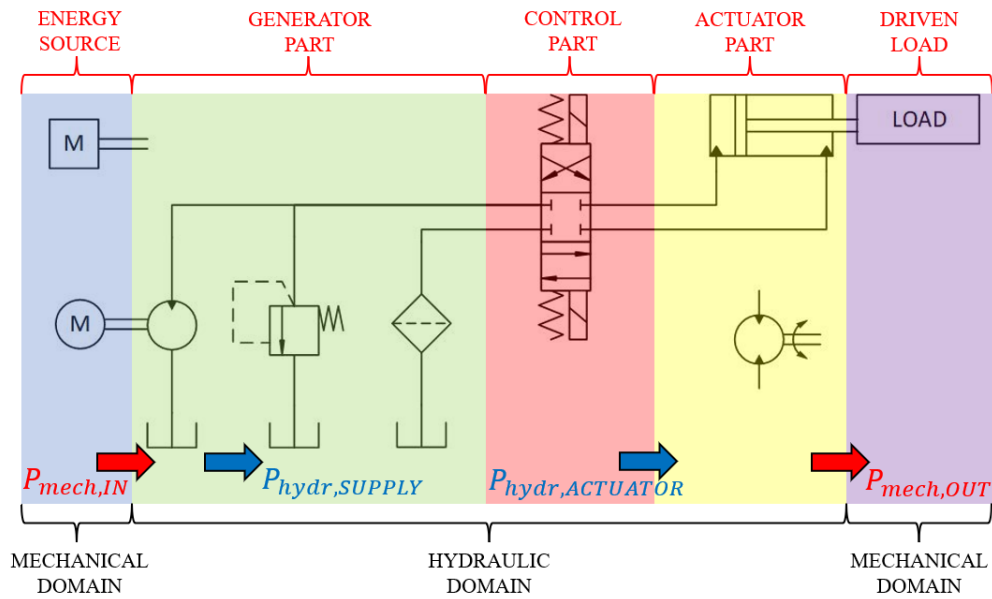


**Figure 1.2: ISO schematic of a basic hydraulic system**

A power loss can be associated with each component of the scheme, and it is related to the intrinsic efficiency of the component. For a common hydraulic system, the most relevant power loss is related to the prime mover: internal combustion engines can achieve efficiencies up to 30% when operating in their sweet spot. Following the workflow, the pump, valves and actuator efficiencies must be considered before obtaining the net output power from the hydraulic input power provided by the prime mover. The net output power is then used to drive the load accomplishing a certain function. An example of power flow of hydraulic systems is shown in Figure 1.3.

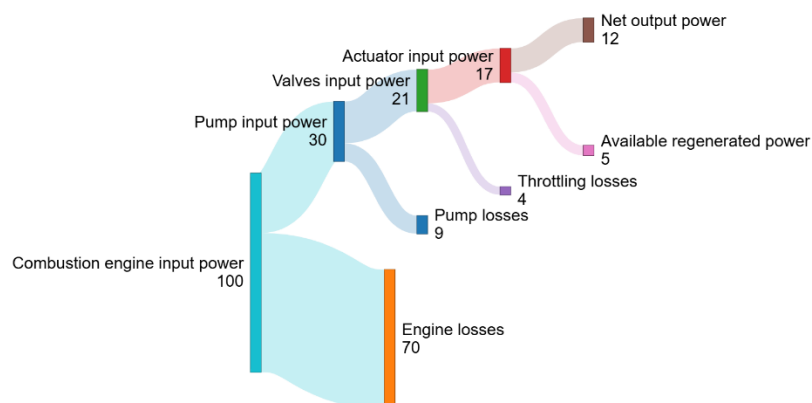


**Figure 1.3: Power flow of hydraulic systems [%]**

## 1.2 MOTIVATION

The increasing concentration of greenhouse gases in the Earth's atmosphere is one of the most pressing challenges of our time. These gases, primarily carbon dioxide (CO<sub>2</sub>), methane (CH<sub>4</sub>), and nitrous oxide (N<sub>2</sub>O), trap heat from the sun and create a “greenhouse effect” that leads to warming the planet. This phenomenon drives significant changes in global climate patterns, resulting in more frequent and severe weather events, heatwaves, rising sea levels, precipitations and storms, wildfires and disruptions to ecosystems [6].

In Figure 1.4 the visual representation of annual CO<sub>2</sub> emissions provides a crucial insight into the scale and trends of carbon dioxide output over time [7]. Human emissions of carbon dioxide and other greenhouse gases are the main factors contributing to the increase in global temperatures. This relationship between global temperatures and greenhouse gas levels has been consistent throughout Earth's history. Figure 1.5 illustrates the global average temperature compared to a baseline, which represents the average temperature from 1961 to 1990. Since that period, average temperatures have increased by more than 0.8°C [8].

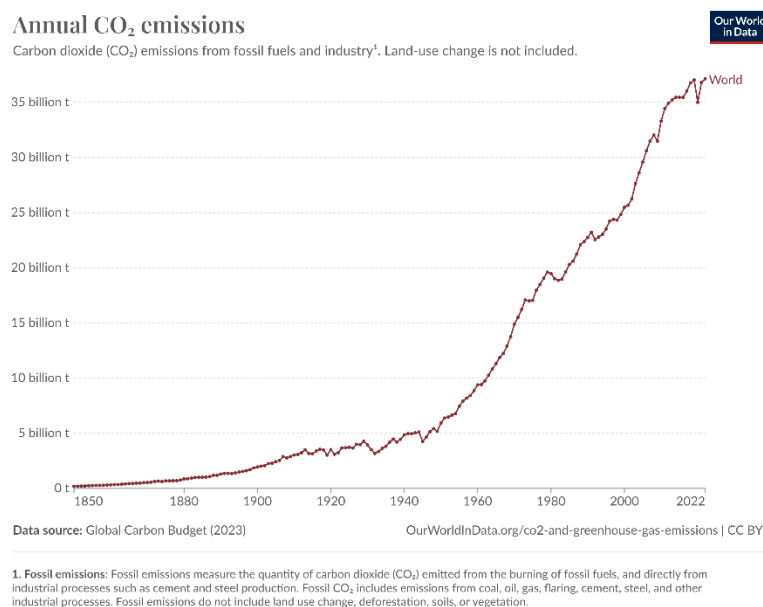


**Figure 1.4: Annual CO<sub>2</sub> Emissions [7]**

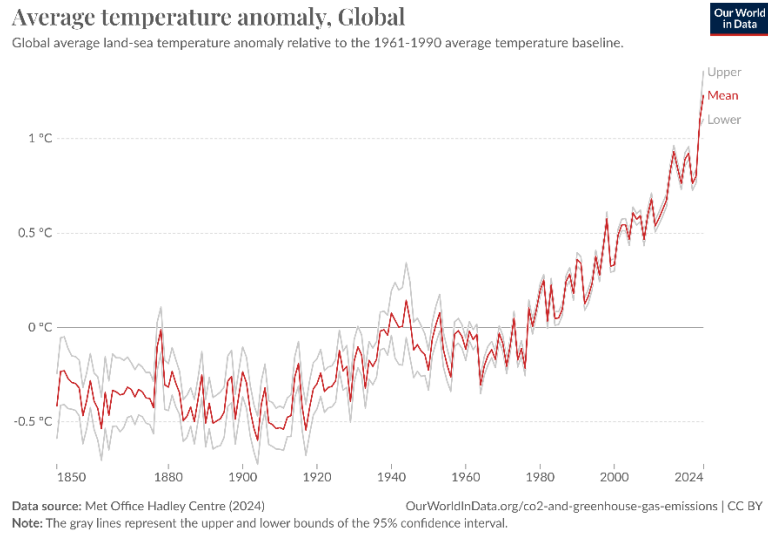


**Figure 1.5: Average temperature anomaly, Global [8]**

According to the United State Environmental Protection Agency (EPA) the transportation sector represents 1/3 of the total greenhouse emission in US [9]. Fluid power applications are included in the agricultural, industry and transportation sectors representing a non-negligible role in total emissions (Figure 1.6). In particular, off-road vehicles and equipment emissions represent the 10% out of the 33% of the transportation sector.

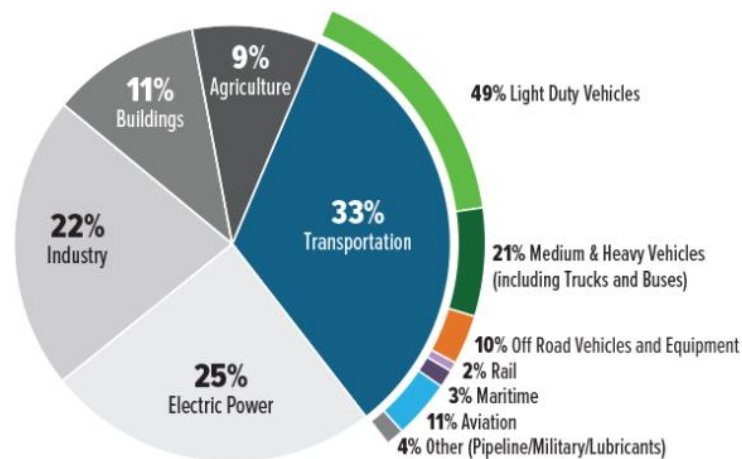


**Figure 1.6: 2019 U.S Greenhouse Emission [9]**

The National Fluid Power Association (NFPA) reviewed the 20 largest customer markets, which represent the 62% of products sales, in order to identify the main

sectors in which fluid power technologies (hydraulics and pneumatics) are employed [10]. From Figure 1.7 it can be stated that the two main fields in which fluid power systems are employed for power transmission are again agricultural (11,73%) and construction machinery (19,59%).

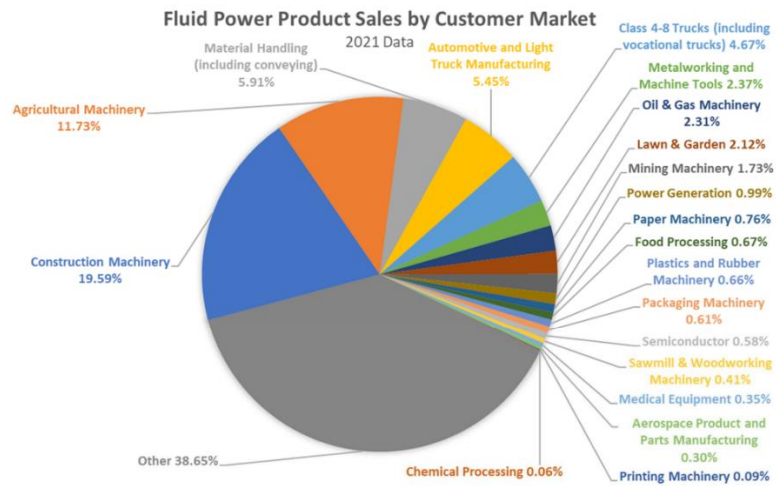


**Figure 1.7: Fluid Power Product Sales by Customer Market [10]**

Construction machinery consumes around 2.68 billion gallons of fuel each year. Despite this significant consumption, the efficiency of hydraulic systems within this machinery shows considerable variability, ranging from 13% to 35% (Table 1.2) [11]. This disparity underscores the need for advancements in technology and practices to increase overall efficiency.

**Table 1.2: Construction machinery fuel consumption and hydraulic efficiency [11]**

<b>Equipment</b>	<b>Total fuel (gallons)</b>	<b>Fuel to Hydraulic (gallons)</b>	<b>Hydraulic efficiency</b>	<b>Energy (Quads)</b>
<b>Excavators</b>	7.79E+08	6.230E+08	35%	8.641E-02
<b>Rough Terrain Forklifts</b>	6.64E+07	1.660E+07	16%	2.303E-03
<b>Rubber Tire Loaders</b>	8.48E+08	4.238E+08	35%	5.878E-02
<b>Loaders/Backhoes</b>	5.13E+08	3.076E+08	22%	4.266E-02
<b>Aerial Lifts</b>	2.09E+07	1.043E+07	13%	1.447E-03
<b>Cranes</b>	9.73E+07	1.945E+07	13%	2.698E-03
<b>Skid Steer Loaders</b>	3.51E+08	2.806E+08	16%	3.891E-02
<b>Total</b>	2.68E+09	1.681E+09	21%	2.332E-01
			<b>Average</b>	

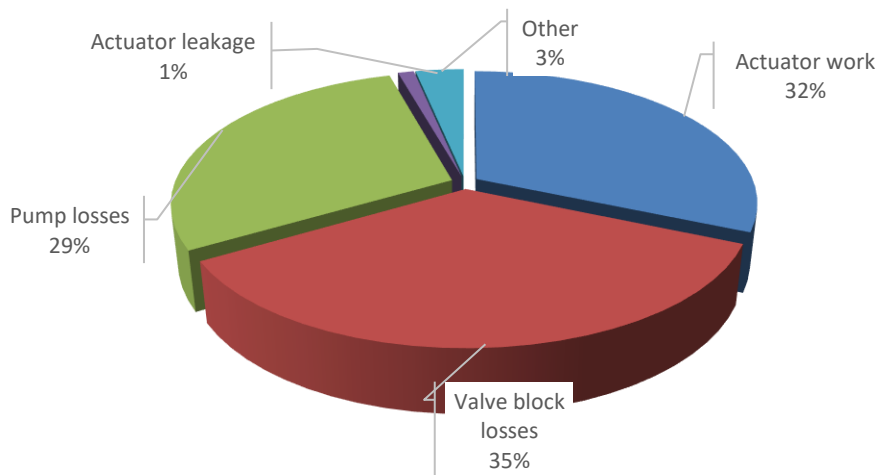
In mobile applications, parasitic losses are associated to the transmission of power from the prime mover (engine or electric motor). Moreover, the power that is transmitted to the load is time varying, hence the required power from the prime mover can experience drastic changes that have a high impact on its efficiency.

In a fluid power system, there are several components that can cause a reduction of efficiency:

- In the pump losses are experienced in the form of internal and external leakages, fluid compressibility and friction. The efficiency of the device can approach 90% in the optimal operating conditions, but due to the time varying loads the overall efficiency can decrease to 75% or even more in case of very low angular speeds [1].
- A non-negligible fraction of losses is due to hoses and pipes. In hydraulic applications, these losses are mainly due to:
  - Major losses (distributed), including friction effects generated in the pipe/hose section considering a constant sectional area and a fully developed flow.

- Minor losses (concentrated), including friction losses caused by singularities - fittings, bends, entrances, couplings - encountered by the fluid during its flow.
- Control valves can experience losses due to internal leakages and metering losses related to pressure drops across the valve to control the flow rate.
- Finally, hydraulic actuators such as cylinders can provide a low quantity of losses mainly due to leakages from piston to rod chambers. Moreover, these devices have the possibility to regenerate power from the load in case of overrunning conditions.

Zimmerman et al. [12] presented the simulation study of a load-sensing excavator hydraulic system to evaluate possible energy savings. Results showed the amount of energy dissipated at different stages of the hydraulic system as shown in Figure 1.8.

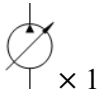
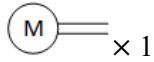
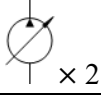
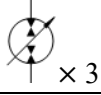
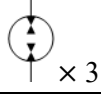


**Figure 1.8: Energy consumption for a load-sensing excavator hydraulic system**

It is indeed of considerable significance the development of new fluid power architectures and components to increase system efficiency, reduce losses, reduce emissions and increase regenerative power. Even if the mobile hydraulics encompass a diverse range of architectures, depending on the single applications, hydraulic excavators are one of the most relevant reference machines when novel solutions are proposed. This is due to reliability, cost and fuel consumption considerations [13].

In a common mobile application for agricultural or construction machinery one prime mover and a limited number of pumps are used to supply power to multiple actuators, and the desired fluid provided to each actuator is regulated by control valves. This last architecture falls in the category of the centralized systems. Patel provided a comprehensive study for the efficiency analysis of hydraulic actuation architectures for mini-excavators [14].

**Table 1.3: Hydraulic architectures energy efficiency increase [14]**

	<b>Prime Movers</b>	<b>Pump-Motor Units</b>	<b>Energy Efficiency Increase</b>
<b>LS</b>	 × 1	 × 1	27%
<b>MPR</b>	 × 1	 × 2	36%
<b>DC</b>	 × 1	 × 3	59%
<b>EHA</b>	 × 3	 × 3	70%

This last study shows how moving towards individualization strategies the overall efficiency of the hydraulic system increases (Table 1.3). However, the transition to this architecture requires high costs since the number of prime movers and hydraulic units must be the same as the number of actuators.

Alongside the advancement of new architectures, vehicle electrification has experienced significant evolution in recent decades, driven by the fluid power industry's emphasis on environmental sustainability. Analysing the state of the art and the trends of electrification in off-highway vehicles, Beltrami et al. [15] stated that:

- A clear convenience in terms of total cost ownership represents an effective driver for electrification.
- Power demand and minimum operational runtime represent technical limits for a widespread electrification. Big machinery with aggressive

duty cycles and in harsh environments are not suitable nowadays for battery electrification.

- A most evident trend is represented by retrofitting of existing vehicles, where the internal combustion engine and the fuel tank are replaced by electric motors and a battery pack.
- The efficiency of electric vehicles is strongly increased by the new technologies regarding hydraulics, actuators and energy recovery systems. However, the introduction of this cutting-edge technologies can increase the upfront costs exceeding the acceptable cost-benefit ratio.

The electrification trend is once again confirmed by the NFPA, which is estimating an increase of electrified machines from 2022 to 2030: agricultural machinery 24%, automotive and track manufacturing 27%, construction machinery 19%, mining machinery 18% [10].

Transitioning from internal combustion engines (ICE) to electric motors, the previously masked noise from hydraulic pumps and motors has become significant in fluid power systems for off-road vehicles. For applications in close proximity to people, noise is a major barrier to the acceptance and adoption of fluid power technology. Beyond environmental considerations, reducing noise from hydraulic components can also improve system control, extend machine lifespan, and enhance reliability. Frequently, the primary challenge in deploying hydraulic systems is the noise and vibration produced by positive displacement machines, which can overshadow the noise generated by valves, loads, and other hydraulic components.

Finally, the required reduction of fuel and energy consumption of off-road vehicles and the consequent increase in the overall system efficiency, the electrification trends in the fluid power field, and the required reduction of noise emission of hydraulic components such as hydraulic pumps-motors are the motivations for the current thesis work.

## 1.3 STATE OF THE ART

Many research activities aimed at electrifying hydraulic systems can be found in the literature. At the same time decentralized systems such as EHAs are always more popular thanks to their high efficiency and compactness. Several examples of EHAs can be found in the aeronautics, robotics and mobile fields. In this study it is mainly considered the research carried by the Maha Fluid Power Research Centre about Electro-Hydraulic Actuators for mobile applications.

Qu et al. [16, 17] proposed a novel open-circuit EHA architecture (Figure 1.9) where the full speed range of the linear actuator was covered using a two-quadrants fixed displacement pump thanks to the use of a bypass valve BPV in parallel to the actuator CYL. This valve was opened in slow and fast working modes adopting a control logic based on the desired flow supplied by the pump and the pressure difference between the two chambers of the actuator. It was shown through experiments that the opening of the bypass valve was causing non-linearities during slow speed working modes due to the introduced throttling losses. Moreover, cavitation was observed during high-speed retractions of the cylinder causing again a non-linear behaviour. Further investigations were conducted on transient load conditions. During this transient the switch of the directional control valve DV introduced non negligible throttling losses due to the high pressure drop and high flow rate. This resulted in cavitating the cylinder chambers, and introducing spikes in the cylinder speed reducing the controllability.

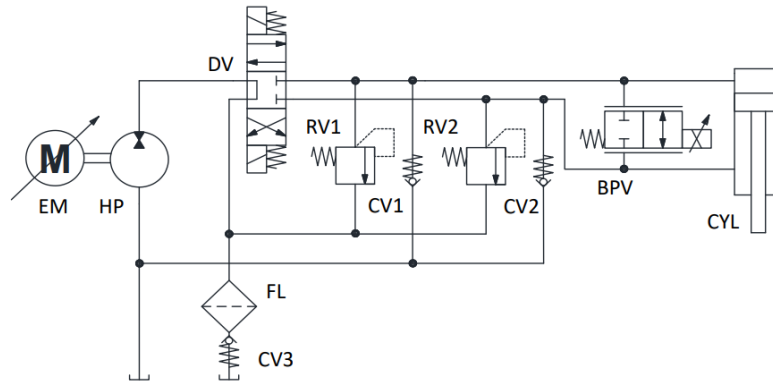


**Figure 1.9: Open-circuit EHA architecture [16]**

The same research group proposed a closed-circuit EHA architecture (Figure 1.10) replicating the same experiments done for the open circuit [18]. In this case a four-quadrants pump-motor was adopted and no reservoir connection was considered. The differential volume of the cylinder CYL was managed by the accumulator ACC. Two directional control valves DV1 and DV2 were implementing the load-holding functionality. However, their pressure drops introduced cavitation issues in the cylinder chambers. A similar control strategy as in [16] was implemented to regulate BPV, but adapted to the functionality of the four-quadrant HP. The robustness of the CYL velocity was tested for different loading conditions. Results showed a non-linear behaviour for slow and high actuator velocities due to the non-linear characteristic curve (pressure drop vs. flow rate) of BPV.

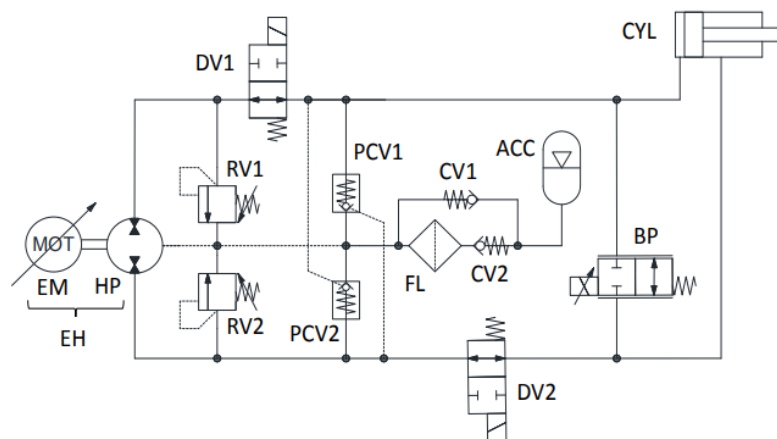


**Figure 1.10: Closed-circuit EHA architecture [18]**

Further studies were conducted to evaluate the efficiency and the power analysis of the hydraulic circuit comparing open- and closed-circuit configurations [19]. Efficiencies up to 80% were obtained in simulation and validated through experiments for both architectures. These results come from the throttling losses reduction given by the adoption of an individualized architecture, as well as from the energy recovery capability in assistive modes. However, high inefficiencies (10-20%) were observed in slow and fast speed operations where the opening of the bypass valve introduced additional throttling losses. The open-circuit performed better in terms of efficiency thanks to the use of a two-quadrants pump-motor intrinsically more efficient with respect to a four-quadrants design used in the closed-circuit. Moreover, the energy stored in the accumulator was not contributing in an incisive way due to the low pressure required in the drain line. However, the considered model was not including the electric motor and inverter losses, which are non-negligible when the overall efficiency and power analysis of the EHA is studied.

The same fluid power centre promoted the development of integrated electro-hydraulic units. Zappaterra et al. [20] proposed an optimization algorithm that utilizes the EM model to derive an optimal EHU design. In particular, an external gear machine (EGM) was integrated with a PMSM. The compact design of the EHU was able to reach a 69% total efficiency at 4000 *rpm* and 60 *bar*. Moreover, the unit was able to operate in all the four quadrants maintaining efficiencies always higher than 50% despite the HU was designed for 2-quadrants. Figure 1.11 shows the 3D model of the EHU where the red components are part of the HM, while the blue components are part of the EM.

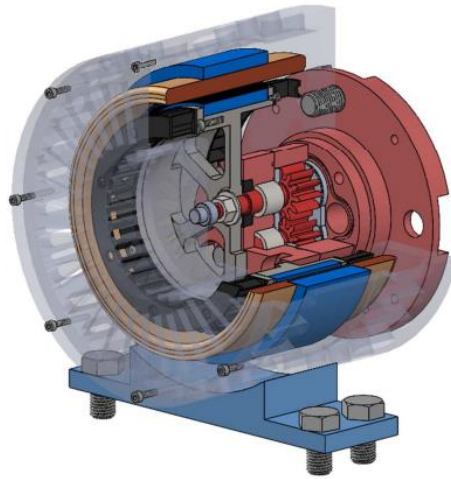


**Figure 1.11: EGM 3D model [20]**

Further studies carried by Zappaterra [21] aimed at designing an optimized internal gear machine (IGM). The proposed EHU allowed for operations up to medium-high pressure levels while using a low-cost EM. The HM integrates seamlessly within an EM in a shaftless embodiment to minimize the number of components enhancing compactness. A wide speed range up to 6000 *rpm* was achieved maintaining an acceptable total efficiency that ranged between 81% and 97%. The morphology of the EHU allowed to cool the EM by using the working fluid. Figure 1.12 shows the 3D model of the EHU. Moreover, a comparison between the IGM and the EGM [20] was done, resulting in a 65% improvement in compactness.

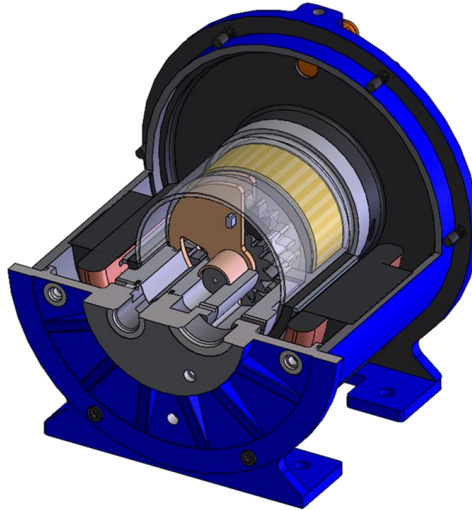


Figure 1.12: IGM 3D model [21]

Further improvements in the design of IGM and EGM brought to two final designs shown in Table 1.4.

Table 1.4: Comparison between EGM and IGM

	<b>EGM</b>	<b>IGM</b>
<b>Volumetric displacement [cc/rev]</b>	10.7	25
<b>Rated voltage [V]</b>	400	700
<b>EM type</b>	PMSM	PMSM
<b>Maximum pressure [bar]</b>	210	210
<b>Maximum power [kW]</b>	15.75	32
<b>Cooling system</b>	Air cooled	Liquid cooled

The discussed EGM [20] was implemented with the open-circuit architecture [16] in a further step for the validation of the EHA proposed by Qu et al. [22, 23]. Results showed a lower system efficiency with respect to previous tests claiming a 70% efficiency [19]. This was due to the low intrinsic efficiency of the EHU which reached values up to only 60% in both resistive extension and assistive retraction. The electric losses due to inverter could be considered negligible, while a maximum of 0.93 kW of power was lost in the hydraulic circuit due to throttling losses. Due to the limited performances of the prototype, the overall system efficiency was reaching a maximum of 54% in assistive extension.

To better validate the proposed EHA, a baseline was established [24]. The considered reference vehicle was a skid-steer loader CASE TV380. Results from this last work showed that an improvement from 20% to 50% in efficiency was achieved in the best-case scenario when the baseline was operated under excessive metering control. The improvements were mainly given by energy regeneration during the lowering phase of the boom, the reduction of throttling losses thanks to the decentralized architecture, and energy savings during idle periods. In particular, only 1/3 of the total energy of the baseline was consumed by the EHA. Limitations raised also in this case from a non-optimal design of the EHU. Higher efficiency improvements could be obtained thanks to well established technologies present in the market.

The simulation models considered in [16] and [18] were assuming isothermal conditions. Further efforts from Qu et al. [25] were aiming at defining a thermal-hydraulic model. The lumped-parameter model was developed on Simcenter Amesim, and it was introducing three correction factors to simplify the modelling process and improve the model accuracy:

- The proportion of heat generation from the pump to the fluid,  $\alpha$ .
- The equivalent heat exchange coefficient for hoses, fittings, and connections,  $h_{line}$ .
- The correction of free convection and radiation,  $\phi_c$ .

The comparison between simulation and experimental results showed average error of less than  $0.8^{\circ}\text{C}$ .

## 1.4 RESEARCH OBJECTIVES

The main technical challenges associated with EHA architectures in mobile hydraulic applications include:

- Most EHA designs aimed at aviation and robotic control, as well as many commercial EHA products, lack energy recovery capabilities and typically operate at lower power levels.

- The use of expensive variable-displacement pumps in certain EHA architectures for aerospace and mobile hydraulics significantly raises the overall cost of these systems.
- EHA systems utilizing fixed-displacement pumps struggle with low-speed performance. Fixed pumps often experience considerable volumetric and torque losses, leading to increased wear on the journal bearings, which results in manufacturers imposing low-speed limitations.
- EHAs are generally sized based on the maximum flow required by each actuator, resulting in considerable oversizing compared to traditional centralized systems where a single pump is supplying multiple actuators.
- Implementing EHA technology in mobile hydraulic applications necessitates alterations to the mechanical structure, which demands more space and restricts operational conditions.

This study will focus on developing an EHA system for mobile hydraulic applications. Both numerical and experimental methods will be employed to validate the efficiency of the studied EHA architectures. The research objectives include:

- Evaluate the performance of a high-efficient EHA architecture with energy recovery capabilities.
- Reducing costs by utilizing a VM-FP configuration as an EHU while ensuring full-speed range operation without requiring the FP to operate at low speeds.
- Proposing a basic sizing method for a scalable EHA design with a similar configuration.
- Develop a simulation model able to serve as a design tool for future sizing and optimization efforts.
- Generate an efficiency map for all four-quadrants to validate performance across various working conditions of the EHA.
- Implementing the EHA on a reference machine without altering the main mechanical structure.

- Analyzing the power management of the machine powered by the proposed EHA and assessing its energy-saving potential.

## **1.5 THESIS STRUCTURE**

The thesis is organized into the following chapters to achieve the research objectives outlined above.

Chapter 2 introduces the Electro-Hydraulic Actuator architecture under study. It discusses the system sizing and presents the selection and operating principles of both hydraulic and electric units. The two hydraulic architectures - open-circuit and closed-circuit - are explained, along with their four-quadrant modes, which are further divided into slow and fast sub-modes. Lastly, the chapter covers the control strategies employed to select the actuation mode, regulate the bypass valve opening, and control the angular speed of the electric unit.

Chapter 3 offers a comprehensive explanation of component sizing and selection. It covers the components used in implementing both hydraulic architectures, including the electric motor, hydraulic pump, accumulator, valves, filter, and manifold.

Chapter 4 discusses the lumped parameter simulation model developed in Amesim Simcenter, which is used to predict the efficiency of the EHA. This model will serve as a design tool for future sizing and optimization efforts.

Chapter 5 provides details on the experimental setup, including the implementation of the EHA system on a reference vehicle, the data acquisition system, and the power electronics used to drive the EHU.

Chapter 6 presents the results from both simulations and experiments. It explores the efficiency across all operating modes, using a four-quadrant efficiency map to compare the two architectures. Additionally, experimental results are discussed to showcase the performance of the EHU and to validate the simulation model developed.

Chapter 7 concludes the thesis by summarizing the key findings, highlighting the main contributions of the research. It provides a reflection on the effectiveness of the proposed EHA architectures, the insights gained from both simulations and experimental results, and their potential applications. Additionally, it offers suggestions for future research directions.

## **2. STUDIED EHA**

The purpose of this chapter is to qualitatively introduce the two EHA architectures under consideration. The system sizing is determined by user requirements, such as maximum loading force and actuating velocity. To meet these requirements, the chosen commercial EHU utilizes a variable-speed electric motor coupled with a fixed-displacement pump (VM-FP). The operating modes for both open- and closed-circuit architectures will be examined, with a further categorization into slow speed, normal speed, and high-speed sub-modes. The electric motor's speed is adjusted according to the selected sub-mode. Operation in the slow and fast speed sub-modes is achieved thanks to the bypass valve.

### **2.1 SIZING OF THE SYSTEM**

An optimized sizing of the system is crucial for both costs and functionality. Regarding the functionality, the two proposed architectures for the EHA should replace the baseline hydraulic system of the reference vehicle. The basic working principle for the actuation of a conventional hydraulic cylinder (double acting: the sliding piston divides the cylinder body into two volumes, each one connected to a different port) is shown in Figure 2.1. Each port is used to supply flow to the linked chamber in order to perform the extension (bore, or piston, side supplied) or the retraction (rod side supplied). In the figure the red colour represents the fluid under high pressure while the blue one represents the fluid under low pressure.

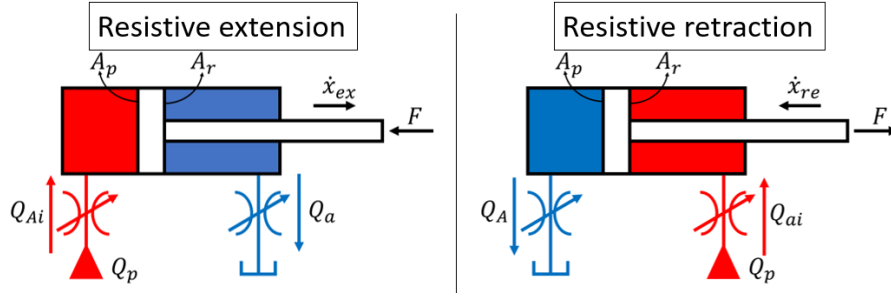


Figure 2.1: Working principle of hydraulic actuators

Typical parameters characterizing a cylinder are [1]:

- Piston stroke  $s$ , maximum linear travel of the piston.
- Piston diameter  $D$ , which defines the bore influence area:

$$A_p = \frac{\pi D^2}{4} \quad (2.1)$$

- Rod diameter  $d$ , which defines the rod influence area  $A_r$ , given by the difference between the bore area and the rod area:

$$A_r = \frac{\pi (D^2 - d^2)}{4} \quad (2.2)$$

- Area ratio  $\lambda$ , defined as the ratio between piston area and rod area.  $\lambda$  is always greater than 1 since  $A_p$  is always greater than  $A_r$ :

$$\lambda = \frac{A_p}{A_r} = \frac{D^2}{D^2 - d^2} > 1 \quad (2.3)$$

When extending under a resistive load the piston chamber is supplied. Ideally the supplied flow  $Q_{Ai}$  is equal to the flow commanded by the pump  $Q_p$ , and the rod velocity is determined by the influence area of the piston:

$$\dot{x}_{ex} = \frac{Q_{Ai}}{A_p} = \frac{Q_p}{A_p} \quad (2.4)$$

On the contrary, when retracting under a resistive load the rod chamber is supplied. Ideally the supplied flow  $Q_{ai}$  is again equal to the flow commanded by the pump  $Q_p$ , and the rod velocity is determined by the influence area of the rod:

$$\dot{x}_{re} = \frac{Q_{ai}}{A_r} = \frac{Q_p}{A_r} \quad (2.5)$$

Comparing these two equations, it can be noticed that the retraction is faster than the extension considering the same  $Q_p$ . A relation between retraction and extension speed can be derived using the area ratio definition:

$$\frac{\dot{x}_{re}}{\dot{x}_{ex}} = \frac{A_p}{A_r} = \frac{Q_A}{Q_a} = \lambda \quad (2.6)$$

As said before, the sizing of the system is accomplished by considering the maximum output power from the accumulator side. This mechanical power is obtained as the product of the actuator velocity  $\dot{x}$  and the loading force  $F$ :

$$P_{CYL} = F \dot{x} \quad (2.7)$$

Since the extension and retraction velocities can be different, also the output power is varying passing from one mode to the other. Moreover, the applied force is dependent from the mechanical structure of the reference application, hence it is also varying depending on velocity and position. It can be stated that a relationship for the output power between extension and retraction cannot be derived.

In Figure 2.2 a basic EHA architecture schematic is shown in order to explain how the differential flow is managed by the system. The considered EHU is a VM-FP hence the flow supplied by the pump is controlled by regulating the angular speed of the electric motor. During the resistive modes the hydraulic pump-motor is working in in pumping mode.

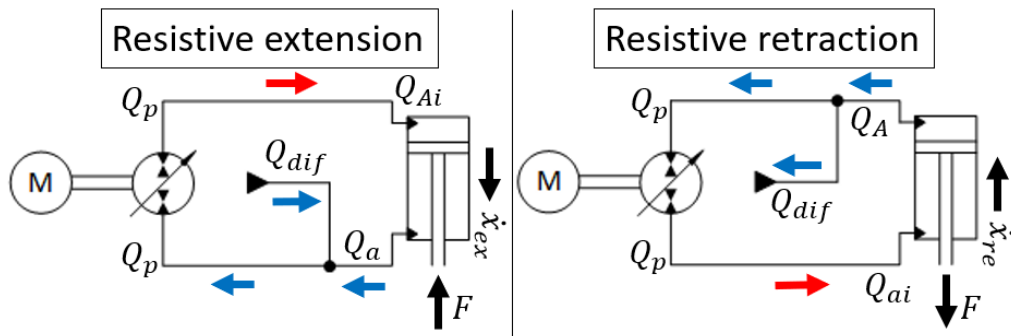


Figure 2.2: Working principle of a basic EHA drive in resistive modes

During both extension and retraction, the EHA supplies flow to the high-pressure chamber. Due to the differential area of the cylinder, a differential flow  $Q_{dif}$  should be provided as low-pressure flow source.

The same considerations can be done for the assistive (or overrunning) modes as shown in Figure 2.3. In this case the extension and retraction velocities can be redefined considering the new influence areas, always related to the high-pressure chambers. During the assistive modes the hydraulic pump-motor is working in motoring mode.

$$\dot{x}_{ex} = \frac{Q_{ai}}{A_r} = \frac{Q_p}{A_r} \quad (2.8)$$

$$\dot{x}_{re} = \frac{Q_{Ai}}{A_p} = \frac{Q_p}{A_p} \quad (2.9)$$

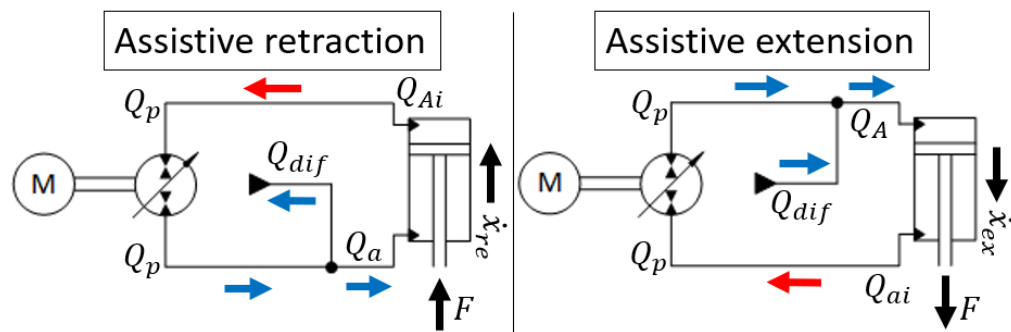
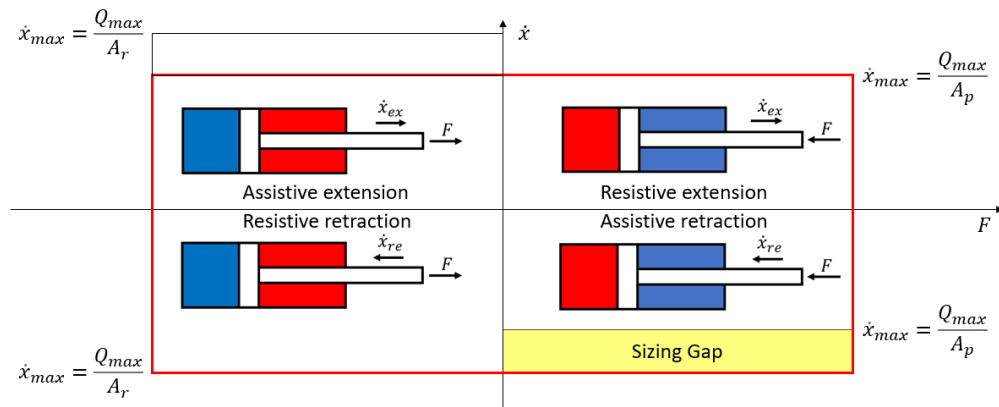


Figure 2.3: Working principle of a basic EHA drive in assistive modes

Considering the switch from a resistive extension to an assistive retraction (Equations 2.4 and 2.9), it can be noticed that the area ratio has no impact on the speed's relationship. The speed during extension and retraction can be the same in the studied EHA assuming an ideal system. This is a consistent difference with respect to conventional hydraulic systems. Due to this behaviour a sizing gap is obtained when designing the EHA as shown in Figure 2.4.



**Figure 2.4: Four-quadrants representation of the system sizing**

In conclusion, two are the methods for sizing the EHA system:

- Size according the maximum extension velocity (resistive extension): in this case the sizing gap occurs during the assistive retraction limiting the performance of the reference application.
- Size according the maximum retraction velocity (resistive retraction): in this case no sizing gap occurs and an additional operating region is achieved in assistive extension. However, since higher velocities can be obtained in extension the system is over dimensioned for this operating mode.

The choice of the sizing method is crucial for the further steps of sizing and selecting the components for the architecture, such as valves, filters, accumulators, hydraulic unit and electric unit. The sizing of all these elements has a direct impact over the costs of the EHA. The final choice adopted is to size

according to a resistive retraction, since oversizing means having higher costs with the advantage of a better functionality.

In the following section the sizing for the hydraulic and electric units is discussed.

### 2.1.1 HYDRAULIC UNIT

When sizing the hydraulic unit, it is important to consider the maximum flow that the device can supply. This quantity will define the maximum velocity of the actuator related to the device performances as stated before.

The pump flow  $Q_p$  is determined by the angular speed at the shaft  $n$ , the volumetric displacement  $V_d$  of the device (fixed when considering FP) and the volumetric efficiency  $\eta_{vol}$ , which is an expression of the leakages occurring in the hydraulic unit:

$$Q_p = n V_d \eta_{vol} \quad (2.10)$$

Hence, the maximum flow that can be supplied by the pump-motor is limited by the maximum shaft speed:

$$Q_{max} = n_{max} V_d \eta_{vol} \quad (2.11)$$

Once  $Q_{max}$  is obtained, the maximum extension and retraction velocities for the actuator can be derived according to Figure 2.4.

The maximum speed of the shaft is a limitation that comes from the pump provider. In order to operate in a sweet spot for the hydraulic unit, a minimum speed is provided too. At low speeds the volumetric efficiency of the device can fall drastically providing low performances for the whole system. From this consideration a minimum flow  $Q_{min}$  supplied by the pump-motor can be derived:

$$Q_{min} = n_{min} V_d \eta_{vol} \quad (2.12)$$

Again, the minimum velocity for each mode can be obtained once  $Q_{min}$  is known. This condition will provide a limited controllability of the system at low speed,

but the issue can be solved thanks to the use of a bypass valve as explained in the subsequent paragraphs.

One more important requirement for the EHA is that the pressure differential output from the pump  $\Delta p$  should meet the peak pressure required by the system, this will allow the EHA to control the loads of the original application.

$$\Delta p = \frac{T \eta_{mech}}{V_d} \quad (2.13)$$

To motivate the choice of the hydraulic unit, a comparison between different types of positive displacement machines is proposed in Table 2.1.

**Table 2.1: Positive displacement machines types and characteristics [26]**

Type of Machine	Pros	Cons	Speed [rpm]		Pressure [bar]
			Min	Max	
<b>Axial Piston Machines</b>	<ul style="list-style-type: none"> <li>• Good efficiency</li> <li>• Low inertia of rotating parts</li> </ul>	<ul style="list-style-type: none"> <li>• High production costs</li> <li>• Long design</li> </ul>	5 to 20	300 to 18000	100 to 450
<b>Radial Piston Machines</b>	<ul style="list-style-type: none"> <li>• High pressure level</li> <li>• High torques (displacement)</li> <li>• Good efficiency</li> </ul>	<ul style="list-style-type: none"> <li>• High production costs</li> </ul>	1 to 10	50 to 12000	120 to 400
<b>Vane Machines</b>	<ul style="list-style-type: none"> <li>• Compactness</li> <li>• Low flow pulsation</li> </ul>	<ul style="list-style-type: none"> <li>• Low efficiencies</li> <li>• Sensitive against pressure peaks</li> </ul>	10 to 400	1000 to 4000	50 to 250
<b>Annular Gear Machines</b>	<ul style="list-style-type: none"> <li>• High power density</li> <li>• Compactness</li> <li>• Robustness</li> </ul>	<ul style="list-style-type: none"> <li>• Very low efficiencies</li> </ul>	10 to 50	200 to 2000	Up to 200
<b>External Gear Machines</b>	<ul style="list-style-type: none"> <li>• Low production costs</li> <li>• High power density</li> <li>• Robustness</li> </ul>	<ul style="list-style-type: none"> <li>• Low efficiencies</li> <li>• Noise emission</li> </ul>	300 to 700	2000 to 8000	80 to 350
<b>Internal Gear Machines</b>	<ul style="list-style-type: none"> <li>• Low production costs</li> <li>• High power density</li> <li>• Robustness</li> <li>• Low noise emission</li> </ul>	<ul style="list-style-type: none"> <li>• High production costs</li> </ul>	300 to 1500	2000 to 5000	30 to 300

Thanks to their advantages in terms of production costs, power density and robustness, external gear machines are selected as hydraulic units in this study. In particular, a novel architecture for this type of pumps-motors was provided by the project sponsor, which features reasonably good efficiencies and low noise and vibration emissions. More details about this device will be discussed in the subsequent paragraphs.

## 2.1.2 ELECTRIC UNIT

Combustion engines are the main culprits when talking about greenhouse emissions in large cities. Electric motors represent a good alternative to ICEs for their properties.

An electric motor is a device that converts electrical energy into mechanical energy. Generally, the conversion happens thanks to the interaction between the magnetic field and the electric current passing through wire windings. This generates a torque applied at the motor shaft [27]. In the case of hydraulic systems, the electric motor shaft is linked to the hydraulic unit to convert the mechanical energy into hydraulic energy. Electric motors can feature various architectures and properties. The most important types of electric units used for mobile applications are shown in Table 2.2.

**Table 2.2: Electric motors types and characteristics [15, 27, 28, 29]**

Type of Machine	Pros	Cons
<b>Brushed DC Motor</b>	<ul style="list-style-type: none"> <li>• Wide constant power speed range</li> <li>• Good controllability</li> <li>• Linear torque-current curve</li> </ul>	<ul style="list-style-type: none"> <li>• Low reliability</li> <li>• Restricted maximum speed</li> <li>• Low efficiency</li> <li>• Low power density</li> </ul>
<b>Permanent Magnet Brushless DC Motor (BLDC)</b>	<ul style="list-style-type: none"> <li>• Simple rotor position estimation</li> <li>• High efficiency</li> <li>• Very high power density</li> </ul>	<ul style="list-style-type: none"> <li>• High costs due to rare-earth magnets</li> <li>• Limited constant power speed range</li> <li>• Limited control flexibility</li> </ul>
<b>Permanent Magnet Synchronous Motor (PMSM)</b>	<ul style="list-style-type: none"> <li>• High efficiency</li> <li>• High power density</li> <li>• High torque density</li> <li>• Compact designs available</li> <li>• Good heat dissipation</li> </ul>	<ul style="list-style-type: none"> <li>• Limited speed range</li> <li>• High cost due to rare-earth magnets</li> <li>• Risk of demagnetization</li> </ul>
<b>Induction Machines (IM)</b>	<ul style="list-style-type: none"> <li>• Low costs</li> <li>• Robustness</li> <li>• High reliability</li> <li>• High efficiency under high-speed cruising conditions</li> <li>• High speed range</li> <li>• Easy to control</li> </ul>	<ul style="list-style-type: none"> <li>• Lower power density with respect to Permanent Magnet Motors</li> <li>• Lower efficiency with respect to Permanent Magnet Motors</li> <li>• Narrow speed range</li> </ul>
<b>Switched Reluctance Motor (SRM)</b>	<ul style="list-style-type: none"> <li>• Simple structure</li> <li>• Robustness</li> <li>• Good efficiency</li> <li>• High speed operation</li> <li>• Low rotor heat generation</li> <li>• High torque at low speeds</li> <li>• Good torque density</li> <li>• Wide constant power speed region</li> <li>• Fast dynamics due to low inertia and structure</li> <li>• Low cost</li> </ul>	<ul style="list-style-type: none"> <li>• High torque ripple</li> <li>• Loud noise</li> <li>• Lower power density with respect to Permanent Magnets Motors</li> <li>• Hard to control</li> </ul>
<b>Synchronous Reluctance Motor (SynRM)</b>	<ul style="list-style-type: none"> <li>• High efficiency</li> <li>• Small size</li> <li>• Low costs</li> <li>• Robustness</li> <li>• Fault tolerance</li> <li>• No need of permanent magnets</li> <li>• Higher torque density with respect to IMs</li> <li>• Smoother low speed torque with respect to SRM</li> </ul>	<ul style="list-style-type: none"> <li>• Low power factor</li> <li>• Challenging to control</li> <li>• Hard manufacturing</li> </ul>
<b>Permanent Magnet Synchronous Reluctance Motors (PMSynRM)</b>	<ul style="list-style-type: none"> <li>• High performance without rare-earth PMs</li> </ul>	<ul style="list-style-type: none"> <li>• Hard manufacturing and installment process</li> <li>• High torque ripples</li> </ul>

PMSMs are widely used in EHA applications [23] thanks to their high power density. Moreover, their small size makes them perfect when an optimal design

for integrated EHUs is needed. However, in the context of this study a commercial SynRM is considered. The benefits of this type of machines are stimulating ongoing research into the product in the past decade, making them become a more suitable solution when a trade-off between performances and costs is required.

The rotor design of SynRMs distinguish these devices from IMs and PMSMs. In particular SynRMs feature:

- High reliability and an easier maintenance thanks to the low winding and bearing temperature, and the lack of a cage or PMs in the rotor structure.
- Low cost due to the lack of PMs.
- Fast dynamic response thanks to their small size and low moment of inertia.
- High speed range due to the wide constant-power operation.
- High efficiency thanks to the cold rotor operation.
- High power density and high torque per ampere.

Finally, it can be stated that SynRMs can provide high performance as PMSMs, but with cost and maintenance that is comparable with IMs [29].

In the context of comparisons between SynRM and IM using the same stator, Boglietti et al. demonstrate that synchronous reluctance motors have 10% to 15% higher rated torque due to lower rotor losses. However, copper losses in the stator end-windings impose limitations [30].

The SynRM generates reluctance torque due to variations in magnetic reluctance, also known as magnetic resistance. Magnetic flux naturally travels towards areas of lowest magnetic resistance. As a result, the flux produced by the stator moves toward the rotor's lowest magnetic resistance. If the rotor is misaligned with this flux, the reluctance torque will cause the rotor to turn toward the path of least magnetic resistance. In this context, the saliency ratio creates magnetomotive force (MMF), which drives the rotor's rotation through reluctance torque [29]. The internal structure of a synchronous reluctance motor is shown in Figure 2.5.

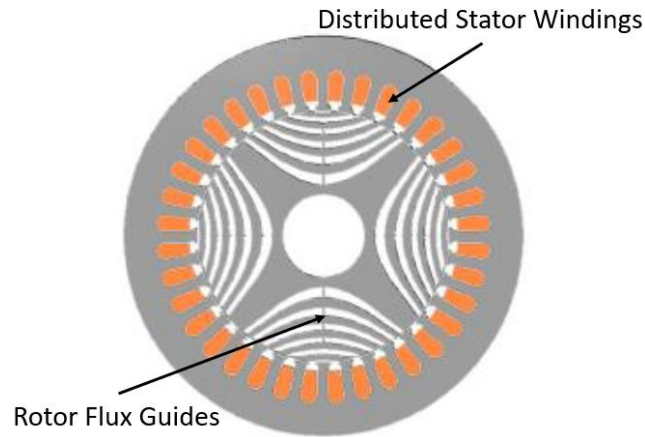


**Figure 2.5: SynRM internal structure [31]**

Heidari et al. present a comparison between SynRM and PMSynRM. These two types of machines have same stator structure, however the flux barriers of the SynRM are filled with PM in the PMSynRM in order to obtain an additional magnetic torque component. The cross-section comparison of the two machines is shown in Figure 2.6 [32].

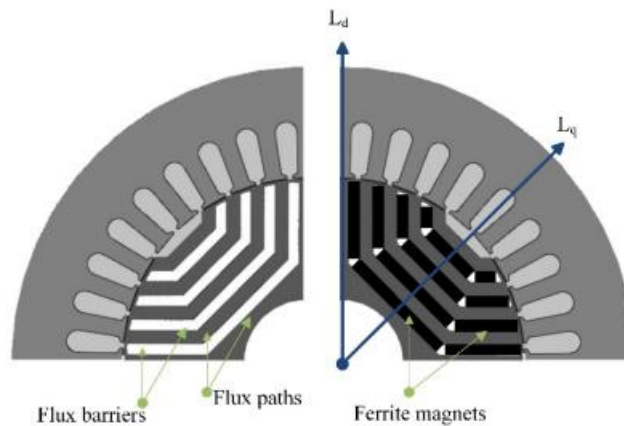


**Figure 2.6: Stator and rotor structure of SynRM (left side) and PMSynRM (right side) [32]**

The flux paths provide a low magnetic reluctance on the d-axis, while the flux barriers are used to avoid the flux to flow in the direction of the q-axis. Hence a higher reluctance is obtained in the q-axis, and the inductance  $L_d$  is bigger than  $L_q$ . The ratio between these two quantities is known as saliency ratio  $\zeta$ , and it defines the reluctance torque and the power factor of the machine.

$$\zeta = \frac{L_d}{L_q} \quad (2.14)$$

$$PF = \frac{\zeta - 1}{\zeta + 1} \quad (2.15)$$

$$T_e = \frac{3}{2}p(L_d - L_q) i_d i_q \quad (2.16)$$

In the case of PMSynRM an additional term  $\Phi_m i_d$ , given by the presence of PM, is included in the torque equation 2.16. The output torque of the electric unit corresponds to the input torque of the hydraulic unit. The two units have same applied rotational speeds.

The desired speed of the SynRM  $\omega_e$  sets the voltages of the d-q reference frame:

$$V_{ds} = R_s i_d + \frac{d\Phi_d}{dt} - \omega_e L_q i_q \quad (2.17)$$

$$V_{qs} = R_s i_q + \frac{d\Phi_q}{dt} - \omega_e L_d i_d \quad (2.18)$$

Where flux equations are defined as follows:

$$\Phi_d = L_d i_d \quad (2.19)$$

$$\Phi_q = L_q i_q \quad (2.20)$$

Maximum speed and torque of the electric unit should be compliant with the required parameters of the hydraulic unit.

## 2.2 HYDRAULIC ARCHITECTURES

In this section the two studied architectures for the EHA are discussed. In particular each component functionality for both the open and closed hydraulic circuit will be discussed.

A formal definition of open and closed hydraulic circuit can be expressed as follows [33]:

- If the pump does not have a pre-defined high- and low-pressure compartment, it is said to work in a closed-circuit.
- When the pump only operates against high pressure on one side, it is working in an open-circuit.

## 2.2.1 OPEN CIRCUIT

Figure 2.7 shows the ISO schematic for the open-circuit architecture.

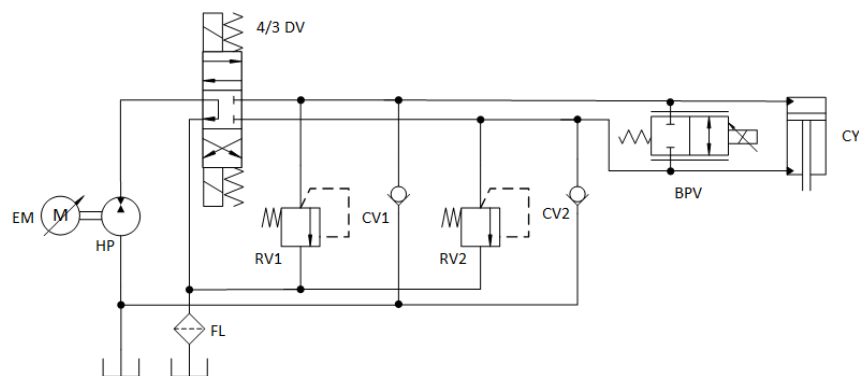


**Figure 2.7: Open-circuit EHA system schematic**

The EHU is composed by a fixed displacement pump and a variable speed electric motor. In the open circuit architecture, a two-quadrants pump-motor HP is employed. The low-pressure line is always connected to the inlet of the hydraulic unit, while the high-pressure line is connected to the outlet. The low-pressure line is also the suction line from the tank in this configuration. The four-ports, three-positions directional control valve (4/3 DV) has the role of supplying rod and bore sides of the cylinder according to the operating condition, hence the full functionality of the four-quadrants can be achieved. A proportional, two positions, two ports bidirectional control valve, also called bypass valve (BPV) for brevity, accounts for operations in the sizing gap mentioned in Section 2.1. One more purpose of this valve is to control low speed actuations as it will be discussed in the next sections. The BPV valve is positioned in parallel to the hydraulic cylinder (CYL). Two check valves (CV1 and CV2) are used to avoid

cavitation problems in fast operation modes. Two relief valves (RV1 and RV2) constitute a safety function in case the maximum pressure allowed in the circuit is exceeded. Finally, a filter (FL) is used for maintaining the oil clean as it can influence the performance of the whole circuit. Filters act on the solid contamination which can affect mechanical parts in relative motion. For this architecture a suction filter is considered since it can be placed between the reservoir and the pump inlet.

Thanks to the optimized design of the two quadrants pump-motor the efficiency of the open circuit architecture is expected to be higher with respect to the efficiency of the closed-circuit architecture discussed in the next section. Two-quadrants hydraulic units are asymmetric since the inlet port is directly connected to the suction line in which a lower pressure is expected. However, the open-circuit shows some issues when dealing with transitions from resistive to assistive loads [16]. To improve the controllability of the system, as well as the efficiency in some critical operating regions the closed-circuit architecture will be studied and implemented on the reference vehicle.

### 2.2.2 CLOSED CIRCUIT

Figure 2.8 shows the ISO schematic for the closed-circuit architecture.

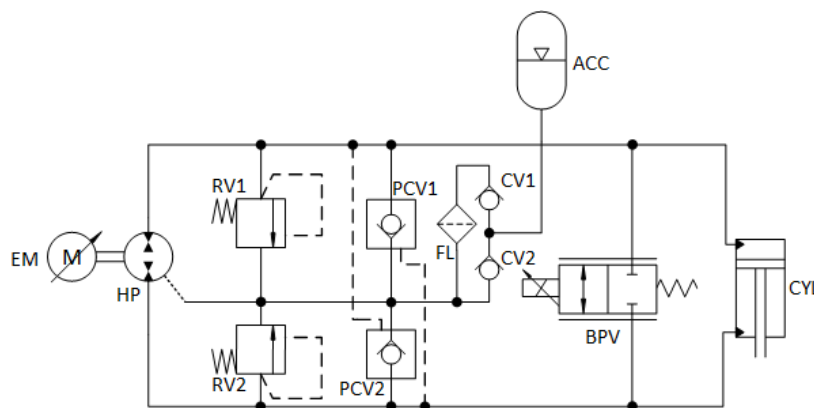


**Figure 2.8: Closed-circuit EHA system schematic**

The EHU is again composed by a fixed displacement pump and a variable speed electric motor. In the closed-circuit architecture, a four quadrants pump-motor HP is employed. Hence, the low- and high-pressure lines of the pump are not

fixed. All the four-quadrant operations are allowed by the hydraulic pump since it can act as a pump or motor in both directions of flow. The drain of HP is connected to the so-called drain line employed also to charge or discharge the accumulator ACC. This last element is used to take care of the differential volume of the cylinder. The charging and discharging of ACC are regulated by the pilot operated check valves (PCV1 and PCV2), which guide flow to the accumulator when high pressure is sensed on the opposite line. In this architecture FL is a in line filter since a tank connection is not present. The flow through FL is regulated by CV1 and CV2. In particular the fluid is cleaned during the charging phase of ACC, and flow is passing through CV1. When discharging ACC flow is passing through CV2 bypassing FL. The BPV is placed again in parallel to CYL to account for slow/fast operations. Two relief valves (RV1 and RV2) are used as a safety function when high pressure arise in the system. Therefore, flow is diverted from the high-pressure line to the low-pressure line passing through the pilot operated check valves.

It is important to remark that a lower efficiency of the system is expected due to the non-optimal design of four-quadrants hydraulic units, which have a symmetric structure due to the switching of the high- and low-pressure lines at the ports of the device.

## 2.3 ACTUATION MODES

In this section the four-quadrant operating conditions for both open- and closed-circuit will be discussed. A precise numbering is assigned to each mode:

- 1, resistive extension.
- 2, assistive extension.
- 3, resistive retraction.
- 4, assistive retraction.

This numbering follows a counter-clockwise rotation in the considered force vs. actuator linear speed chart starting from the top-right quadrant.

Each mode will be divided in main, slow and fast speed sub-modes. Slow and fast speed sub-modes can be operated thanks to the bypass valve, of which the functioning will be discussed.

In particular all quadrants present main and slow speed sub-modes, while in assistive retraction an additional fast speed mode is considered to account for the sizing gap discussed in Section 2.1. In order to distinguish the sub-modes, a letter is assigned to each sub-mode according to the following criteria:

- a, main speed.
- b, slow speed.
- c, fast speed.

Hence, a sub-mode is defined by a number followed by a letter. If for example a slow speed assistive retraction is considered, the equivalent code is 4.b.

### **2.3.1 FOUR QUADRANT MODES**

A graphical representation of the four quadrant modes is given considering on the x-axis the load force  $F$  and on the y-axis the actuator linear velocity  $\dot{x}$ . Positive velocities are considered for extension motion of the actuator, while negative velocities are considered for retraction motion. Regarding  $F$ , positive load forces are assumed in the direction of retraction, while negative forces are assumed in the direction of extension. In the 1<sup>st</sup> and 3<sup>rd</sup> quadrants actuation velocity and load force are in the opposite direction having a resistive mode. Instead, in the 2<sup>nd</sup> and 4<sup>th</sup> quadrants actuation velocity and load force are in the same direction having an assistive mode. Only in assistive modes energy regeneration can be achieved.

During the resistive modes HP is working as a pump converting the mechanical power from EM in hydraulic power, while EM is working as a motor converting electric power from the inverter in mechanical power for HP. During the assistive modes HP is working as a motor converting hydraulic power from the circuit into mechanical power for EM, while EM is working as a generator converting mechanical power from HP into electrical power that can be stored in a battery.

The four-quadrant modes for the closed-circuit are shown in Figure 2.9. The high-pressure lines are represented in red, while the low-pressure lines are represented in blue. The arrows give the direction of the flow.

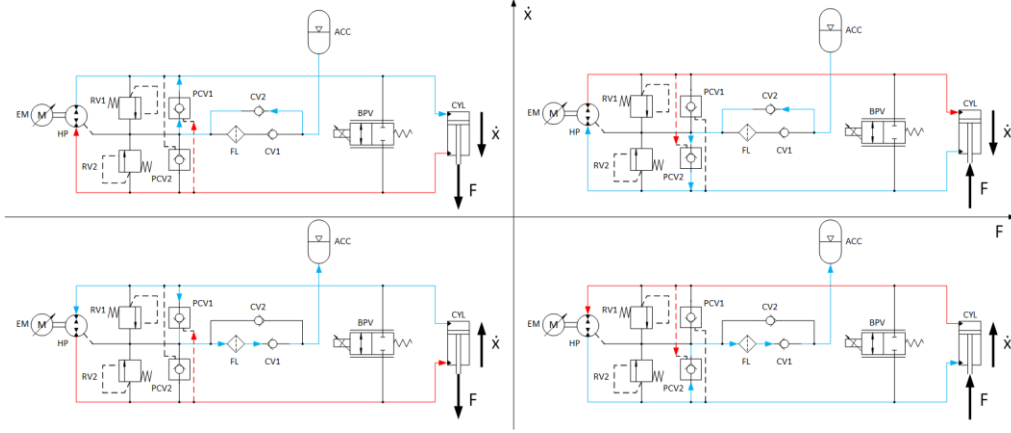


**Figure 2.9: Closed-circuit four-quadrant modes**

It is important to discuss the function of ACC. It stores fluid during the retractions and gives back the same amount of fluid during the extensions. Assuming that a positive flow for the accumulator means exhausting it, the accumulator flow rate can be obtained as in Eq. 2.21.

$$Q_{acc} = Q_A - Q_a \quad (2.21)$$

The accumulator power can be expressed as:

$$P_{acc} = Q_{acc} p_{acc} \quad (2.22)$$

The power that is stored in the accumulator represents a small amount with respect to the other contributions. This is due to the limitation of the drain line for which the condition  $p_{acc} < p_{drain}$  must be respected, as explained in the next chapter.

In the first quadrant (resistive extension, Figure 2.10) HP is supplying flow to the bore side of CYL, while the rod flow rate  $Q_a$  can be derived using the area ratio  $\lambda$  (Eq. 2.6):

$$Q_A = Q_p = n_{des} V_d \eta_{vol} \quad (2.23)$$



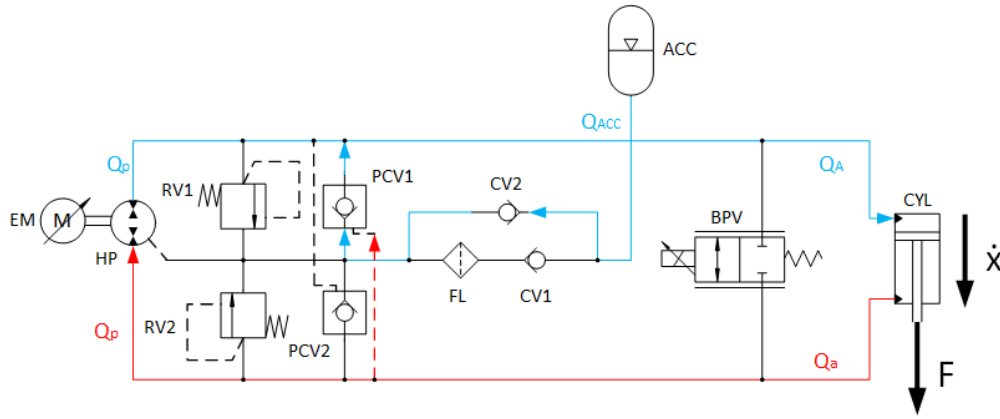


**Figure 2.11: Closed-circuit assistive extension mode**

In the third quadrant (resistive retraction, Figure 2.12) HP is supplying flow to the rod side of CYL, while the bore flow rate  $Q_A$  can be derived using the area ratio  $\lambda$  (Eq. 2.6) .

$$Q_a = Q_p = n V_d \eta_{vol} \quad (2.28)$$

$$Q_A = Q_a \lambda \quad (2.29)$$

The high-pressure chamber regulates the linear velocity of the actuator  $\dot{x}$ .

$$\dot{x} = \frac{Q_a}{A_r} \quad (2.30)$$

To avoid cavitation in the pump, the accumulator is charged from the low-pressure line through PCV1, FL and CV1.

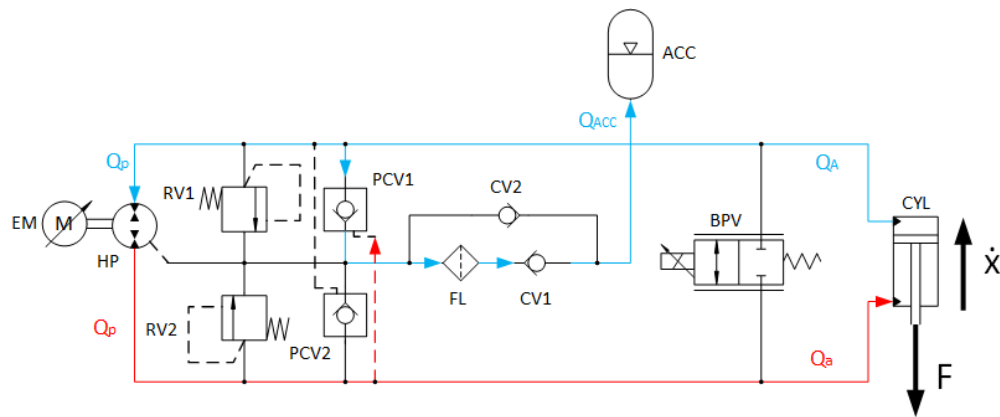


**Figure 2.12: Closed-circuit resistive retraction mode**

In the fourth quadrant (assistive retraction, Figure 2.13) HP is working as a motor. The linear velocity of the actuator  $\dot{x}$  dictates the bore flow rate  $Q_A$ , while the rod flow rate  $Q_a$  can be derived using the area ratio  $\lambda$  (Eq. 2.6).

$$Q_A = Q_p = \dot{x} A_p \quad (2.31)$$

$$Q_a = \frac{Q_A}{\lambda} \quad (2.32)$$

To avoid cavitation in the cylinder, the accumulator is charged from the low-pressure line through PCV2, FL and CV1.

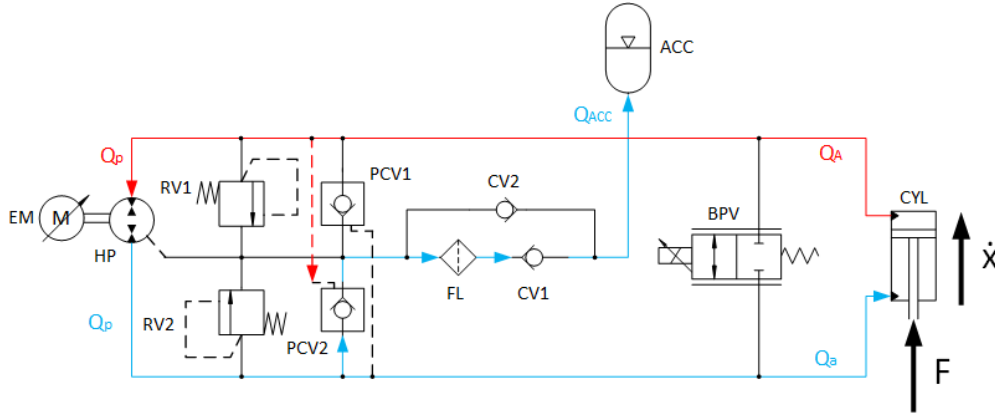


**Figure 2.13: Closed-circuit assistive retraction mode**

It can be noticed that the efficiency has to be computed in different ways according to the mode in which the system is operating. The efficiency is defined as the power in output  $P_{out}$  divided by the power in input  $P_{in}$ :

$$\eta = \frac{P_{out}}{P_{in}} \quad (2.33)$$

The powers included in the system efficiency came from CYL (Eq. 2.7), ACC (Eq.2.22), and HP. In order to define the output power from HP, the efficiency of the of the hydraulic unit has to be defined. Two different efficiencies can be considered for pump and motor modes [1]:

$$\eta_{HP,pump} = \frac{P_{P,hyd}}{P_{P,mech}} = \frac{Q_{P,e} (p_2 - p_1)}{T_{P,e} n_P} \quad (2.34)$$

$$\eta_{HP,mot} = \frac{P_{M,mech}}{P_{M,hyd}} = \frac{T_M n_{M,e}}{Q_M (p_1 - p_2)_e} \quad (2.35)$$

The subscript  $e$  denotes the actual values, which differ from the ideal one.

The efficiency of the hydraulic pump can be further divided into volumetric efficiency and hydro-mechanical efficiency [1]:

$$\eta_{v,P} = \frac{Q_{P,e}}{n_{P,e} V_D} \quad (2.36)$$

$$\eta_{v,M} = \frac{n_{M,e} V_D}{Q_{M,e}} \quad (2.37)$$

$$\eta_{hm,P} = \frac{V_D (p_2 - p_1)_e}{T_{P,e}} \quad (2.38)$$

$$\eta_{hm,M} = \frac{T_{M,e}}{V_D (p_1 - p_2)_e} \quad (2.39)$$

Finally, the system efficiency for all the four quadrants can be defined as:

$$\eta_{1,closed} = \frac{P_{CYL}}{P_{HP,pump} + P_{ACC}} = \frac{F \dot{x}}{Q_P \Delta p_P + Q_{acc} p_{acc}} \quad (2.40)$$

$$\eta_{2,closed} = \frac{P_{HP,mot}}{P_{CYL} + P_{ACC}} = \frac{Q_M \Delta p_M}{F \dot{x} + Q_{acc} p_{acc}} \quad (2.41)$$

$$\eta_{3,closed} = \frac{P_{CYL} + P_{ACC}}{P_{HP,pump}} = \frac{F \dot{x} + Q_{acc} p_{acc}}{Q_P \Delta p_P} \quad (2.42)$$

$$\eta_{4,closed} = \frac{P_{HP,mot} + P_{ACC}}{P_{CYL}} = \frac{Q_M \Delta p_M + Q_{acc} p_{acc}}{F \dot{x}} \quad (2.43)$$

Where  $\dot{x}$  can be derived according to Section 2.1.

Once the efficiency of the hydraulic circuit is computed, the overall efficiency of the system can be obtained by multiplying the electric motor efficiency.

$$\eta_{sys} = \eta_{closed} \eta_{EM} \quad (2.44)$$

The efficiencies of the electric motor in motor and generator modes are:

$$\eta_{EM,mot} = \frac{P_{mech}}{P_e} = \frac{T_e \omega_e}{V I} \quad (2.45)$$

$$\eta_{EM,gen} = \frac{P_e}{P_{mech}} = \frac{V I}{T_e \omega_e} \quad (2.46)$$

Where the mechanical power of the electric motor is equal to the shaft power multiplied by the conversion factor:

$$P_{shaft} = T n \frac{2 \pi}{60} \quad (2.47)$$

The efficiency of the inverter can be considered constant being around 97% for all the operating conditions.

Figure 2.14 gives a graphical representation of the four-quadrant modes for the open-circuit architecture. In this case the accumulator is no more present and the inlet port of the hydraulic unit is directly connected to a reservoir. All the previous equations are still valid with except for Eq. 2.40 - 2.43. Since  $P_{ACC} = 0$ , the hydraulic efficiencies of the open-circuit can be expressed as follows:

$$\eta_{1,open} = \frac{P_{CYL}}{P_{HP,pump}} = \frac{F \dot{x}}{Q_P \Delta p_P} \quad (2.48)$$

$$\eta_{2,open} = \frac{P_{HP,mot}}{P_{CYL}} = \frac{Q_M \Delta p_M}{F \dot{x}} \quad (2.49)$$

$$\eta_{3,open} = \frac{P_{CYL}}{P_{HP,pump}} = \frac{F \dot{x}}{Q_P \Delta p_P} \quad (2.50)$$

$$\eta_{4,open} = \frac{P_{HP,mot}}{P_{CYL}} = \frac{Q_M \Delta p_M}{F \dot{x}} \quad (2.51)$$

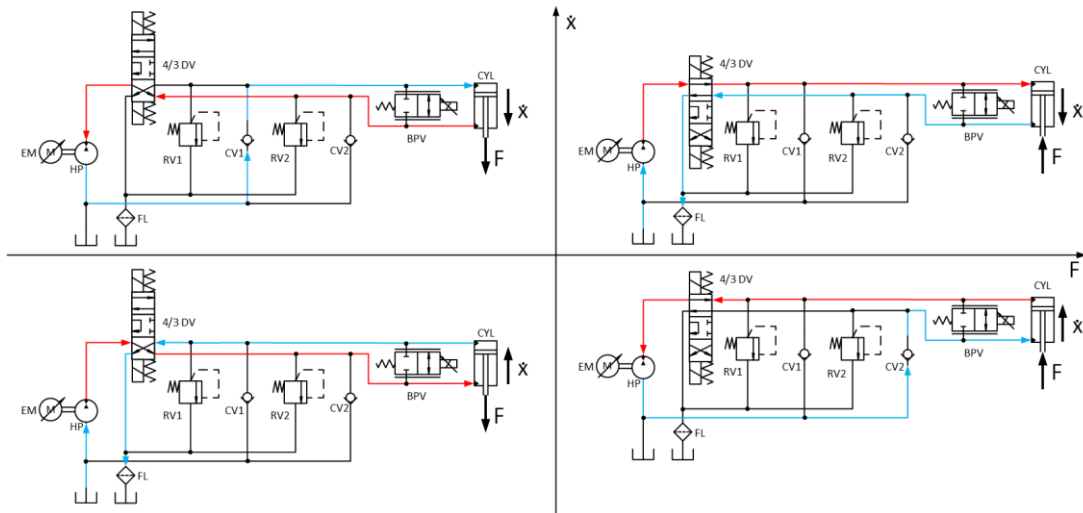


**Figure 2.14: Open-circuit four quadrant modes**

### 2.3.2 SLOW/FAST SUB-MODES

A proportional 2/2 bidirectional valve, also defined as bypass valve (BPV), is implemented in parallel to the actuator in both open- and closed-circuit. This valve is addressing two main features:

- To enable the sizing gap mentioned in Section 2.1.
- To enable slow actuation speeds avoiding to operate the pump in low rotational speed ranges where the total efficiency of the unit is drastically reducing the overall efficiency of the system.

Figure 2.15 shows the full four-quadrants map with slow and fast sub-modes for the closed-circuit.

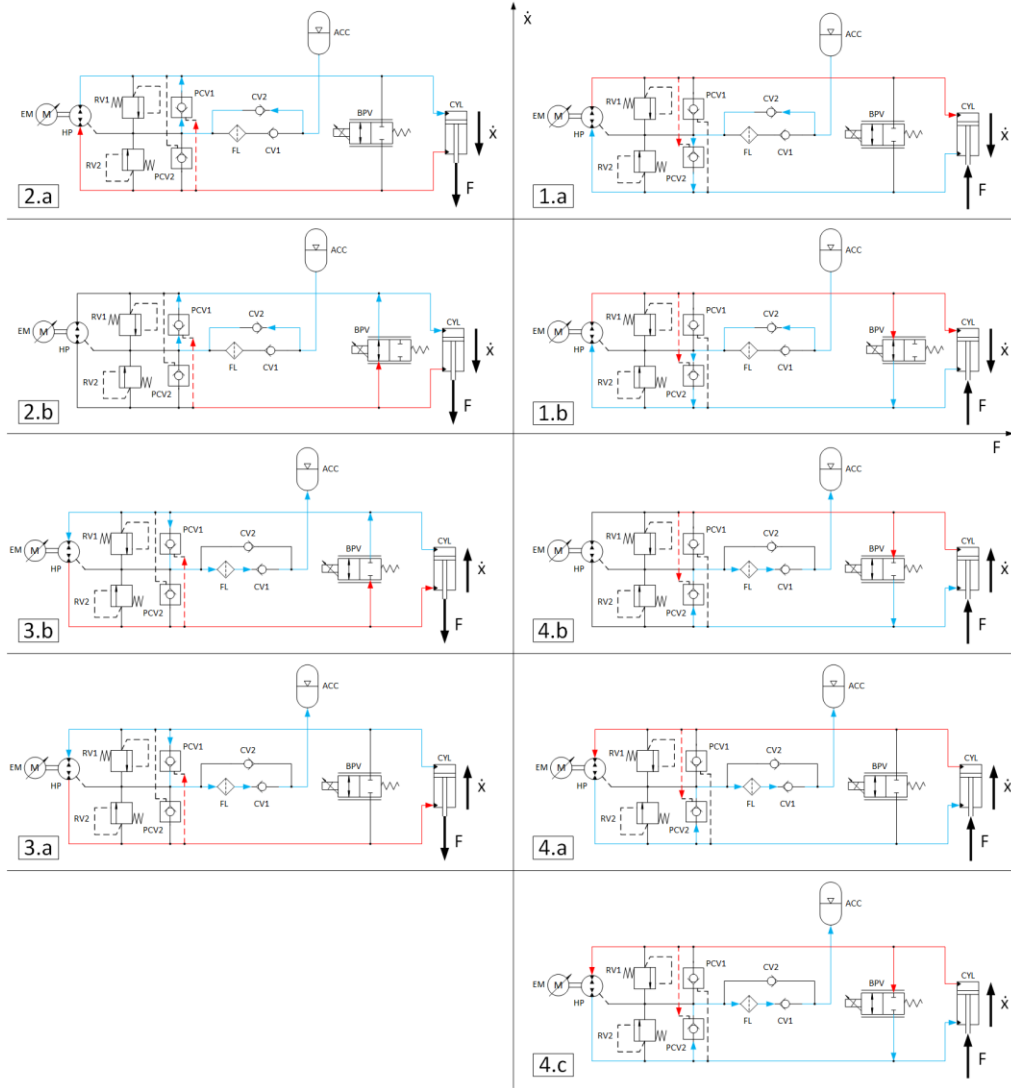


**Figure 2.15: Closed-circuit full four-quadrant map**

Figure 2.16 shows the slow-speed resistive extension (1.b). The rotational speed of HP is set to a minimum  $n_{min}$  and flow is diverted through BPV. The flow passing through BPV is controlled and it can be computed as follows:

$$Q_{bpv} = Q_p - Q_A \quad (2.52)$$

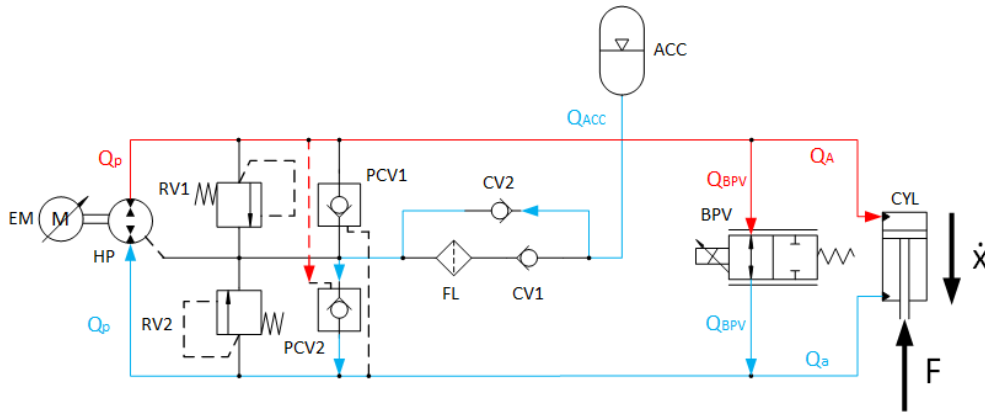
Where in the ideal case:

$$Q_p = n_{min} V_d \quad (2.53)$$

$$Q_A = \dot{x} A_p \quad (2.54)$$

$Q_a$  is obtained from Eq. 2.26, while  $Q_{acc}$  can be computed as follows:

$$Q_{acc} = Q_p - Q_a - Q_{bvpv} \quad (2.55)$$



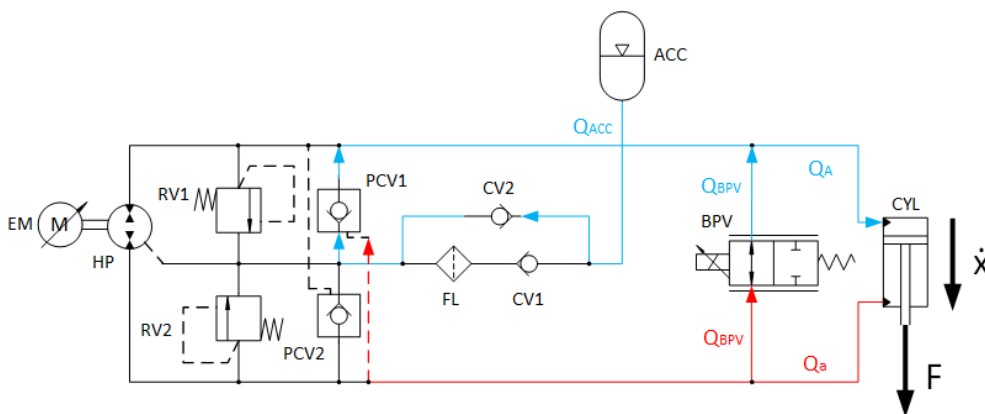
**Figure 2.16: Slow speed resistive extension closed-circuit**

Figure 2.17 shows the slow-speed assistive extension (2.b). The rotational speed of HP is set to zero. The flow in output from the rod chamber is diverted through BPV:

$$Q_a = \dot{x} A_r = Q_{bvpv} \quad (2.56)$$

$Q_A$  can be derived from Eq. 2.29, while  $Q_{acc}$  can be computed as follows:

$$Q_{acc} = Q_A - Q_{bvpv} \quad (2.57)$$



**Figure 2.17: Slow-speed assistive extension closed-circuit**

Figure 2.18 shows the slow-speed resistive retraction (3.b). The rotational speed of HP is set again to a minimum  $n_{min}$  but in the opposite direction, and flow is diverted through BPV. The flow passing through BPV is controlled and it can be computed as follows:

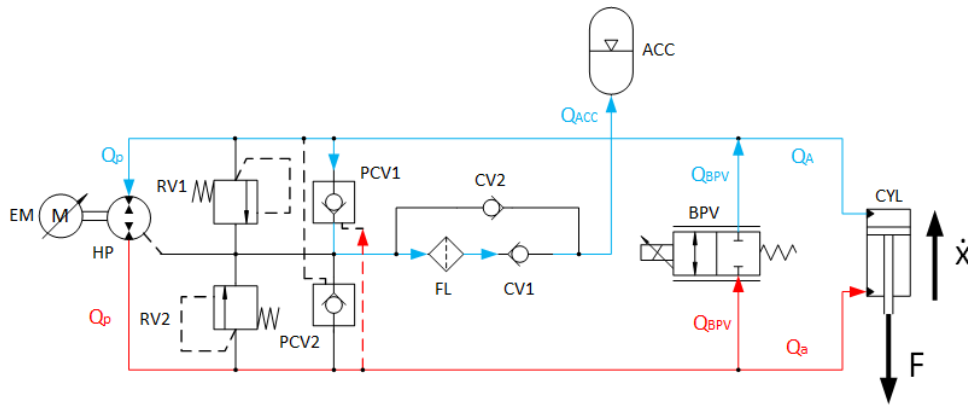
$$Q_{bvp} = Q_p - Q_a \quad (2.58)$$

Where in the ideal case  $Q_p$  is computed as in Eq. 2.53, while the rod side flow is:

$$Q_a = \dot{x} A_r \quad (2.59)$$

$Q_A$  can be derived from Eq. 2.29, while  $Q_{acc}$  can be computed as follows:

$$Q_{acc} = Q_{bvp} + Q_A - Q_p \quad (2.60)$$



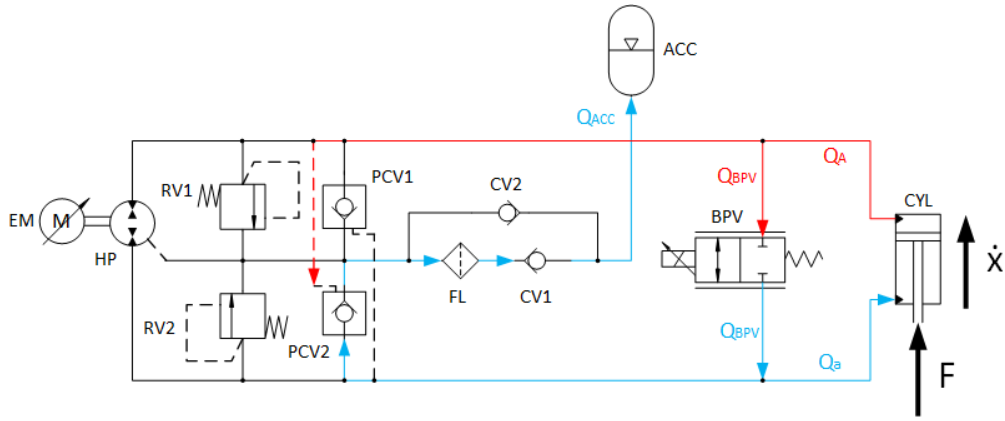
**Figure 2.18: Slow-speed resistive retraction closed-circuit**

Figure 2.19 shows the slow-speed assistive retraction (4.b). The rotational speed of HP is set again to zero. The flow in output from the piston chamber is diverted through BPV:

$$Q_A = \dot{x} A_p = Q_{bvp} \quad (2.61)$$

$Q_a$  can be derived from Eq. 2.32, while  $Q_{acc}$  can be computed as follows:

$$Q_{acc} = Q_{bvp} - Q_a \quad (2.62)$$



**Figure 2.19: Slow-speed assistive retraction closed-circuit**

Figure 2.20 shows the fast-speed assistive retraction (4.b). The rotational speed of HP is set to a negative maximum  $n_{max}$ . The flow in output from the piston chamber is diverted through BPV.

$$Q_p = n_{max} V_d \quad (2.63)$$

$$Q_{bpv} = Q_A - Q_p \quad (2.64)$$

Where  $Q_A$  can be derived from Eq. 2.56, while  $Q_{acc}$  can be computed as follows:

$$Q_{acc} = Q_p + Q_{bpv} - Q_a \quad (2.65)$$

Where  $Q_a$  can be obtained from Eq. 2.26.

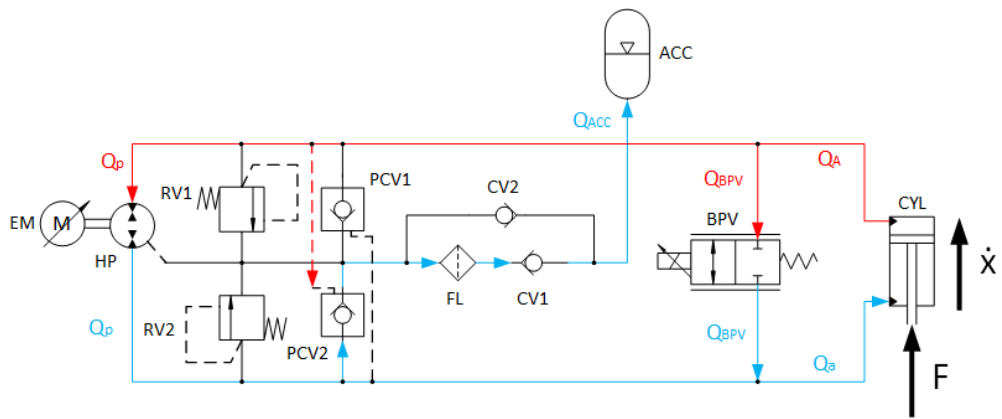


**Figure 2.20: Fast-speed assistive retraction closed-circuit**

The full four-quadrant map for the open circuit is shown in Figure 2.21.

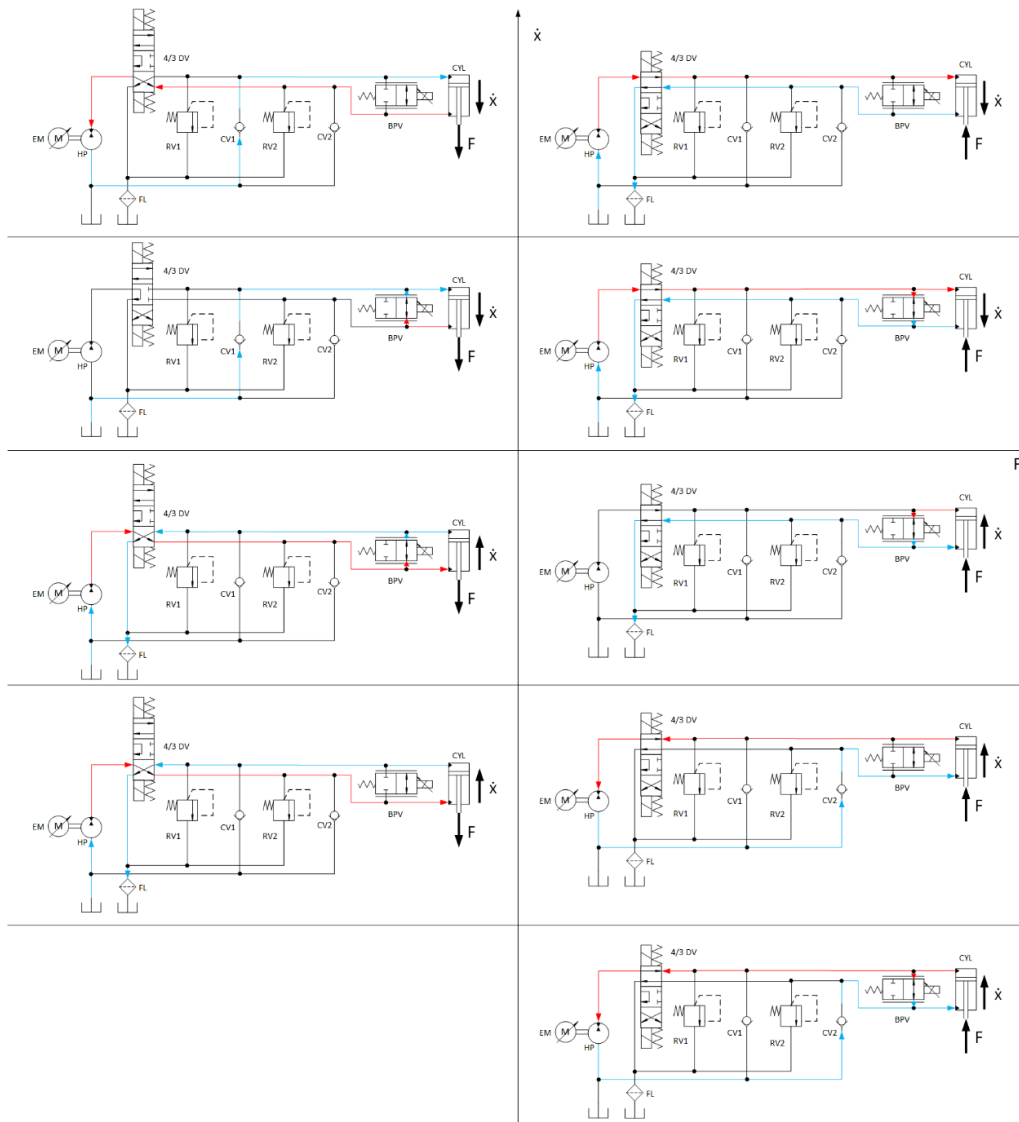


Figure 2.21: Open-circuit full four-quadrant map

## 2.4 CONTROL STRATEGIES

This section is aimed at explaining the control strategies for mode selection, bypass valve and electric motor speed. The selection of the operating mode is of main importance when the input signals for BPV and EM must be commanded. In particular the control strategies for both open- and closed-circuit will be explained. The mode selection and the BPV control are common for both architectures. However, the different type of HP – two-quadrants for the open-circuit and four-quadrants for closed-circuit – require slightly different EM

commands, while an additional 4/3 DV control is necessary to regulate the flow direction in the open-circuit.

### 2.4.1 MODE SELECTION

As for the reference vehicle, the EHA is operated by using a joystick. The input signal commanded by the operator is a velocity command  $i$  defined as follows:

$$i = \frac{\dot{x}_{des}}{\dot{x}_{max}} \quad (2.66)$$

Where  $\dot{x}_{des}$  is the desired linear velocity of the actuator, and  $\dot{x}_{max}$  is the maximum velocity that can be achieved by the cylinder. The sign of  $i$  is defined as positive during extension, while negative during retraction. As shown in Figure 2.4, the maximum speed is dependent on the mode considered.

$$-\dot{x}_{max,re} < \dot{x}_{des} < \dot{x}_{max,ex} \quad (2.67)$$

In ideal case, the maximum velocities in extension and retraction can be computed as follows:

$$\dot{x}_{max,ex} = \frac{Q_{max}}{A_p} = \frac{V_d n_{max}}{A_p} \quad (2.68)$$

$$\dot{x}_{max,re} = \frac{Q_{max}}{A_r} = \frac{V_d n_{max}}{A_r} \quad (2.69)$$

If the efficiency map of HP has been derived, volumetric efficiency  $\eta_{vol}$  should be considered to better regulate the actuator velocity.

To estimate the mode in which the EHA is operating the pressure difference  $\Delta p$  between piston and rod chamber of the cylinder is sensed:

$$\Delta p = p_A - p_a \quad (2.70)$$

Based on  $i$  and  $\Delta p$  the mode can be selected as shown in Table 2.3. The desired rotational speed can be computed according to the table.  $n_{des}$  is defined as positive during extension, which means a clockwise spin of the pump shaft. Therefore, during retraction  $n_{des}$  will be negative, and the shaft spins in the opposite direction.

**Table 2.3: Mode selection**

Speed command $i$	Pressure difference $\Delta p$	Mode	Desired rotational speed $n_{des}$
$i > 0$	$\Delta p > 0$	1	$\frac{\dot{x}_{des} A_p}{V_d}$
$i > 0$	$\Delta p < 0$	2	$\frac{\dot{x}_{des} A_r}{V_d}$
$i < 0$	$\Delta p > 0$	3	$\frac{\dot{x}_{des} A_r}{V_d}$
$i < 0$	$\Delta p < 0$	4	$\frac{\dot{x}_{des} A_p}{V_d}$

Once the  $n_{des}$  has been derived, it can be compared with the maximum and minimum speeds allowed by HP. From this comparison the sub-modes can be defined and listed in Table 2.4.

**Table 2.4: Sub-mode selection**

Speed command $i$	Pressure difference $\Delta p$	Desired rotational speed $n_{des}$	Mode
$i > 0$	$\Delta p > 0$	$ n_{des}  > n_{min}$	1a
$i > 0$	$\Delta p > 0$	$ n_{des}  < n_{min}$	1b
$i > 0$	$\Delta p < 0$	$ n_{des}  > n_{min}$	2a
$i > 0$	$\Delta p < 0$	$ n_{des}  < n_{min}$	2b
$i < 0$	$\Delta p > 0$	$ n_{des}  > n_{min}$	3a
$i < 0$	$\Delta p > 0$	$ n_{des}  < n_{min}$	3b
$i < 0$	$\Delta p < 0$	$n_{max} >  n_{des}  > n_{min}$	4a
$i < 0$	$\Delta p < 0$	$ n_{des}  < n_{min}$	4b
$i < 0$	$\Delta p < 0$	$ n_{des}  > n_{max}$	4c

The desired flow supplied by HP can be computed once  $n_{des}$  is obtained. HP is always affected by losses depending on the pressure difference between inlet and outlet, and the rotational speed of the shaft. Thanks to the control strategy the

effect of the volumetric efficiency can be balanced multiplying  $n_{des}$  by  $\eta_{vol}$  when HP is working in pump mode, and by  $1/\eta_{vol}$  when HP is working in motor mode.

#### 2.4.2 BYPASS VALVE CONTROL

BPV is a two-ports, two-positions, proportional, bidirectional control valve. It is a normally closed monostable valve where the rest position is maintained by a spring. A voltage signal regulates the position of the spool since the valve is solenoid operated. Being BPV proportional, infinite orifice areas are allowed between 0 (valve fully closed) and a maximum (valve fully open).

$$0 < \Omega_{des} < \Omega_{max} \quad (2.71)$$

The maximum orifice area is obtained when the maximum fractional pool position is reached and in turn when the maximum voltage signal is applied to the solenoid.

In order to obtain the desired amount of flow passing through the valve a control logic based on the orifice equation is considered, where the orifice equation is defined as follows:

$$Q = C_f \Omega_0 \sqrt{\frac{2 \Delta p}{\rho}} \quad (2.72)$$

Where  $Q$  is the volume flow rate passing through the orifice when the orifice area  $\Omega_0$ , the fluid density  $\rho$ , the pressure difference across the valve  $\Delta p$  and the orifice coefficient  $C_f$  are considered [1].

The desired orifice area  $\Omega_{des}$  can be derived from Eq. 2.72 as follows:

$$\Omega_{des} = \frac{Q_{bvp}}{C_f} \sqrt{\frac{\rho}{2 \Delta p_{meas}}} \quad (2.73)$$

The input data in the equation are:

- $\Delta p_{meas} = p_A - p_a$ , computed thanks to the pressure transducers located at the two ports of the hydraulic cylinder.
- $Q_{bvp}$ , which is the desired flow rate to compensate the one coming from the pump:

$$Q_{bvp} = V_d (n_{des} - n) \quad (2.74)$$

Where  $n$  is the actual speed sensed at the shaft between electric motor and hydraulic pump.

The command signal of BPV is set as the ratio between the desired orifice area and the maximum area:

$$j = \frac{\Omega_{des}}{\Omega_{max}} = \frac{\frac{Q_{des}}{C_f} \sqrt{\frac{\rho}{2 \Delta p_{meas}}}}{\frac{Q_{max}}{C_f} \sqrt{\frac{\rho}{2 \Delta p_{max}}}} = \frac{Q_{des}}{Q_{max}} \sqrt{\frac{\Delta p_{max}}{\Delta p_{meas}}} \quad (2.75)$$

Where  $\Delta p_{max}$  is the pressure drop across BPV when considering  $Q_{max}$  as flow passing through the valve.  $\Delta p_{max}$  and  $Q_{max}$  are derived from the characteristic curve of the device.  $j$ , that ranges between 0 and 1, is then converted into a voltage signal according to the solenoid properties.

As explained in Section 2.3.2 BPV is operated only during slow and fast sub-modes. The opening of BPV introduces throttling losses that represent a non-negligible quantity with respect to the total losses due to valves, filters, fittings and hoses in the hydraulic system. In general, the power loss due to these elements is computed as follows:

$$P_{loss} = Q \Delta p \quad (2.76)$$

### 2.4.3 PUMP SPEED CONTROL

The speed commanded to EM depends on the mode in which the EHA is operating. As shown in Table 2.3 the  $n_{des}$  is computed according to the high-pressure chamber of CYL. Moreover, the rotational speed of EM is set to zero during slow-speed assistive modes as explained in Section 2.3.2. All the power in input from the cylinder is dissipated in BPV to control the linear speed of the device. However, during the fast assistive retraction (4.c) the speed is set to a maximum. Table 2.5 shows a summary of the EM rotational speed for each mode

in the closed-circuit architecture. To better understand the direction of rotation the absolute value of  $i$  is considered.

**Table 2.5: EM speed in closed-circuit**

Mode	EM speed	BPV	Resistive/Assistive
1a	$ i  n_{max}$	Closed	Resistive
1b	$n_{min}$	Open	Resistive
2a	$ i  n_{max}$	Closed	Assistive
2b	0	Open	Assistive
3a	$- i  n_{max}$	Closed	Resistive
3b	$-n_{min}$	Open	Resistive
4a	$- i  n_{max}$	Closed	Assistive
4b	0	Open	Assistive
4c	$-n_{max}$	Open	Assistive

Figure 2.22 shows a conceptual flow chart for the closed-circuit architecture control. In the flow chart a new parameter  $k$  is introduced to define the operating range of the slow speed modes.

$$k = \frac{n_{min}}{n_{max}} \quad (2.77)$$

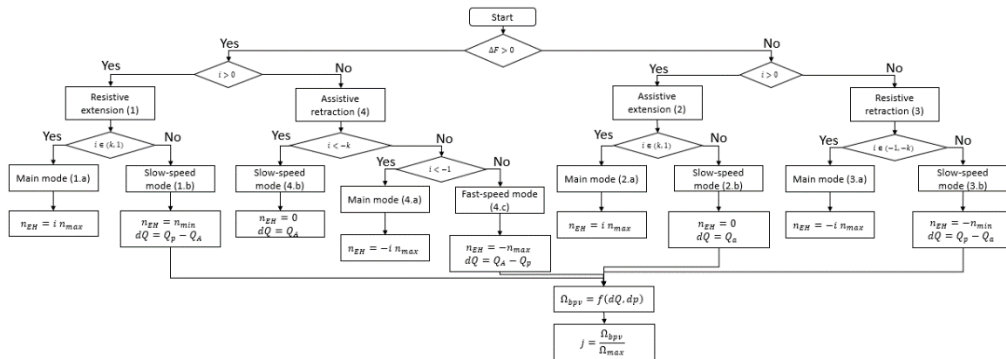


**Figure 2.22: Flow chart closed-circuit**

## 2.4.4 OPEN-CIRCUIT VARIANT

In the open-circuit architecture a two-quadrants HP is used. Therefore, the four-quadrant operating conditions can be achieved only if an additional 4/3 directional valve is implemented. Since the valve is monostable, the normally closed position is also the rest position thanks to two springs. Two solenoids are operated to switch to the two extreme positions. Table 2.6 shows a summary of the modes working conditions for the open-circuit architecture.

**Table 2.6: EM speed and 4/3 DV position in open-circuit**

Mode	EM speed	4/3 DV	BPV	Resistive/Assistive
1a	$ i  n_{max}$		Closed	Resistive
1b	$n_{min}$		Open	Resistive
2a	$ i  n_{max}$		Closed	Assistive
2b	0		Open	Assistive
3a	$ i  n_{max}$		Closed	Resistive
3b	$n_{min}$		Open	Resistive
4a	$ i  n_{max}$		Closed	Assistive
4b	0		Open	Assistive
4c	$-n_{max}$		Open	Assistive

## **3.COMPONENTS SIZING AND SELECTION**

This chapter will provide an in-depth discussion of the various components selected for the closed-architecture system. These components are essential for ensuring the functionality, reliability, and performance of the system, and their selection has been made with careful consideration of the specific requirements of the closed-circuit EHA design. Moreover, the components for the open-circuit based on previous research from Maha Lab [16] will be briefly explained.

### **3.1 CLOSED-CIRCUIT COMPONENTS**

The selection of the electric motor and of the hydraulic unit are accomplished based on the sizing discussed in Section 2.1. In particular, these two components are cutting-edge technologies provided by the sponsor “Settima Meccanica”, and their partner “Spin Engineering Solutions”. The valves and the filter choices are based on the accumulator sizing as it will be discussed. Moreover, a manifold is designed to accommodate all the cartridge valves and the filter.

#### **3.1.1 ELECTRIC MOTOR**

The considered electric motor is a 3-Phase Synchronous Reluctance Motor (Figure 3.1) designed from “Spin Engineering Solutions” [34]. The main advantages of the electric unit are:

- High efficiency up to 95%.
- Robustness and high power density.
- Competitive production costs: no brushes, no conductors in the rotor, no rare earth.
- No overheating in the rotor.
- Low rotor inertia and high dynamic response.

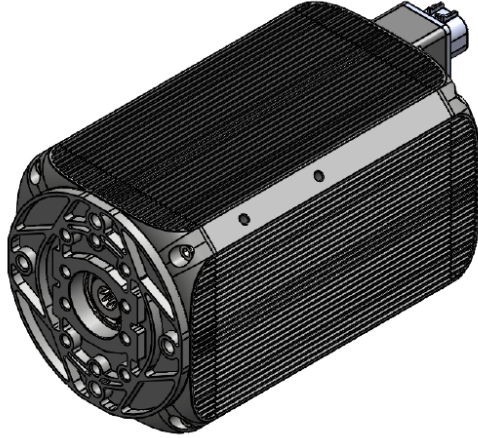


**Figure 3.1: 3D model of synchronous reluctance motor**

The most important parameters of the electric motor are shown in Table 3.1.

**Table 3.1: Electric motor parameters**

Description	Symbol	Unit	Value
Peak Torque @ 0 rpm	$T_{peak}$	$Nm$	92
Peak Power @ 3.2 krpm	$P_{peak}$	$kW$	31
Peak Current	$I_{peak}$	$A_{rms}$	75
Max Speed	$n_{max}$	$rpm$	5000
Number of poles	$2p$	-	6
Rotor Inertia	$J_r$	$kg\ cm^2$	81
Motor Weight	$M$	$kg$	31.5
Cooling System	-	-	Liquid cooling Water - Glycol
Motor Rated Power	$P_{mot}$	$kW$	15
Inverter Power Supply	$U$	$V_{dc}$	650

To accurately replicate the behaviour of an electric motor in a simulation, efficiency and power loss maps are generated from prior testing of the motor. These maps, which capture the motor's performance across various operating

conditions, are then used as input data for the simulation model, ensuring a realistic representation of the motor behaviour.

### **3.1.2 HYDRAULIC PUMP**

A key demand from the industrial sector is to develop a more favourable working environment, which translates to increased efficiency, reduced production costs, and improved quality of life for employees. Undoubtedly, minimizing operational noise contributes significantly to reaching these objectives.

Hydraulic pumps for high-pressure operations produce noise and vibrations that are often unacceptable for a wide range of scenarios, as for example mobile applications. Parameters influencing emissions of hydraulic noise are cavitation, pressure peaks rising from trapped fluid between gear teeth and flow ripples [34].

To reduce the noise emission, hydraulic units from Settima Continuum series (Figure 3.2) are implemented for the current EHAs. In particular, two different designs are considered for open- and closed-circuit. A two-quadrants HU featuring a helical rotor profile for the open-circuit, and a four-quadrant HU featuring a bihelical rotor profile for the closed-circuit. Unlike traditional gear pumps, the helical rotor design of the Continuum does not entrap any fluid volume, allowing for smooth fluid transmission and a significant reduction in pulsations. The features of the external gear pump/motor can be summarized as follows:

- Less noise compared to standard gear and vane pumps.
- Extremely Low vibration and pulsation.
- High efficiency for a wide range of speeds.
- Stable performances at variable speeds, also in case of sudden speed changes.

**SETTIMA®**



**Figure 3.2: Continuum external gear pump/motor**

According to the sizing of the EHA, an 18 *cc/rev* HU is implemented. However, the selection of components and the design of the manifold discussed in the next sections are accomplished taking in mind the possible implementation of a 22 *cc/rev* hydraulic machine. Therefore, future experiments with higher volumetric displacements can be performed with the current hardware.

The efficiency of the Continuum 4Q was tested on the multi-purpose test rig at Maha Lab to derive main flow rate, drain flow rate and torque maps used to model the unit in simulation. Tests are performed considering different oil temperatures. Two different circuit are considered to test the unit in both pumping and motoring mode as shown in Figure 3.3.

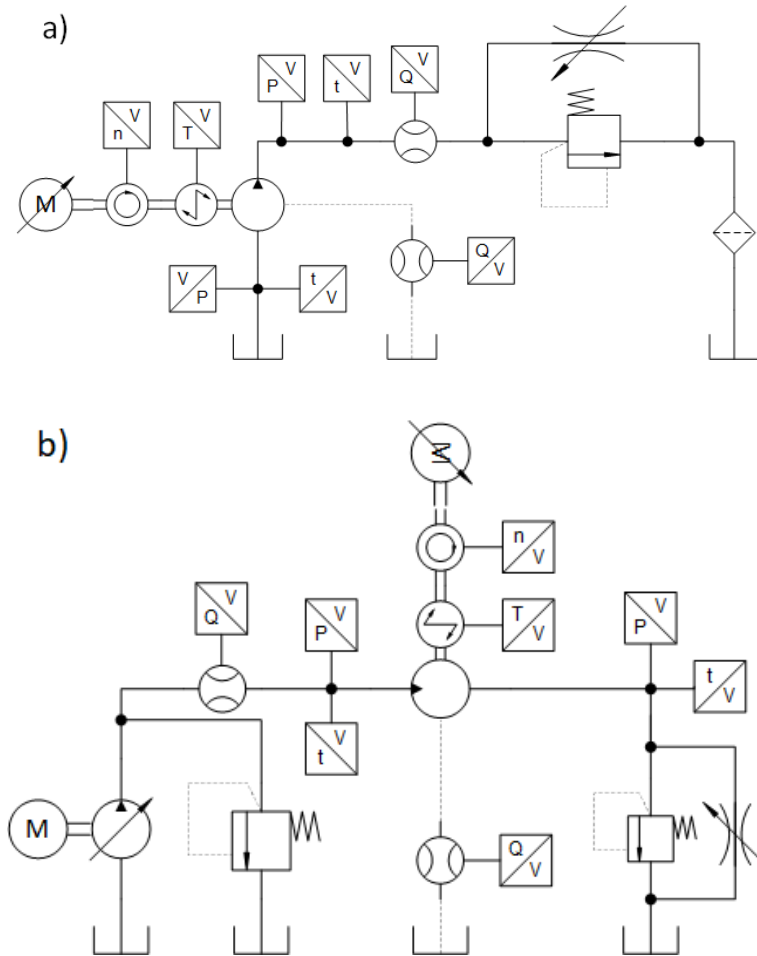


**Figure 3.3: Circuits for testing pumping mode (a) and motoring mode (b)**

In order to avoid low volumetric and hydro-mechanical efficiency regions the device will be operated in a specific rotational speed range. From the obtained maps a minimum speed can be derived for the HU. The main parameters for the implemented hydraulic machines are shown in Table 3.2.

**Table 3.2: Hydraulic pump parameters**

<b>Description</b>	<b>Symbol</b>	<b>Unit</b>	<b>Value</b>
Volumetric displacement	$V_d$	<i>cc/rev</i>	17.8
Max Speed	$n_{max}$	<i>rpm</i>	3000
Min Speed	$n_{min}$	<i>rpm</i>	500
Maximum operating pressure	$p_{max}$	<i>bar</i>	300
Maximum drain pressure	$p_{drain}$	<i>bar</i>	10
Pump shaft inertia	$J_p$	<i>kg cm<sup>2</sup></i>	73.4
Pump Weight	$M$	<i>kg</i>	4.1

### 3.1.3 ACCUMULATOR SIZING AND SELECTION

Since the closed-circuit architecture is not provided of a tank connection as the open-circuit, an accumulator is needed to compensate the differential volume from the actuator. The sizing of the accumulator is based on the reference vehicle for which the final implementation is considered. The skid steer loader will be introduced in the next sections when the experimental setup will be discussed. A general step by step procedure will be introduced for the sizing:

1. Considering a linear actuator, derive the volumes for the two cases of full instroke and full outstroke corresponding to rod and bore sides volumes respectively:

$$V_p = s A_p \quad (3.1)$$

$$V_r = s A_r \quad (3.2)$$

Where  $A_p$  and  $A_r$  are piston and rod side areas computed as in Eq. 2.1 and Eq. 2.2, while  $s$  is the cylinder stroke.

2. Compute the volume variation of the accumulator considering that for lifting/lowering operation two cylinders are employed:

$$\Delta V = 2(V_p - V_r) \quad (3.3)$$

3. Compute the minimum gas pressure according to the pressure drops during the discharging phase of the accumulator (Figure 3.4). The line pressure of the system cannot go below 0 bar, cavitation problems happen in this scenario. A reasonable margin pressure for the line can be set at 1 bar. The pressure drops estimated from the datasheets are considered in this step for each valve or filter the flow encounters. During the discharge phase pressure drops arise in check valve and pilot operated check valves.

$$p_1 = \Delta p_{cv} + \Delta p_{pcv} + p_{line} \quad (3.4)$$

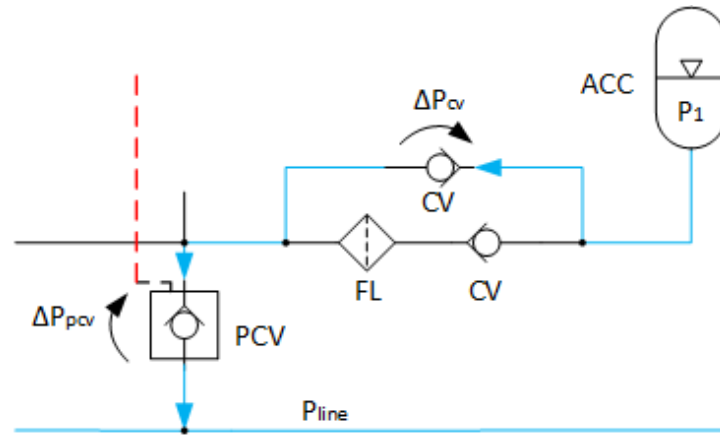


**Figure 3.4: Accumulator discharge**

4. Compute the pre-charge pressure of the accumulator:

$$p_0 = p_1 \cdot 0.9 \quad (3.5)$$

The pre-charge pressure ensures that a minimum amount of fluid is kept into the accumulator to compensate leakages from the cylinder.

5. Consider a suitable polytropic index:  $\gamma = 1.4$ , where 1.4 is the index used for an adiabatic reaction with nitrogen as gas. An adiabatic reaction can be assumed since the full charge/discharge of the accumulator is completed in few seconds (fast reaction with no exchange of heat). Moreover, the gas used to pre-charge the accumulator during experiments is nitrogen.

6. The maximum gas pressure is constrained by the drain line pressure. Due to the shaft sealing of hydraulic pump, the pressure at the drain should be kept lower than 10 bar.  $p_2$  can be computed taking into account the pressure drops of the hydraulic components when the accumulator is in charging phase (Figure 3.5). The pressure drops encountered are the filter pressure drop and the check valve pressure drop.

$$p_2 = p_{drain} - \Delta p_{cv} - \Delta p_{fl} \quad (3.6)$$

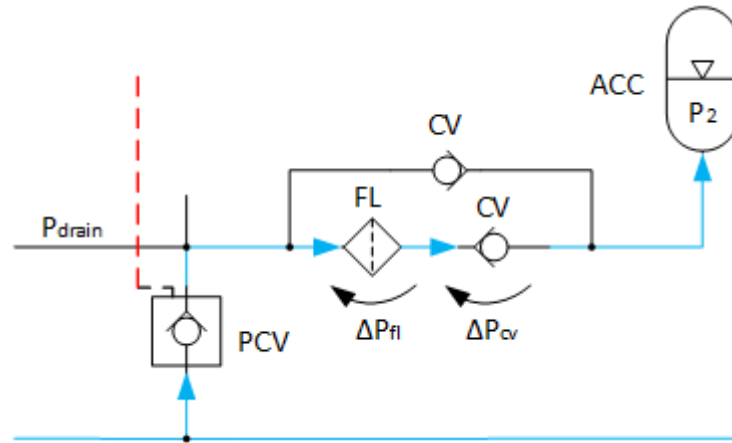


**Figure 3.5: Accumulator charge**

7. The maximum gas volume ( $V_2$ ) can be derived from the polytropic relationship (Figure 3.6), while the minimum gas volume ( $V_1$ ) can be obtained as difference between maximum and differential volumes:

$$V_1 = V_0 \left( \frac{p_0}{p_1} \right)^{\frac{1}{\gamma}} \quad (3.7)$$

$$V_2 = V_1 - \Delta V \quad (3.8)$$

8. By fixing the accumulator gas volume  $V_0$ , compute the estimated maximum gas pressure  $p_{2,est}$  according to the polytropic behaviour of the gas (Figure 3.6). The obtained value must be lower than the one computed in point 6. Absolute pressures must be used in equations in which the polytropic behaviour is considered.

$$p_{2,est} = \left[ \frac{p_0 V_0^\gamma}{V_2^\gamma} \right] < p_2 \quad (3.9)$$

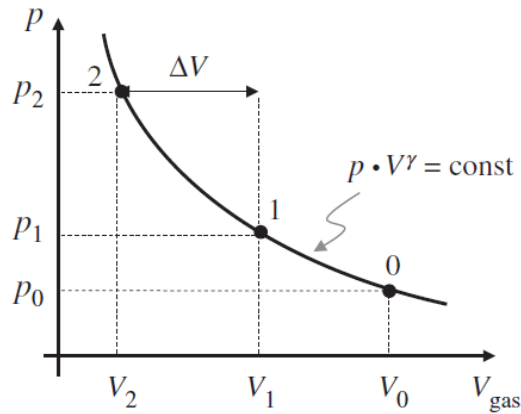


Figure 3.6: Polytropic behaviour of the gas inside the accumulator [1]

9. Once  $V_1$  is computed, the minimum rest volume in the accumulator can be obtained. The presence of the rest volume is due to setting conditions of the pre-charge pressure explained in point 4.

$$V_{rest} = V_0 - V_1 \quad (3.10)$$

The choice of the accumulator can be finalized once valves and filter are selected. The pressure drops are a very important parameter for the sizing of the accumulator. Due to the big sizes, high weights and high costs of these components a big attention should be paid to their sizing. Even slightly bigger pressure drops can cause to increase the size of the accumulator to the next possible one according to the market availability.

According to the valves/filter selection presented in the next section, the accumulator selected for the closed-circuit implementation is an Hydac accumulator of the series SB330 [35]. Some accumulator information are reported in Table 3.3.

Table 3.3: Accumulator properties

Code	Effective Gas Volume [L]	Maximum Flow Rate [L/min]	Maximum Pressure [bar]	Weight [kg]	Length [mm]	Diameter [mm]
SB330-10A1/112S1-262C	9.3	908.5	262	14	533	219

### 3.1.4 VALVES AND FILTER SELECTION

From the considerations made during the accumulator sizing it is clear that valves and filter are selected according to the minimum pressure drop criterion. In this way a wider pressure range can be obtained for the accumulator downsizing the device.

A selection is accomplished considering the best valves and filters for the closed-circuit implementation from different producers. For brevity the final choice is shown in this section, while the whole selection is reported in Appendix A.

In order to obtain lower pressure drops and downsize the accumulator, the selected valve will withstand higher flows than required. Considering valves with higher capacity means also an increase in costs. However, costs are still saved considering smaller accumulators at the cost of bigger valves.

In Table 3.4 are shown the maximum flow rate and the maximum pressure to which valves and filter are subjected in the closed-circuit (Figure 2.8). The maximum pressure of the system is set by the relief valves and it must be greater than the maximum load pressure.

$$p_{rel} > p_{max} = p_A = \frac{F + p_a a}{A} \quad (3.11)$$

**Table 3.4: Valve/filter maximum operating conditions**

<b>Valve/Filter</b>	<b>Maximum Flow Rate [L/min]</b>	<b>Maximum Pressure [bar]</b>
PCV1	38.3	206
PCV2	38.3	206
CV1	38.8	10
CV2	22.4	10
RV1	54	206
RV2	54	206
FL	38.3	10
BPV	38.3	206

The maximum flow rate of PCV1, PCV2, FL and CV1 are expected in resistive retraction when the maximum rotational speed of HP is considered ( $n = 3000 \text{ rpm}$ ). Around  $0.5 \text{ L/min}$  are added to the flow rate of CV1 because of the drain flow coming from HP. The maximum flow rate of CV2 is expected in resistive extension when a negative maximum rotational speed of HP is considered ( $n = -3000 \text{ rpm}$ ). RV1 and RV2 should be able to handle all the flow coming from HP at the maximum rotational speed ( $Q = V_d n_{max}$ ). The maximum flow passing through BPV is obtained in fast-speed assistive retraction, and it can be computed as in Eq. 2.64.

Based on the maximum operating conditions, the valves and filter shown in Table 3.5 represent the final selection. Since the pressure drop depends on the flow rate passing through the valve, two different pressure drops can be derived from the characteristic curve of each device when charging ( $Q_{acc} = 38.3 \text{ L/min}$ ) and discharging ( $Q_{acc} = 22.4 \text{ L/min}$ ) the accumulator.

**Table 3.5: Closed-circuit valves and filter**

Valve/Filter	Brand	Code	$Q_{max}$ [L/min]	$p_{max}$ [bar]
PCV	Sun Hydraulics	CKGB-XAN [36]	227.125	344.74
CV	Sun Hydraulics	CXFA-XAN [37]	151.416	344.74
RV	Sun Hydraulics	RDDA-LAN [38]	94.63	344.74
FL	Sun Hydraulics	FLHAXDN [39]	151.42	151.42
BPV	Rexroth	KKDSR1NB/HCG12N0K4V [40]	38	350

### 3.1.5 MANIFOLD DESIGN

Manifolds simplify the complexity of hydraulic circuits by minimizing the number of lines and fittings. By reducing the need for fittings, they not only decrease the potential for leaks but also help to lower the likelihood of assembly errors and make component replacements easier. Additionally, manifolds shorten line lengths, which helps to reduce pressure drops, improve response times, and enhance flow patterns. They feature larger passageways between ports, making them highly reliable and adaptable. Maintenance and repairs typically involve less downtime, and operators require a lower skill level to work with them [41].

An “enblocking” type manifold is designed. The name refers to a manifold with a single block receiving cartridge type valves and providing internal passages for interconnections and for ports leading to the outside. It is machined from a solid block of metal and it contains a large number of control elements interconnected by drilled passages.

Figure 3.7 shows the closed-circuit manifold schematic. The elements inside the blue, dashed line are screwed into the manifold block. The ports numbering is given for each external connection, which represents a hose interface.

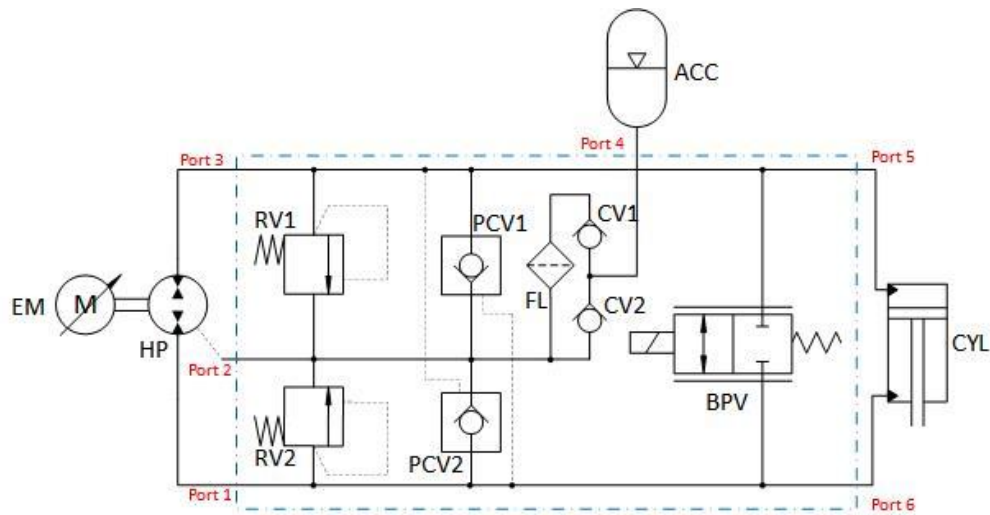


**Figure 3.7: Closed-circuit manifold schematic**

Flow rate requirements determine the appropriate inside diameter of a hydraulic hose. Engineers use the continuity equation to specify flow conditions that will ensure that the fluid velocity is appropriate. Nomograms as the one shown in Figure 3.8 [42] are helpful when sizing hoses. Recommended fluid velocity for suction lines can reach a maximum of  $1.6 \text{ m/s}$ , and for pressure lines the suggested range is from  $3$  to  $7.6 \text{ m/s}$ .

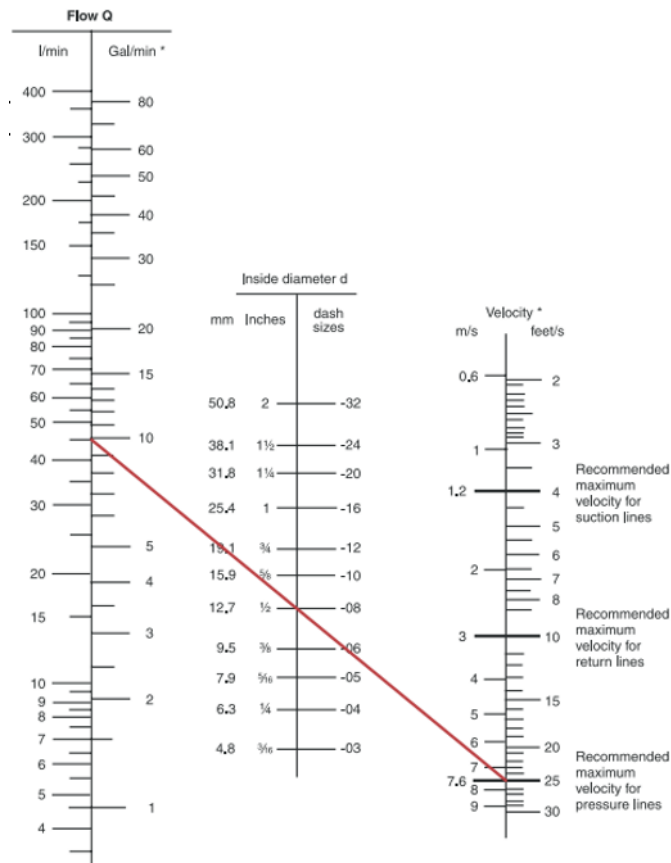


Figure 3.8: Hydraulic hose sizing nomogram [42]

In the considered design a direct connection to tank is not provided, but the accumulator maximum pressure is low such that higher internal diameters of the hose must be considered. For all the remaining hoses the pressure line limitations can be considered. The discussion about hose sizing is relevant also for the port size choice in the manifold. In order to avoid an excessive use of fittings, which introduce discontinuities in the flow, the port diameters must be as close as possible to the corresponding hose internal diameter.

By knowing the maximum flow rate through the hoses from the circuit sizing, and by setting a reasonable fluid velocity, the sectional area of hoses and ports can be computed. The design of the manifold is based on the usage of the 22 cc pump.

$$A = \frac{Q}{\dot{x}_{fluid}} \quad (3.12)$$

Table 3.6 shows the maximum operating conditions of the ports in the manifold and their minimum and maximum diameter based on the recommended fluid velocity discussed before.

**Table 3.6: Operating conditions of the manifold ports**

<b>Port</b>	<b><math>Q_{max}</math> [L/min]</b>	<b><math>p_{max}</math> [bar]</b>	<b>Min port size [mm]</b>	<b>Max port size [mm]</b>	<b>Connected to</b>
1	66	206	15.16	25.62	Hydraulic Pump
2	2.5	10	2.95	4.99	Hydraulic Pump drain
3	66	206	15.16	25.62	Hydraulic Pump
4	49.3	10	13.10	22.14	Accumulator
5	112.8	206	19.81	33.49	Cylinder Bore side
6	66	206	15.16	25.62	Cylinder Rod side

SAE port threads are considered, and aluminium is the option of the material since it can fit the pressure requirements (20.6 MPa as maximum system pressure). The dimensions of the manifold are 190 mm × 190 mm × 150 mm.

Table 3.7 lists the components in the manifold referring to the information given in Figure 3.7. The maximum flow rates among the operating conditions are computed according to the use of a 22 cc/rev hydraulic unit.

**Table 3.7: List of components in the manifold**

Component	Brand	Code	Cavity	Maximum flow rate [L/min]	Maximum pressure [bar]
PCV1	Sun Hydraulics	CKGB-XAN	T-17A	46.8	206
PCV2	Sun Hydraulics	CKGB-XAN	T-17A	46.8	206
CV1	Sun Hydraulics	CXFA-XAN	T-5A	49.3	206
CV2	Sun Hydraulics	CXFA-XAN	T-5A	27.4	206
RV1	Sun Hydraulics	RDDA-LAN	T-10A	66	206
RV2	Sun Hydraulics	RDDA-LAN	T-10A	66	206
FL	Sun Hydraulics	FLHAXDN	T-16A	49.3	206
BPV	Rexroth	KKDSR1NB/HCG12N0K4V	R/T-13A	46.8	206

The maximum pressure of the system is determined by the relief pressure of the RDDA-LAN valve. The maximum flow rates are calculated based on the most demanding actuation modes of the EHA, which are resistive retraction and resistive extension. For the BPV, the most demanding mode is fast retraction.

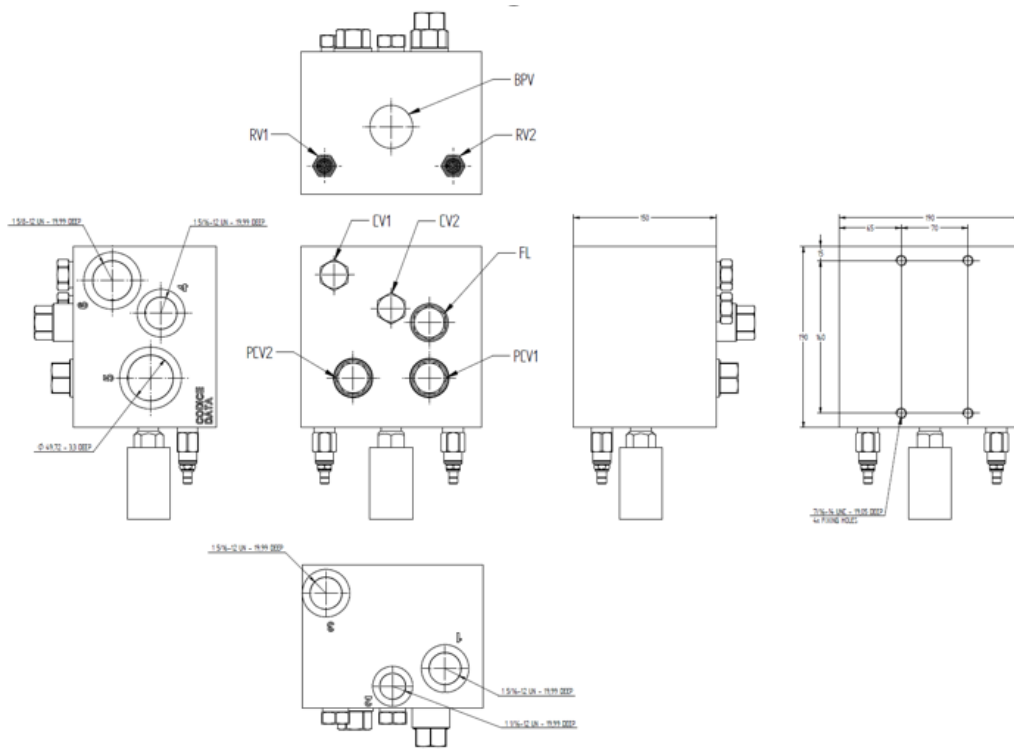
The final size of ports and channels connecting the valves and filter in the manifold body are reported in Table 3.8. The computed fluid velocities are always below the pressure line limit of  $7.6 \text{ m/s}$ , except for the input channel of the relief valves. Additionally, the losses in the manifold are minimal due to the very short flow paths the fluid must travel. Since the requirements for the  $22 \text{ cc/rev}$  HP unit have been met, the same will apply to the  $18 \text{ cc/rev}$  unit.

**Table 3.8: Fluid velocity in the manifold with 22 cc/rev HP**

	<b>Diameter [mm]</b>	<b>Max flow rate [L/min]</b>	<b>Fluid speed [m/s]</b>
1	22	66	2.89
2	19	2.5	0.15
3	22	66	2.89
4	15.25	46.8	4.27
5	22	112.8	4.95
6	22	66	2.89
In RV	13.5	66	7.68
Out RV	15.25	66	6.02
In CV	17.5	46.8	3.24
Out CV	19	46.8	2.75
BPV	11.8	46.8	7.13
In FL	22	46.8	2.05
Out FL	19	46.8	2.75
PCV	22	46.8	2.05

The valves and filter positions on the manifold faces are shown in Table 3.9. The bottom side serves as the mounting surface on the platform, featuring four mounting holes. The top and front sides are used for the cartridge valves and filter. The ports are located on the back and right sides of the manifold. Specifically, ports 1 and 3 are used for the HP inlet/outlets, while port 2 is for the pump drain, all of which are positioned on the back side. Ports 5 and 6 are for the piston and rod connections of the CYL, while port 4 connects the accumulator to the manifold, and these are all located on the right side.

**Table 3.9: Manifold drawing**



The port positions have been carefully designed to facilitate easy and efficient piping when connecting the HP, manifold, accumulator, and CYL, as described in the following sections.

### **3.2 OPEN-CIRCUIT VALVES AND FILTER**

Table 3.10 shows the valves selected by Qu [15] for the experimental setup of the open-circuit architecture. The simulation model of the open-circuit will be based on these components to match future experiments aimed at comparing the two possible architectures of the EHA.

**Table 3.10: Hydraulic components open-circuit**

<b>Component</b>	<b>Brand</b>	<b>Product Number</b>
Check valve	Rexroth	0431250027A0000 [43]
Relief valve	Rexroth	DBDS 6 K1X/315 [44]
2/2 Bypass valve	Rexroth	KKDSR1NB/HCG12N0K4V [40]
4/3 directional valve	Rexroth	4WE10G5X/EG12N9K4/M [45]
Filter	Rexroth	50LEN0063-H6XLA00-V5,0-M-R3 [46]

# 4.SIMULATION MODEL

This chapter will discuss the simulation model, which is created using the Simcenter Amesim [47] platform, employing the lumped parameter method. Its purpose is to simulate the systems under investigation and serve as a design tool for future sizing and optimization efforts. The mechatronic system built in simulation takes elements from different libraries (thermal-hydraulic, mechanical, electronic drives) to derive realistic results in terms of power loss and efficiency.

## 4.1 CONTROL LOGIC

The Amesim simulation is composed by components from different libraries. It is indeed important to specify how the different sub-models communicate and how the control logic of the entire system is set (Figure 4.1).

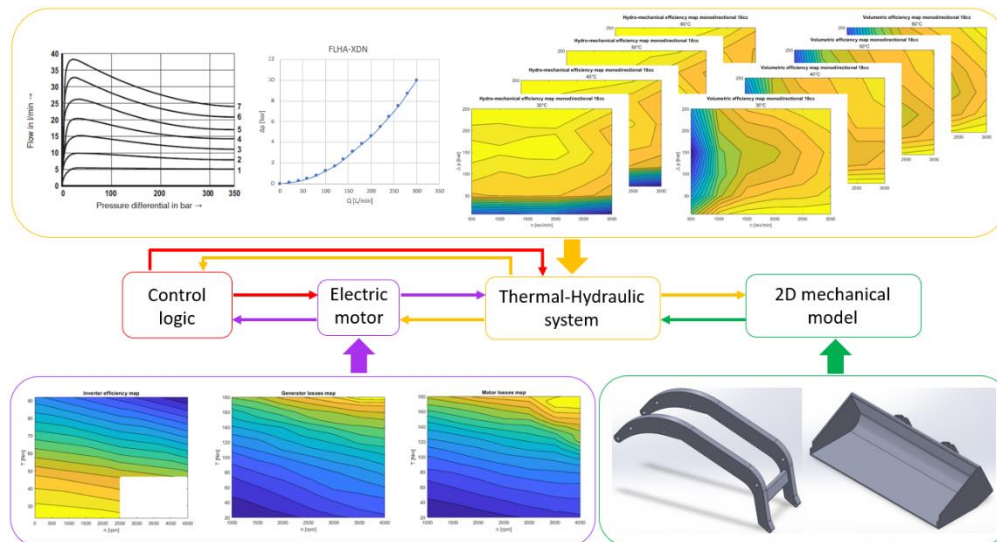


Figure 4.1: Simulation model in Amesim Simcenter

The signal/control library is used to generate signals to pilot physical systems. Signals processed by the control library are then send to the electric drive, thermal-hydraulic and mechanical libraries.

The electric drives library is used to model the synchronous reluctance motor. From the characterization made by the sponsor a power loss map is implemented into this model for both motor and generator modes. While a constant efficiency for the inverter is assumed based on the datasheet maps.

The thermal hydraulic library is used to model the hydraulic circuit composed by hydraulic unit, valves, filter, accumulator, actuator and hoses. For further evaluations related to the cooling system of the architecture the heat transfer model is indeed fundamental. Input to the hydraulic components are efficiency maps for the hydraulic unit and characteristic curves for valves and filters. Maps can be implemented also for different temperatures in this library.

Additionally, the 2D mechanical library can be considered to study the kinematics of the boom and bucket structure. Since the load in the actual experimental setup cannot be controlled, the load applied to the structure of the reference vehicle is given by filling the bucket with weights. This library provides a realistic behavior of the mechanical structure under the performed experiments. Input to the model are the 3D models of the boom and bucket from the reference vehicle.

Regarding the control logic, it is divided into different structures. The mode selection logic tells us in which sub-mode of the four-quadrants we are operating. Based on the pressure difference between piston and bore chambers and on the joystick command one of the four quadrants is selected. The desired rotational speed of the hydraulic pump is computed based on the mode since the linear speed of the actuator is dependent on the retraction or extension motion (Table 2.3). The desired speed is then compared with the minimum and maximum rotational speeds set for the hydraulic pump, and from this comparison an additional sub-mode selection is obtained (Table 2.4). The electric motor rotational speed is limited according to the corresponding sub-mode (Table 2.5). The speed command is then converted into a suitable torque command required by the

electric motor model. In particular a PI anti-windup controller is used to derive the torque command.

The electric motor is dictating the hydraulic pump rotational speed, which will define the flow supplied to the cylinder through the hydraulic circuit. The external force applied at the cylinder side will define the pressures in bore and rod chambers.

During slow and fast actuation mode the bypass valve is opening based on the orifice equation. Inputs to this logic are the sub-mode signal, the desired and the actual speed of EM, which can be converted in flow rates multiplying by the volumetric displacement, and the pressures in the cylinder chambers. This logic provides a signal for the solenoid of the proportional valve.

Figure 4.2 shows the signals exchange between the different control strategies and the physical system adopted in simulation.

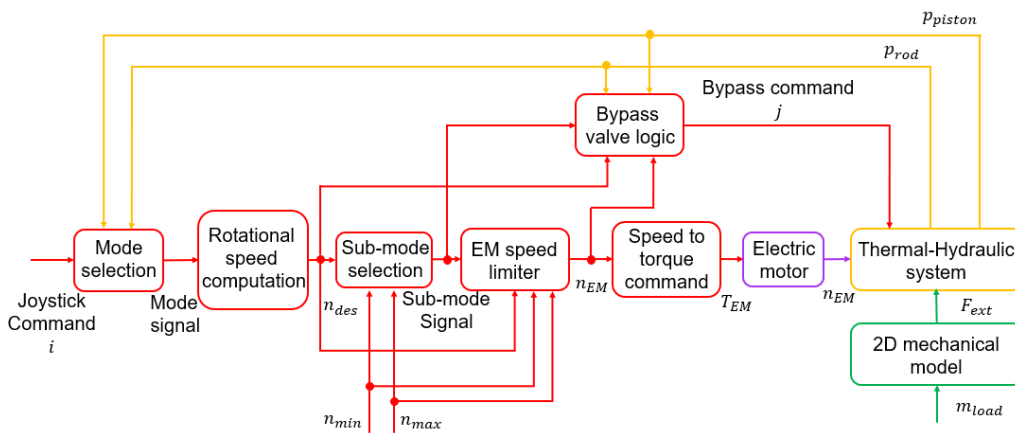


Figure 4.2: Simulation signals exchange

## 4.2 THERMAL-HYDRAULIC MODEL

The Thermal-Hydraulic Library focuses on designing hydraulic systems where changes in fluid temperature significantly affect overall performance. This library employs a transient heat transfer method to model thermal behaviours in liquids, including energy transfer and convection, and to analyse how these liquids' temperatures evolve within a hydraulic system.

HP is modelled considering Eq.2.36 – 2.39. Moreover, a parameter called “percentage of heat generated by friction transferred to the fluid”  $K_{heat}$  is introduced to evaluate the power loss due to friction. This parameter represents an additional degree of freedom to improve the accuracy of the temperature prediction, which can be challenging since the heat interaction can vary among the types of pumps.

$$P_{loss} = \left(1 - \frac{K_{heat}}{100}\right) P_{frict} \quad (4.1)$$

Where  $P_{frict}$  is computed in pump and motor mode as follows:

$$P_{frict}^P = P_{mech} - P_{hyd}^P = T \omega - Q_{in} (p_2 - p_1) \quad (4.2)$$

$$P_{frict}^M = P_{hyd}^M - P_{mech} = Q_{out} (p_1 - p_2) - T \omega \quad (4.3)$$

Fundamental input for the pump model of the four-quadrant pump of the closed-circuit are maps for the main volumetric flow rate, the external drainage volumetric flow rate and the shaft torque. These maps can be derived from a previous pump characterization. Instead, the two-quadrants pump employed in the open-circuit (not provided of drain port) has as input volumetric and hydro-mechanical efficiency maps provided by the sponsor.

All valve and filters models are based on the orifice equation (Eq. 2.72), from which the power losses due to throttling can be obtained (Eq. 2.76). In particular, FL is modelled as a fixed orifice in which flow rate vs. pressure drop characteristic curves can be included.

RV serves to control the upstream pressure in a hydraulic circuit, safeguarding hydraulic components from excessive pressure. Typically, the valve remains closed. However, when the pressure differential across the valve surpasses the specified cracking pressure (equivalent pressure of the spring preload), the valve opens, allowing fluid to flow through and maintaining the pressure at the cracking level.

$$\Delta p = p_2 - p_1 - p_{crack} \quad (4.4)$$

CV allows flow only in one direction, due to a sliding element held by a spring against the seat. This element is modelled again by Eq. 4.4.

PCV functioning is similar to the one of CV. Additionally, a drain port is used to sense the pressure in the hydraulic system. This pressure, also known as “pilot pressure”, commands the opening of the valve.

$$p_3 = \frac{p_1 - p_2 + p_{crack}}{p_{ratio}} + p_2 \quad (4.5)$$

The fractional valve opening for PCV is expressed as:

$$x_v = \frac{p_2 - p_1 - p_{crack} + (p_3 - p_2) p_{ratio}}{p_{sat} - p_{crack}} \quad (4.6)$$

Where  $p_{sat}$  is the saturation pressure, which is the minimal differential pressure when the valve is fully open.

ACC consists of a liquid phase linked to port 1 and a gas phase that is in pressure equilibrium. The behaviour of the gas is modelled using a polytropic gas law, where  $C_{poly}$  is the polytropic constant determined by the initial or pre-charge pressure and the effective gas volume.

$$C_{poly} = p V_g^\gamma = p_0 V_0^\gamma \quad (4.7)$$

Since charging and discharging of the accumulator require few seconds, no heat exchange is modeled between the liquid and gas phases. The liquid phase is therefore supposed to be adiabatic. The volume of gas is computed from the polytropic law, while the temperature of the gas is calculated from the perfect gas law.

$$V_g = \left( \frac{C_{poly}}{p_1} \right)^{\frac{1}{\gamma}} \quad (4.8)$$

$$T_g = \frac{p V_g}{c m_g} \quad (4.9)$$

CYL converts hydraulic energy into translational kinematic energy. Its model is described by the force balance and the thermal pressure build up equation. In the force balance the viscous friction is included.

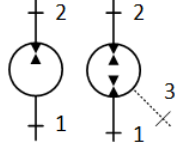
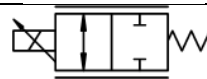
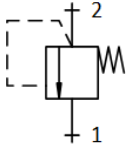
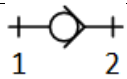
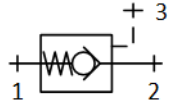
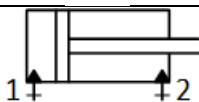
$$F = (p_1 - p_{atm}) A_p - (p_2 - p_{atm}) A_r + \dot{x} k_{visc} \quad (4.10)$$

$$\frac{\partial p}{\partial t} = \frac{B_T}{V} \left( \sum Q_{in} - \sum Q_{out} - \frac{\partial V}{\partial t} \right) - \frac{B_T}{\rho} \frac{\partial \rho}{\partial t} \Big|_p \frac{\partial T}{\partial t} \quad (4.11)$$

An additional heat flow rate to dead volume coefficient  $\dot{\phi}$  is considered to determine the variation of temperature at the two ports of CYL. This parameter is introduced as  $K_{heat}$  to increase the accuracy of the model.

As a summary, Table 4.1 provides a list of the main hydraulic components modelled in simulation.

**Table 4.1: Modelling hydraulic components in simulation**

Component	Symbol	Equations
HP		Eq 2.36 -2.39 Eq. 4.1 – 4.3
BPV		Eq. 2.72
4/3 DV		Eq. 2.72
FL		Eq. 2.72
RV		Eq. 2.72 Eq. 4.4
CV		Eq. 2.72, 4.4
PCV		Eq. 2.72, 4.5, 4.6
ACC		Eq. 4.7 – 4.9
CYL		Eq. 4.10, 4.11

Hoses are modelled as series of hydraulic resistances and hydraulic capacitances based on the system configuration. Hence, they are also defined by the orifice equation (Eq. 2.72) and the thermal pressure build up equation (Eq. 4.11). A thermal exchange coefficient  $k_{th}$  is considered to derive the heat exchange by convection with the outside of the hose.

$$dh = k_{th} \pi D L (T_{ext} - T_{int}) \quad (4.12)$$

Figure 4.3 and Figure 4.4 represent the closed-circuit and the open-circuit thermal-hydraulic model in Simcenter Amesim environment.

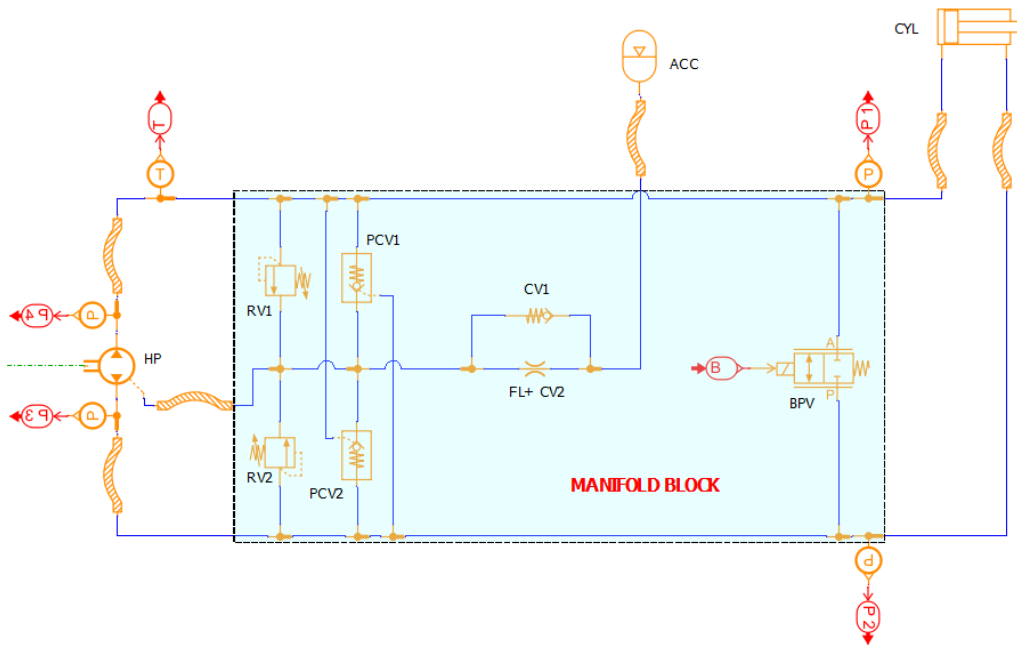


**Figure 4.3: Graphical representation of the thermal-hydraulic closed-circuit system in Simcenter Amesim**

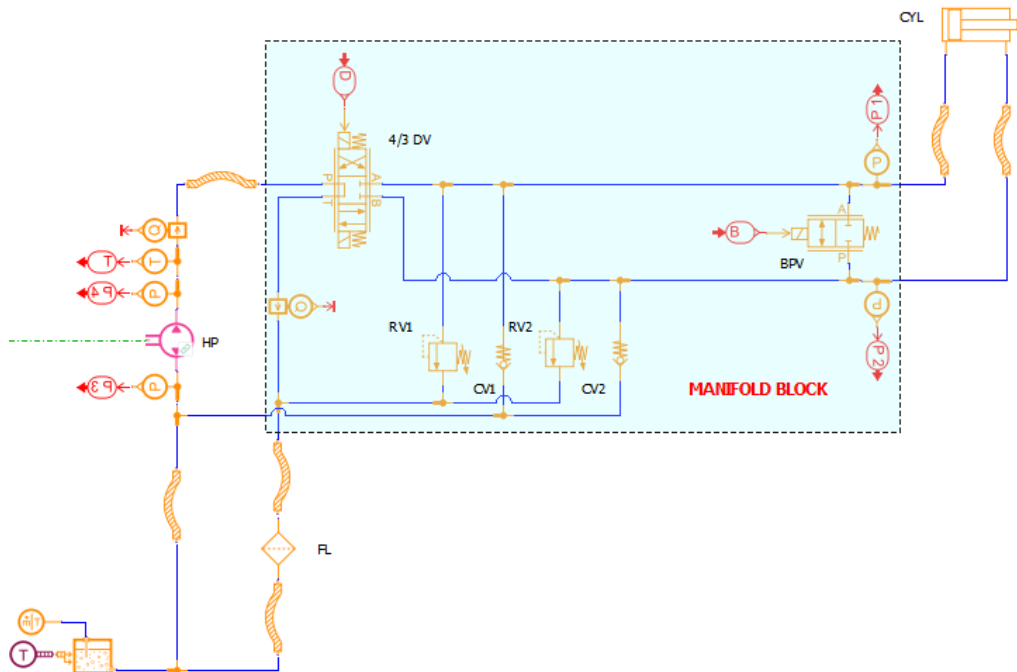


**Figure 4.4: Graphical representation of the thermal-hydraulic open-circuit system in Simcenter Amesim**

### 4.3 ELECTRIC MOTOR MODEL

Synchronous reluctance motors do not have a specific model in Simcenter Amesim. The advantages of these devices are resulting in an increasing interest for the technology. However, SynRM are not common electric drives in nowadays systems.

To model the considered electric motor an average model of an electric drive is considered. The functioning of the model is indeed independent from the technology of the machine and the inverter. The equations representing the model are Eq. 2.45 and Eq. 2.46. Inputs to this model are losses maps including both motor and generator modes of the EU, and additional parameters as shown in Table 3.1.

An inverter efficiency map can be considered to derive the input electric power to EM in resistive modes, as well as the output electric power of the whole system in assistive modes. The map is derived by the datasheets of the considered inverter.

$$P_{el,in} = \frac{V I}{\eta_{inv}} \quad (4.13)$$

$$P_{el,out} = V I \eta_{inv} \quad (4.14)$$

A high and almost constant efficiency can be assumed for the inverter in the considered operating conditions. It is worth to recall that the electric motor is working in the rotational speed range 500 – 3000 *rpm*, while the maximum expected torque applied to EM is around 60 *Nm*.

### 4.4 2D MECHANICAL MODEL

Figure 4.5 presents a graphical representation of the mechanism model created in the Simcenter Amesim platform. The focus is primarily on the boom and bucket functions. Key parameters, including position of joints, mass, and moment of

inertia of bodies, are incorporated into the model, ensuring that its behaviour closely aligns with the baseline measurements.

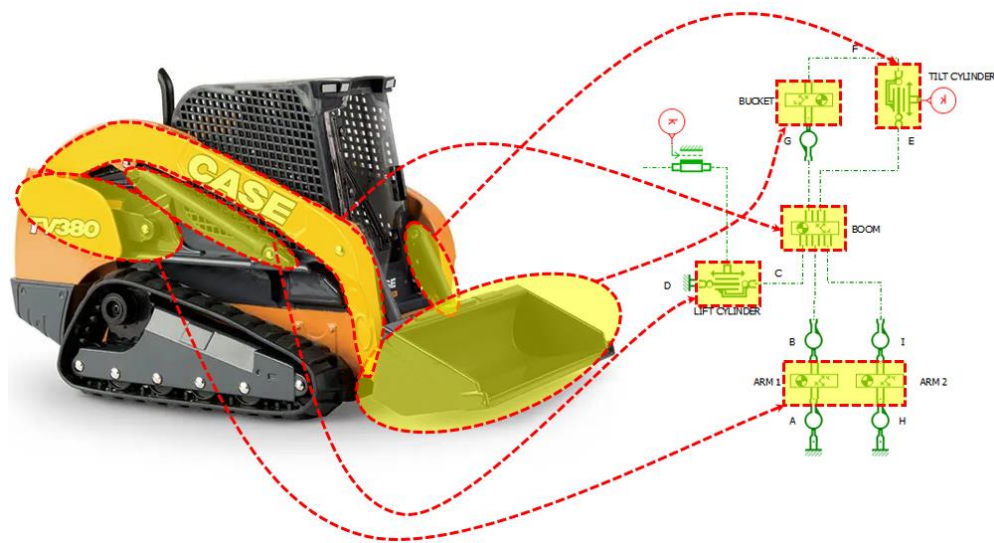


**Figure 4.5: 2D mechanical model of boom and bucket in Simcenter Amesim**

The 2D mechanical library can reproduce a synchronous motion of the reference vehicle (Figure 4.6) to evaluate the correctness of the simulation model. Mass and inertia are the main input parameters for the bodies, such as boom, bucket and arms. Moreover, an item location for each port should be specified. Lift and tilt cylinder are used to have a graphical representation of the actuators in animation. These last blocks are connected to the actuators of the thermal-hydraulic library. The revolute pairs (A, B, C, etc.) are defined by a rotary spring stiffness and a rotary damping coefficient. All the information about the mechanical model of boom and bucket are derived by the 3D drawing and the datasheet of the reference vehicle.

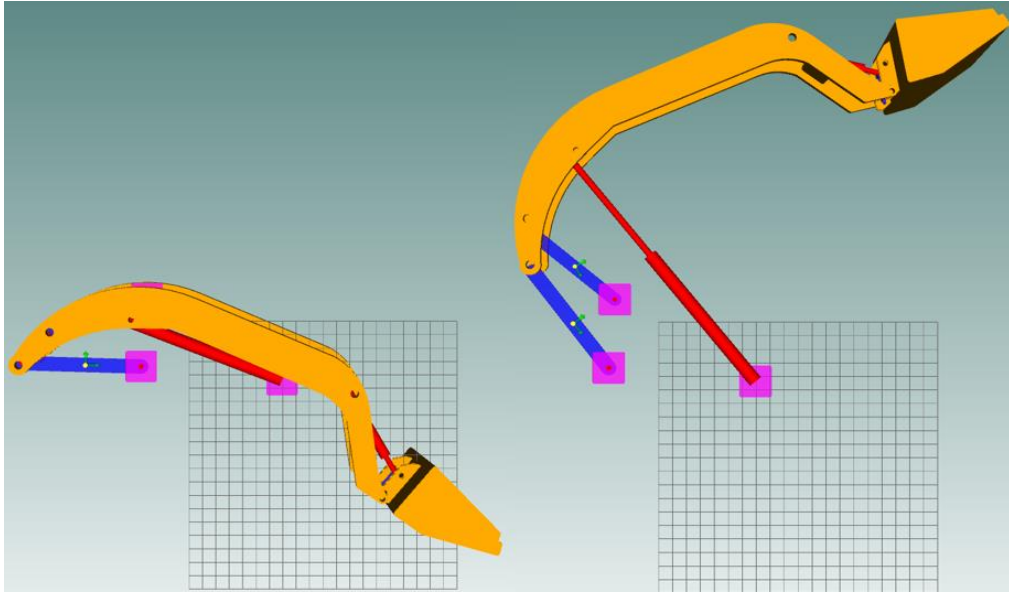


**Figure 4.6: Synchronous 2D mechanical model of the reference vehicle**

## 5. EXPERIMENTAL SETUP

This section will describe the instrumentation of the reference vehicle with the closed-circuit EHA. The application of the EHA is represented by a compact skid steer loader on which an open centre hydraulic system is mounted. In order to instrument the EHA some minor modifications on the baseline system are needed. The considered hydraulic configuration, the data acquisition system and the power electronics used in the experimental setup will be explained.

### 5.1 REFERENCE VEHICLE

The reference vehicle is a compact skid steer loader CASE TV380 from Case New Holland. The machine present in Maha laboratory is shown in Figure 5.1. The baseline hydraulic circuit is provided of different functions such as boom, bucket, hydraulic couplers and auxiliary functions. The ISO schematic of the baseline open centre circuit is shown in Figure 5.2. This study will focus on boom and bucket functions for which the closed-circuit EHA is implemented.



**Figure 5.1: Reference vehicle CASE TV380**

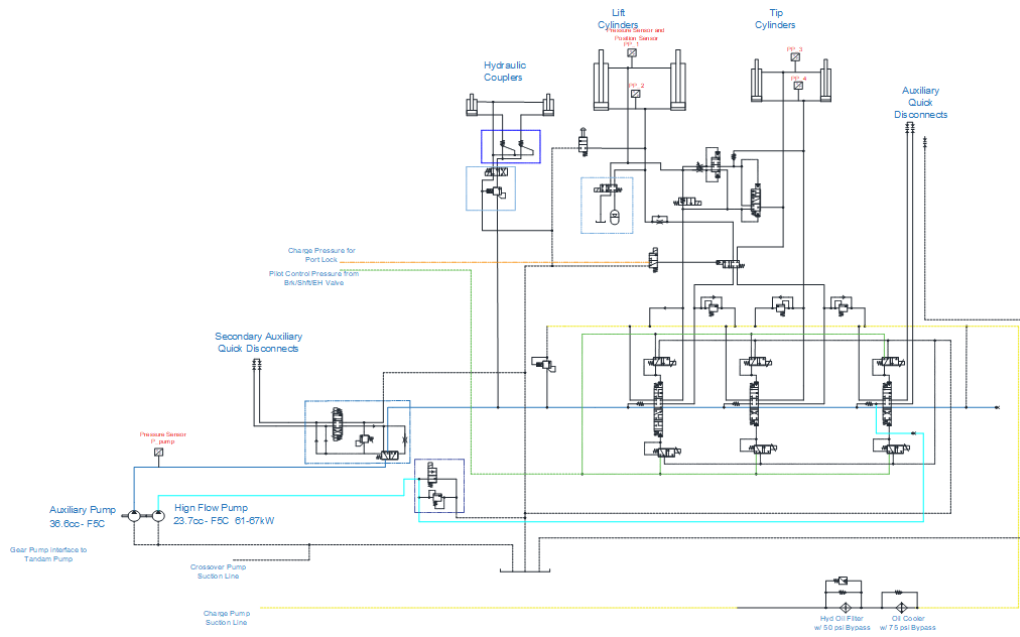


**Figure 5.2: ISO schematic of the baseline open centre hydraulic circuit**

The baseline machine is mounting an internal combustion engine, which drives two gear pumps in a tandem configuration. Since the two pumps are FP, the higher is the rotational speed of the ICE, the higher is the supplied flow to the actuator systems. In Table 5.1 are provided some information about the reference vehicle [48].

**Table 5.1: CASE TV380 specifications**

<b>ENGINE</b>		
Type	Diesel, Turbo – Direct Injection	
Cylinders	4	
Engine speed	1150 - 2500 <i>rpm</i>	
Maximum power	67 <i>kW</i>	
Peak torque	383 <i>Nm</i>	
<b>HYDRAULICS</b>		
Pump type	Gear	
Volumetric displacement	Standard aux.: 36.6 <i>cc/rev</i> High flow aux.: 20.4 <i>cc/rev</i>	
Standard flow	91.5 <i>L/min</i>	
Optional high flow	142.5 <i>L/min</i>	
Relief pressure	210 <i>bar</i>	
<b>HYDRAULIC CYLINDERS</b>		
Lift cylinders	Bore diameter	69.85 <i>mm</i>
	Rod diameter	45 <i>mm</i>
	Stroke	886.5 <i>mm</i>
	Close length	1205 <i>mm</i>
Bucket cylinders	Bore diameter	76.2 <i>mm</i>
	Rod diameter	38.1 <i>mm</i>
	Stroke	410 <i>mm</i>
	Close length	610 <i>mm</i>
<b>PERFORMANCE SPECS</b>		
Tipping load		3447 <i>kg</i>
Breakout force	Bucket cylinders	39 <i>kN</i>
	Lift cylinders	28 <i>kN</i>
Cycle times	Raise	4.7 <i>sec</i>
	Lower	2.7 <i>sec</i>
	Dump	2.6 <i>sec</i>
	Roll back	2 <i>sec</i>

The fundamental operation of open center hydraulic systems (Figure 5.3) involves creating two distinct paths for the pump flow, each characterized by different throttling areas. One path leads to the actuator, while the other returns fluid to the tank. The speed of the actuator is influenced by how the pump's output flow is distributed between these two paths, with this distribution depending on the throttling areas and the load pressure [1].

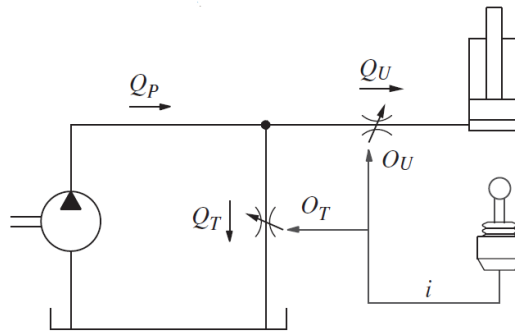


**Figure 5.3: Principle of operation of open centre system [1]**

Most open center systems work in conjunction with a fixed displacement pump and utilize two variable orifices: one for the actuator line and another for the return line. The operator's command signal adjusts the opening of these orifices, thereby controlling the actuator's speed based on the pump flow, orifice sizes, and the load on the actuator.

Open center systems are popular in hydraulic applications for two main reasons. Firstly, their valve layout is straightforward, allowing for effective flow metering using a single spool. Secondly, the combined operation of the two metering orifices offers dynamic control of the actuator.

Energy efficiency in a basic open center circuit is generally low when the actuator requires only a fraction of the available flow. In contrast, efficiency improves significantly when the required flow aligns closely with the pump's output rate. Moreover, the common efficiency of this kind of system features values under 30%.

## 5.2 HYDRAULIC CONFIGURATION

As discussed, the EHA is going to replace the baseline hydraulic system for the boom and bucket actuation systems. As a first step, only the boom actuation is implemented since it represents the most demanding function regarding the applied loads. Since the linear actuators of the boom function have a bigger area ratio and stroke with respect to the bucket actuator, all the hydraulic components are sized and selected according to this function.

The structural configuration of the cylinders in boom and bucket actuation defines the operating conditions in the four-quadrants of the corresponding EHA. In particular the boom is operating in resistive extension and assistive retraction, while the bucket is operating in assistive extension and resistive retraction. Moreover, each actuation system is composed by two cylinders which are kinematically joint by the structure.

Modifications in the baseline hydraulic circuit are needed to install the EHA. In particular, high pressure ball valves (BV1 and BV2) are installed as shown in Figure 5.4 to decouple the open center system from the EHA for the boom function.

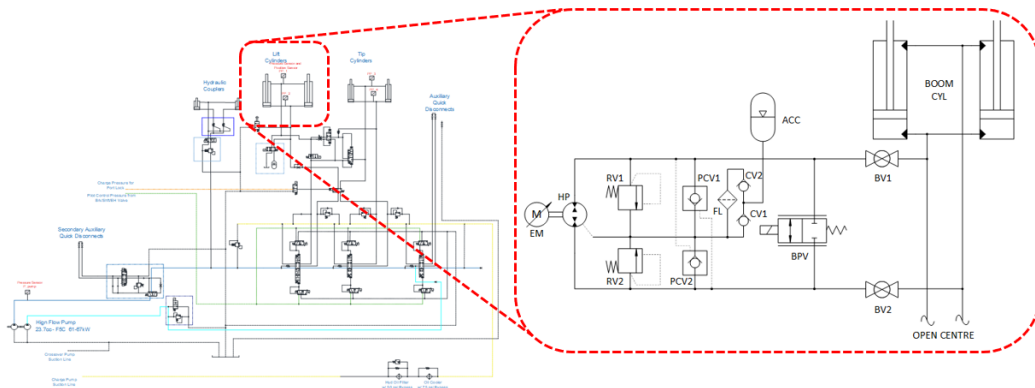
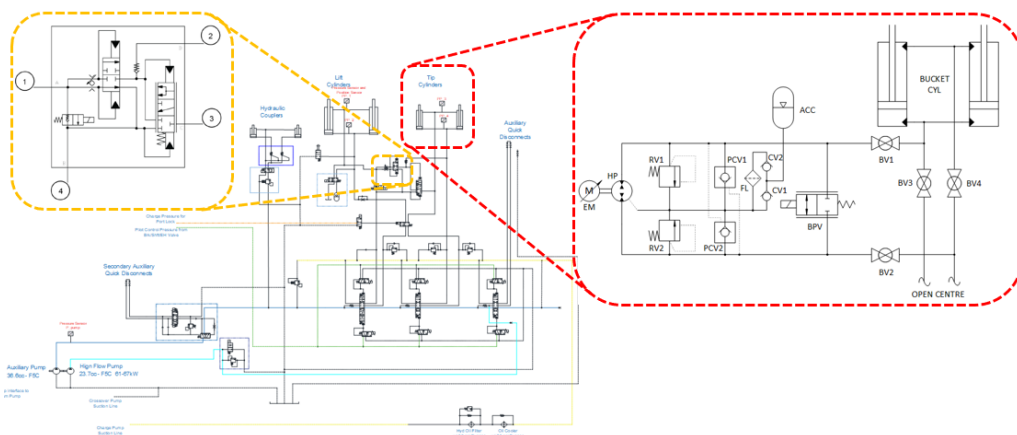


**Figure 5.4: Boom EHA implementation**

Furthermore, the baseline hydraulic circuit is provided of a self-levelling function for the bucket operation (Figure 5.5). As the loader boom cylinder extends, hydraulic fluid from the rod port is directed to port 1. The fluid entering port 1 can flow through both an adjustable orifice and a fixed orifice in the flow divider

spool. The size of the adjustable orifice determines how the flow is divided. The remaining fluid flows through the fixed orifice, exiting at port 4 to return to the control valve and then to the tank. The fluid that passes through the adjustable orifice flows out of port 2, where it is directed to the base end of the bucket cylinders. The resistance encountered during the movement of the bucket cylinders generates sufficient pressure to activate the unloading spool in the self-levelling valve. As the bucket cylinders extend, fluid from their rod port enters port 3, bypassing the open unloading spool, then flows around the flow divider spool and out of port 4 back to the control valve and the tank.

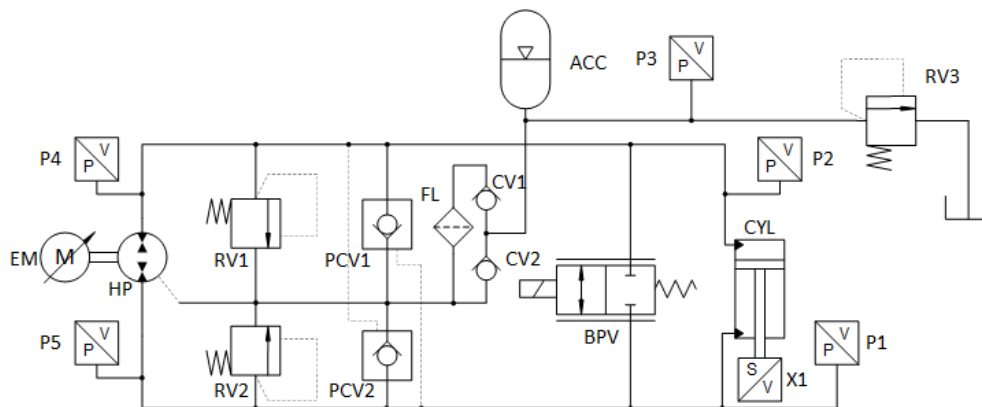
To avoid recirculation of fluid between boom and bucket functions, two additional ball valves (BV3 and BV4) are added on the bucket side. Further efforts could be directed to include the self-levelling function in a combined control logic of the EHAs in future works.



**Figure 5.5: Bucket EHA implementation**

The ISO schematic of the experimental setup is represented in Figure 5.6. Five pressure transducers are implemented. P1 and P2 are used to estimate the pressure difference between piston and rod chambers of the cylinder. This measure is crucial for the mode selection logic and the control of the bypass valve. P3 is measuring the pressure at the accumulator port. This transducer is implemented to evaluate the charging and discharging of the device. Moreover, it is important to monitor the pressure in the drain line, which must be lower than 10 *bar* to guarantee the proper functioning of the shaft sealing of the pump. The relief

pressure of RV3 is set as the maximum pressure of the accumulator such that the pressure of the drain line is kept under the limit. RV3 is relieving directly into the tank of the skid steer, but its switch is never expected in a normal operation of the hydraulic system. The pressure transducers at the inlet/outlet ports of the hydraulic unit (P4 and P5) are implemented to estimate the pressure difference across the device. Even if P1 and P2 are connected to the same hydraulic lines of P5 and P4 respectively, they are not suitable to estimate the pressure difference due to pressure drops in hoses, fittings and manifold. P4 and P5 are used to evaluate the hydromechanical efficiency (Eq. 2.38 – 2.39) of HP. A displacement transducer X1 is applied on CYL. From the time derivative of this last measure the linear velocity of the actuator can be computed. The volumetric flow rate supplied by the pump to CYL can be then derived based on the actuating mode (Eq. 2.4 – 2.5 and Eq. 2.8 – 2.9). From  $Q$  the volumetric efficiency of HP can be obtained from Eq. 2.36 and Eq. 2.37. Moreover, torque and rotational speed of the hydraulic unit are equal to the electric motor one assuming a rigid connection.



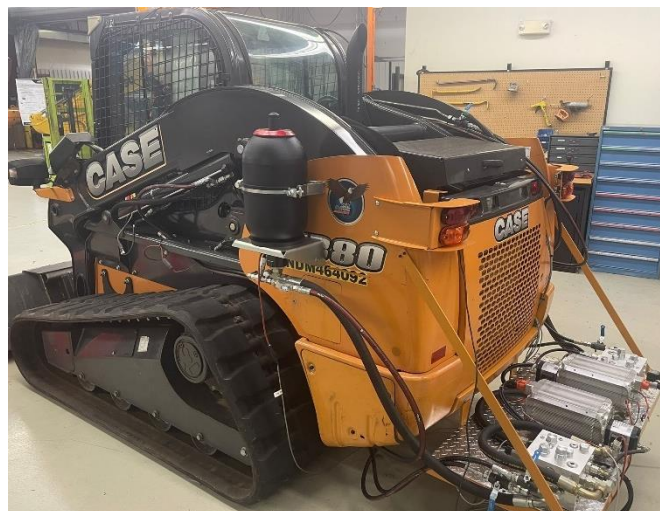
**Figure 5.6: Conceptual architecture of the experimental setup**

Table 5.2 lists all the main hardware used on the reference vehicle.

**Table 5.2: Hardware list of the EHA implementation on skid-steer**

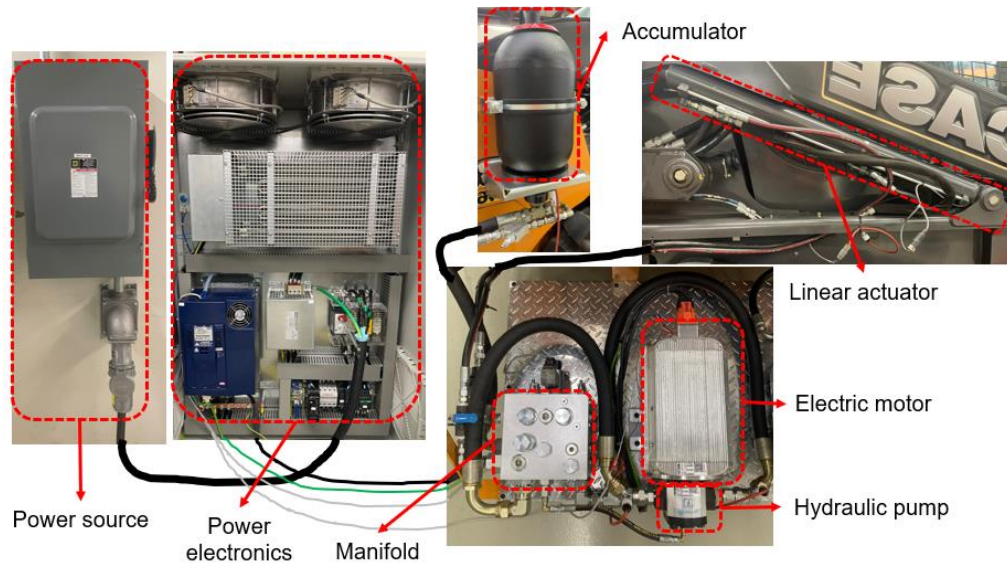
<b>Hardware</b>	<b>Manufacturer</b>	<b>Product number</b>	<b>Number of parts</b>
External gear pump	Settima	Continuum 4Q	1
Pilot operated check valve	Sun Hydraulics	CKGB-XAN	2
Check valve	Sun Hydraulics	CXFA-XAN	2
Relief valve	Sun Hydraulics	RDDA-LAN	2
Filter	Sun Hydraulics	FLHAXDN	1
Proportional 2/2 bidirectional valve	Rexroth	KKDSR1NB/HCG12N0K4V	1
Accumulator	Hydac	SB330-10A1/112S1-262C	1
Cylinder	CNH	CNH TV380 boom cylinder	2
Electric motor	Spin	3-phase synchronous reluctance	1

Figure 5.7 shows a picture of the CASE TV380 implementing the closed-circuit architecture. The considered EHAs system (boom and bucket) are mounted on a platform in the back of the reference vehicle, with this configuration no modifications are applied on the baseline hydraulic circuit. The accumulators are mounted on the side panels of the skid steer.



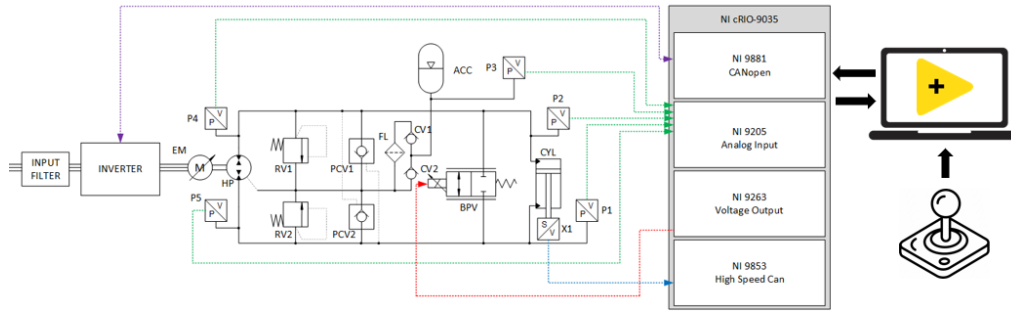
**Figure 5.7: CASE TV380 implementing closed-circuit EHA**

Figure 5.8 shows in detail how the experimental setup is implemented on the reference vehicle. The power source is connected to the inverter box as it will be explained in the next section. Moreover, the electric motor is driven by the inverter, and it is connected through the shaft to the hydraulic pump. The manifold is implementing all the valves and filter of the hydraulic circuit, and it is providing an easy connection between HP, accumulator and linear actuators through hoses.



**Figure 5.8: Experimental setup implemented on the skid steer loader**

The data acquisition (DAQ) is implemented by setting up a National Instrument CompactRIOs and a controller laptop (Figure 5.9). To apply the input command  $i$  a joystick is used, and it is connected through USB to the laptop. All the pressure transducers are connected to the Analog Input module of the cRIO controller, while the displacement transducer is communicating with the High-Speed CAN module. The opening of the bypass valve is commanded through the Voltage Output module. The controller is commanding an angular speed to the inverter through the CANopen module, and at the same time it is acquiring the actual torque, rotational speed, electrical power at the interface with the electric motor and other diagnostic signals from the inverter.



**Figure 5.9: Conceptual schematic of the data acquisition system**

Table 5.3 lists the electric hardware used in the data acquisition system. LabVIEW is used for data acquisition and to instrument control, while MATLAB is used to conduct post-processing of the acquired data.

**Table 5.3: Electrical hardware list of the data acquisition system**

	Hardware	Manufacturer	Code	Number of parts
ECU	Controller	National Instruments	NI cRIO-9035	1
	Analog Voltage Output module		NI 9263	1
	Analog Voltage Input module		NI 9205	1
	High-Speed CAN module		NI 9853	1
	CANopen module		NI 9881	1
Sensors	500 bar pressure transducer	Parker	2020009	4
	35 bar pressure transducer		2020008	1
	Linear transducer	Rota	ELC 3209	1
Coil	Prop. 2/2 directional valve (24V)	Rexroth	R901022180	1
Others	Joystick	Logitech	963290-0403	1
	5V converter	EKYLIN	K240505	1
	DC power step-up regulator	NE	SR-700-24	1

## 5.3 POWER ELECTRONICS

A power electronics setup is developed to drive the electric machine as shown in Figure 5.10. The input for the power electronics setup is a 3-phase high-voltage (440VAC) that is used to drive the electric machine. The input filter is used to remove interferences produced by the inverter. The fused disconnect switch monitors electrical flow within the device, automatically disconnecting power when it detects dangerous fluctuations or interruptions. The 3-phase fuse serves as a safety device, providing overcurrent protection for the electrical circuit, and an additional fuse is connected to the 24V power supply. The 24V power supply is connected to inverter and fans through the contactors. The emergency relay is used to detect failures allowing power to be removed from the contactors. The braking resistor is dissipating the electric energy generated by the electric motor during assistive modes since a battery is not included in this stationary experimental setup. The thermostat is sensing the temperature within the box, and it is used to regulate the turning on/off of the fans through the contactors. The inverter is supplied by the 3-phase high voltage to drive the electric motor, and by the 24VDC for the control section. The inverter with its control section regulates the input voltage, so that the synchronous reluctance motor can be properly controlled. The power from the inverter to EM is again filtered by the inverter.

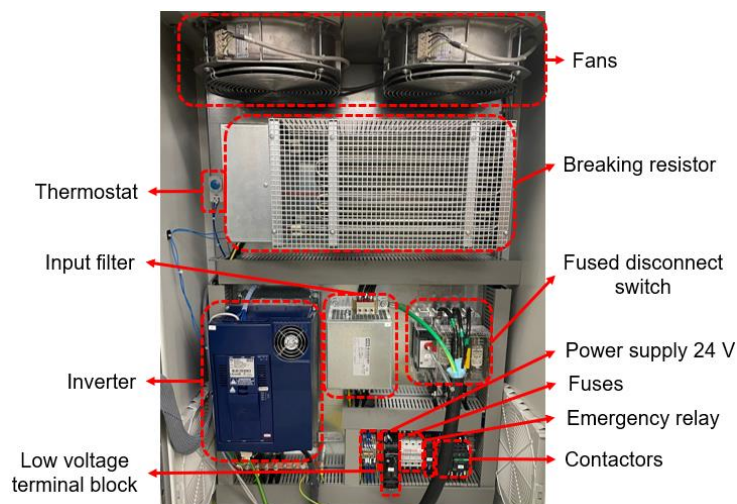


Figure 5.10: Power electronics setup

Table 5.4 lists the components for the power electronics setup.

**Table 5.4: Electrical components of the power electronics setup**

<b>Hardware</b>	<b>Manufacturer</b>	<b>Code</b>	<b>Number of parts</b>
Fan	Ebm-papst	W2D250-HJ02-12	2
Braking resistor	KEB	21BR226-6103	1
Inverter		21F6A14-3411	1
Input filter		20E6T60-3000	1
Fused disconnect switch	Wimex	C2F3160	1
24V power supply	Omron	S8VK-T12024	1
3-phase fused	Mersen	CMC103SP	1
Fuse		CMC101	1
3-phase emergency relay	Schneider electronic	RM17TG20	1
Contacteur		LC1D18BD	2
Thermostat	STEGO	111019-00	1

# 6. RESULTS

This chapter will discuss the results obtained from the studied EHAs (open-circuit and closed-circuit). In particular the two configurations will be compared in terms of efficiency through the four-quadrant map in simulation. Furthermore, the results obtained in terms of power flow and efficiency for the implemented closed-circuit will be evaluated to validate the simulation model and demonstrate the high efficiency of the electro-hydraulic circuit.

## 6.1 SIMULATION RESULTS

In this section are shown simulation results for both open- and closed-circuit. The power flow within the proposed EHA system is analysed to assess the efficiency and losses at each component, with particular focus on typical operating conditions. Moreover, efficiency maps are derived from the power computation for different operating points.

Since the electro-hydraulic system can be utilized for a vast range of applications for off-road vehicles, the cylinder configuration of the CASE TV380 and its 2D mechanical model are not considered in this first phase. In particular the power flow analysed is not considering the mechanical power to/from the cylinder (according to resistive/assistive mode), which is affected by the leakages occurring between piston and rod chambers, and the friction losses typical of each actuator.

### 6.1.1 OPEN-CIRCUIT RESULTS

The simulation results shown for the open-circuit EHA are referred to the simulation model shown in Figure 6.1.

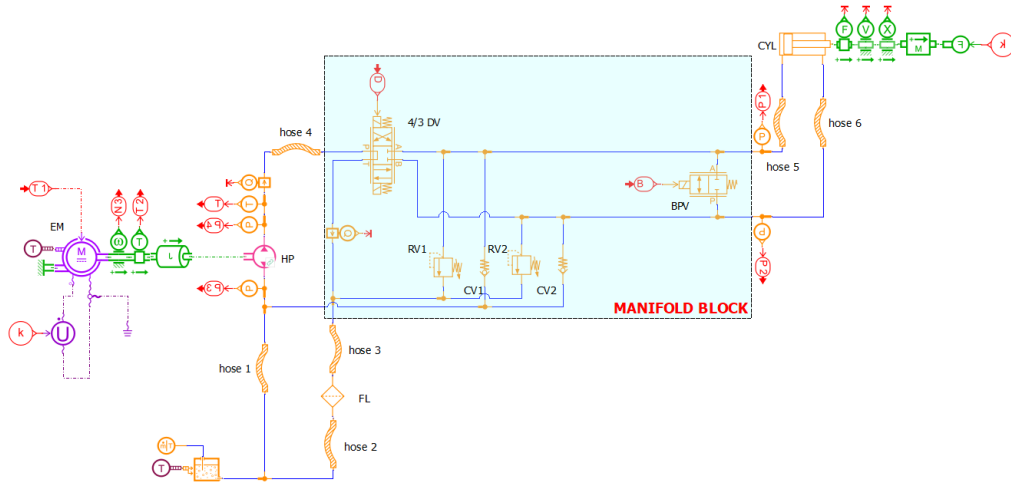


**Figure 6.1: Simulation model open-circuit**

The power computation at each interface of the EHA system can be defined according to resistive and assistive modes:

1. Wall electric power:

- Resistive mode:

$$P_{el} = V I \eta_{inv} \quad (6.15)$$

- Assistive mode

$$P_{el} = \frac{V I}{\eta_{inv}} \quad (6.16)$$

2. Inverter electric power

$$P_{inv} = V I \quad (6.17)$$

3. Electric motor mechanical power:

$$P_{EM} = T \omega \quad (6.18)$$

4. Pump hydraulic power:

- Resistive mode:

$$P_{HP,P} = Q_P (p_2 - p_1) \quad (6.19)$$

- Assistive mode:

$$P_{HP,M} = Q_M (p_1 - p_2) \quad (6.20)$$

5. Hydraulic system power, which is equal to the cylinder hydraulic power generally defined as follows:

$$P_{cyl,hyd} = Q_{in} p_{in} - Q_{out} p_{out} = F \dot{x} \quad (6.21)$$

In an ideal cylinder the hydraulic power can be considered equal to the mechanical output power from the device.

This last power is dictated by the cylinder motion as follows:

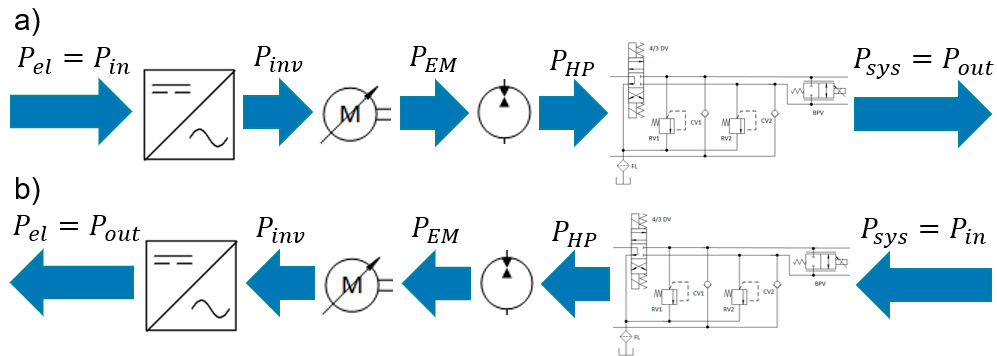
- Extension:

$$P_{sys} = Q_A p_A - Q_a p_a \quad (6.22)$$

- Retraction:

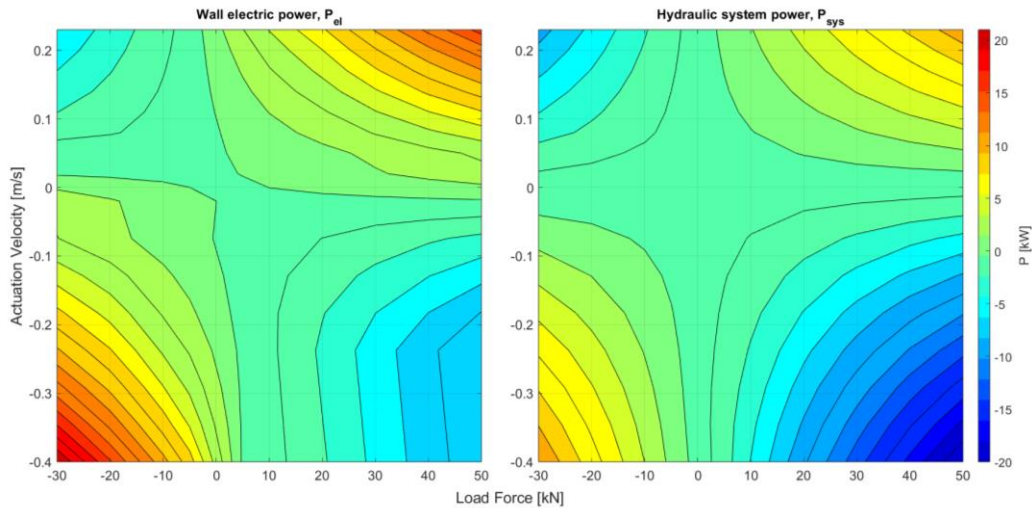
$$P_{sys} = Q_a p_a - Q_A p_A \quad (6.23)$$

Figure 6.2 shows the power flow in resistive and assistive modes for the open-circuit architecture.



**Figure 6.2: Open-circuit power flow: resistive modes (a), assistive modes (b)**

The power maps at each interface of the open circuit are obtained considering steady-state signals. The commanded actuation velocity and the applied force are varied to extract the power at several data points. Figure 6.3 shows the four-quadrant maps for the electric wall power and the hydraulic system power in the open-circuit EHA.



**Figure 6.3: Power maps of open-circuit from simulation**

It can be observed that the power spans from 21  $kW$  (resistive retraction wall electric power) to 20  $kW$  (assistive retraction hydraulic system power). A positive power means that power follows the arrow direction in Figure 6.2 (a). During resistive modes the input power is represented by the wall electric power supplied to the inverter, while the output power is represented by the hydraulic power from the hydraulic system supplied to the cylinder. During assistive modes the input power is represented by the hydraulic power supplied by the cylinder to the hydraulic system, while the output power is represented by the electric power in output from the inverter.

To further explain the performance of the open-circuit system, Figure 6.4 shows the power flow of the EHA in resistive extension and assistive retraction considering in both cases 50  $kN$  as force load and 50% actuation velocity command.



**Figure 6.4: Power flow of open-circuit EHA: 50% actuation velocity command, 50 kN load force**

In both the operating conditions the main source of losses is represented by the two-quadrants hydraulic unit. During resistive extension HP features 75.8% overall efficiency operating at 1458 *rpm* and 132 *bar* of pressure difference. The same efficiency is maintained during assistive retraction when HP operates at 2583 *rpm* and 126 *bar*. HP shows a quite high efficiency working as a motor and can regenerate energy with a power of 7.82 *kW*. Additional losses are given by EM which maintains a very high efficiency in both conditions, 92.6% in resistive extension and 94.1% in assistive retraction. As said previously, the inverter efficiency is set constant at 97%. A negligible contribution is given by the hydraulic system composed by valves, filter and hoses. In particular, a higher power loss is observed during assistive retraction (0.26 *kW*) when the commanded actuation velocity is higher due to the area ratio of the cylinder, and as a consequence the volumetric flow rates are higher too.

Finally, the efficiency of the overall system and of each device can be obtained as the ratio of the input power and the output power considering the correct power flow direction for assistive and resistive modes. The efficiency maps for all the four quadrants of electric motor, hydraulic pump and hydraulic system are shown in Figure 6.5. In this figure the colour pattern used is the same for all the three images to better visualize the contribution of each element in the total efficiency of the system. The black reference lines divide the map into the four quadrants. The white dashed lines divide the four-quadrant modes into the slow, main and fast sub-modes.

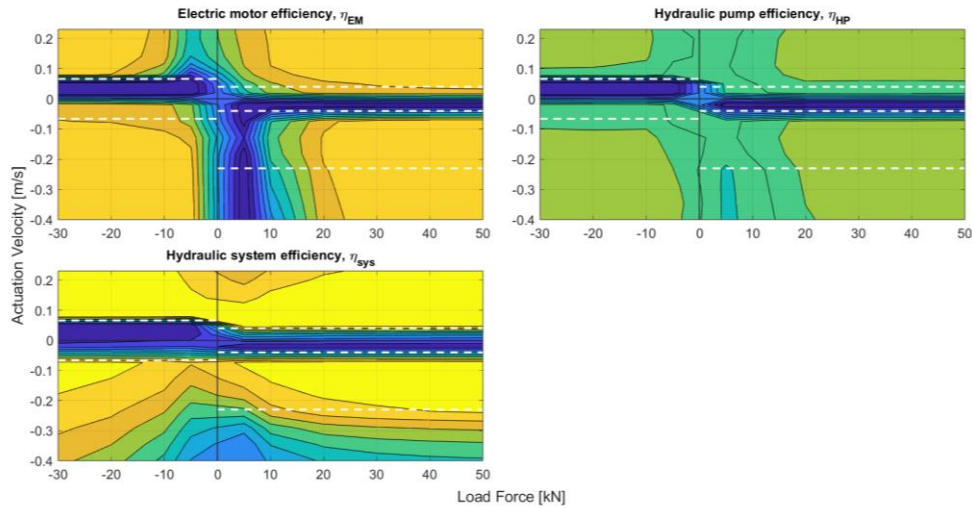


**Figure 6.5: Efficiency maps of the open-circuit EHA electric motor, hydraulic pump and hydraulic system from simulation**

Figure 6.6 shows how the efficiency is mainly driven by the hydraulic pump, which exhibits generally around 70% in both pumping and motoring modes.

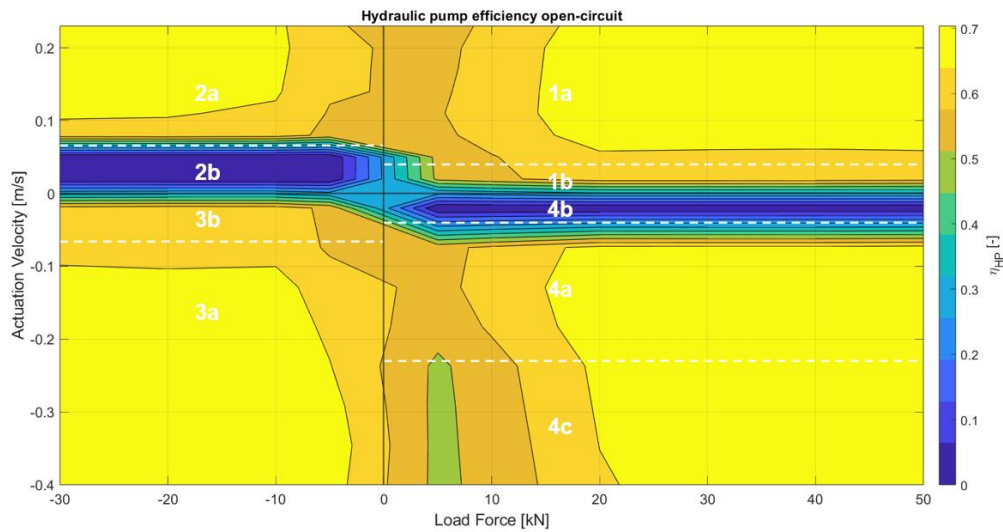


**Figure 6.6: HP efficiency map of the open-circuit EHA from simulation**

As shown in Figure 6.7 the electric motor is subjected to higher efficiencies (90%) for most of the operating conditions. In general, the efficiency of the EHU is very low in case of low rotational speed required at the shaft. Moreover, the efficiency of EM is not defined for most of the range 0 to 10 kN of the assistive retraction mode. In case of low applied loads and high retraction velocities the

input power from the overrunning load is not sufficient to reach the commanded actuation velocity of CYL. Hence, in this scenario electric power is required from the inverter to maintain the electric motor rotational speed as shown in Figure 6.8, and no power is regenerated.

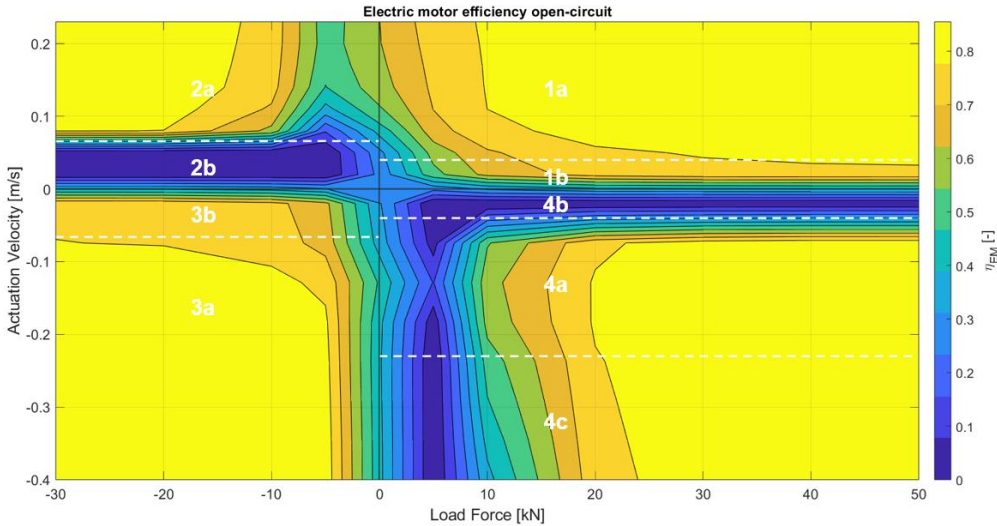


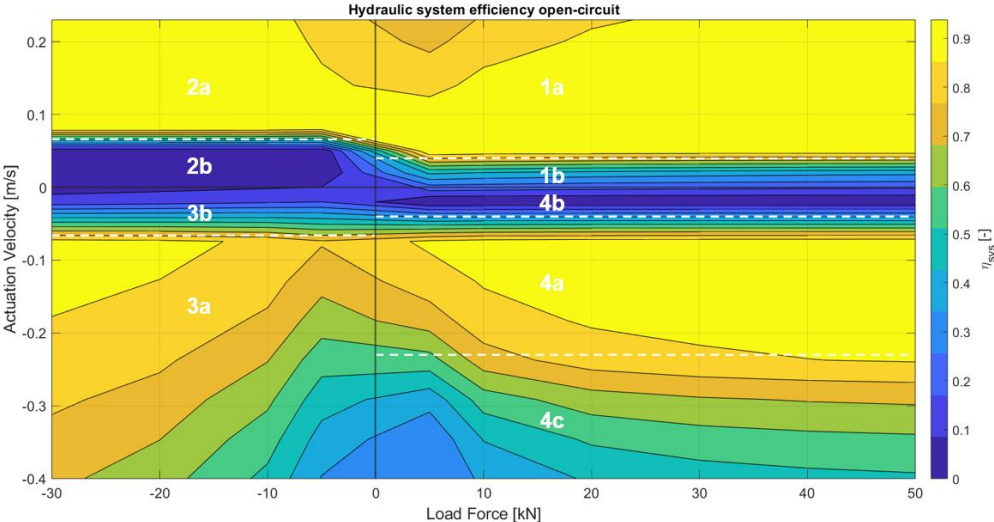
Figure 6.7: EM efficiency map of the open-circuit EHA from simulation



Figure 6.8: Power flow of open-circuit EHA: 75% actuation velocity command, 5 kN load force

Regarding the hydraulic system efficiency, shown in Figure 6.9, it experiences a higher efficiency (more than 90%) in the extension modes and variable efficiencies during the retraction modes (between 90% and 40%). During retraction the higher throttling losses in valves and hoses are expected due to the higher flow rates. Moreover, when low forces are applied the throttling losses experienced in the 4/3 directional control valve represent a non-negligible

contribution with respect to the overall power level, especially when the maximum flow rate of  $54 \text{ L/min}$  is supplied by HP.



**Figure 6.9: Hydraulic system efficiency map of the open-circuit EHA from simulation**

The efficiency map of the overall system for the open-circuit is shown in Figure 6.10.

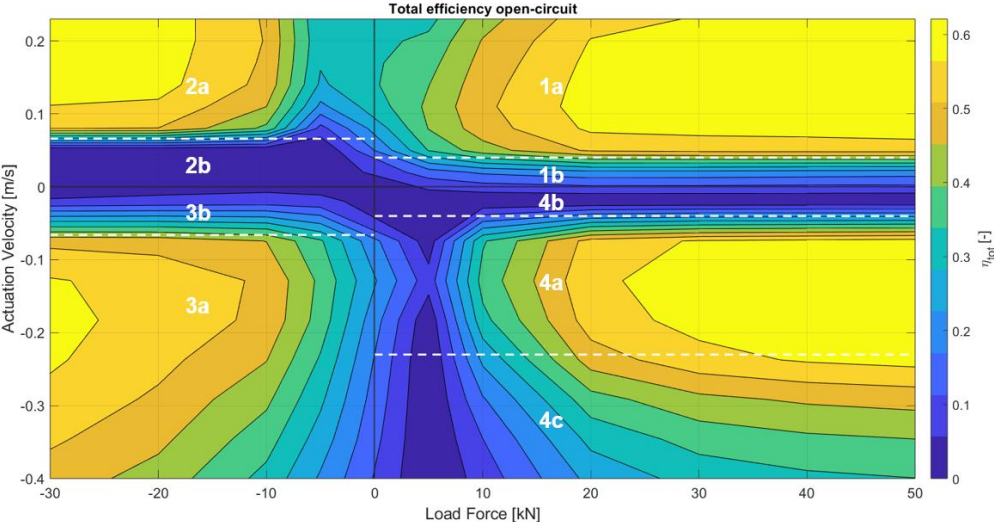


**Figure 6.10: Efficiency map of the open-circuit EHA from simulation**

As shown in Figure 6.10, the efficiency of the overall system for the open-circuit EHA can reach up to 68.28% in resistive extension. Moreover, the efficiency of the architecture ranges between 50% and almost 68% in most of the map regions.

The maximum efficiency is always expected when high loads are applied to the cylinder.

Regarding the low efficiency regions, these are expected when the bypass valve is opening. Hence, the slow-speed sub-modes and the fast assistive retraction sub-mode are affected by this last behaviour. As discussed in Section 2.4.2 the opening of BPV introduces throttling losses that are proportional to the volumetric flow rate passing through the valve. In areas 1b, 2b, 3b, and 4b power is dissipated through the valve to slower the motion of CYL, while in 4c the high flow rates due to the required fast retraction are resulting in higher losses as shown in Eq. 2.76.

In sub-modes 1b and 3b the pump is set to its minimum rotational speed (500 rpm), and part of pump power is converted into heat in BPV. In sub-modes 2b and 4b the rotational speed of EM and HP is set to zero, and no energy can be regenerated in this condition because all the power in input from the cylinder side is dissipated into BPV. However, these low-speed actuation conditions happen for a limited range of velocity between  $-0.06\text{ m/s}$  and  $0.06\text{ m/s}$ . The required power consumption in this range is low as shown in Figure 6.3.

### 6.1.2 CLOSED-CIRCUIT RESULTS

The simulation results shown for the closed-circuit EHA are referred to the simulation model shown in Figure 6.11.

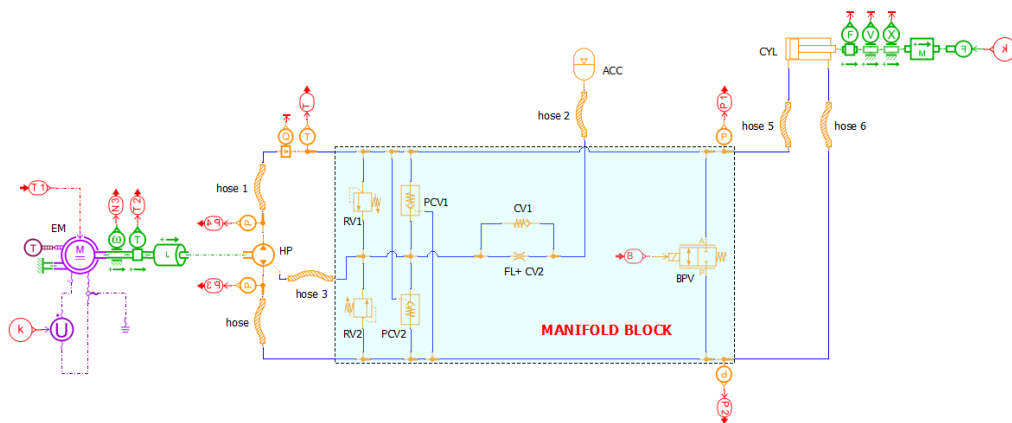
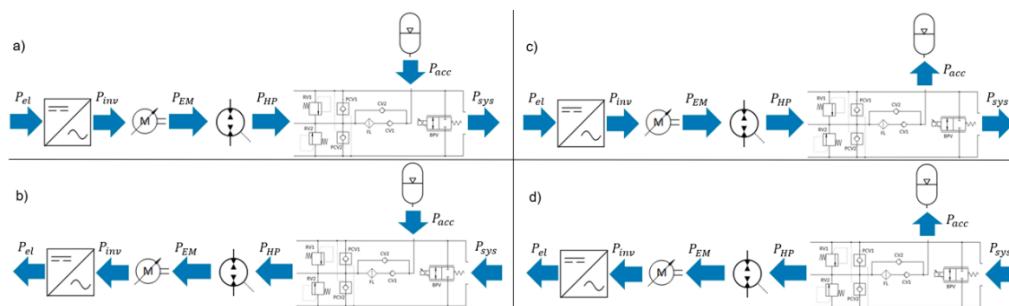


Figure 6.11: Simulation model closed-circuit

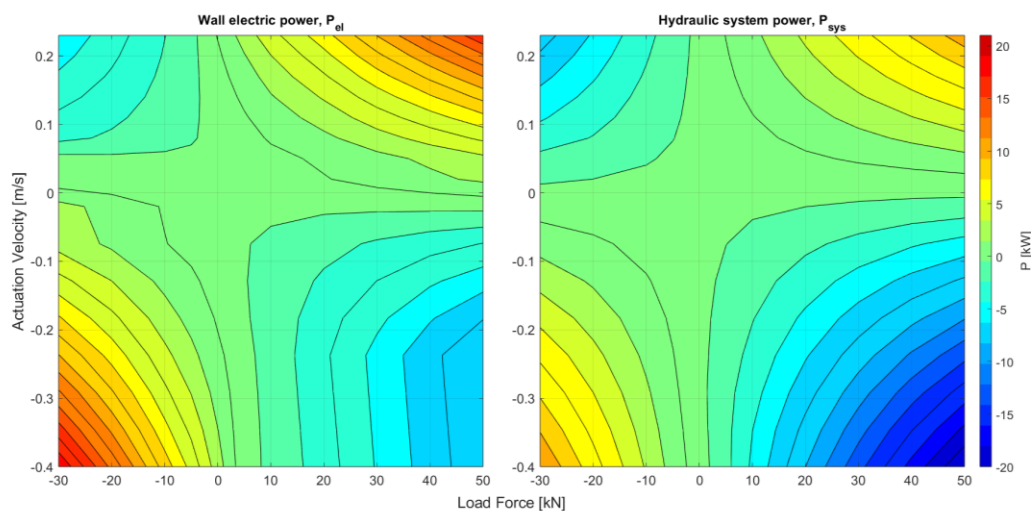
The power computation at each interface of the EHA system follows Eq. 4.1 – 4.6. Additionally, the power stored and delivered by the accumulator can be computed according Eq. 2.22. As shown in Eq. 2.40 – 2.43, the accumulator power can represent an input or an output to the EHA system according to the extension or retraction actuation of CYL.

Figure 6.12 shows the power flow in resistive extension, assistive extension, resistive retraction and assistive retraction modes for the closed-circuit architecture.



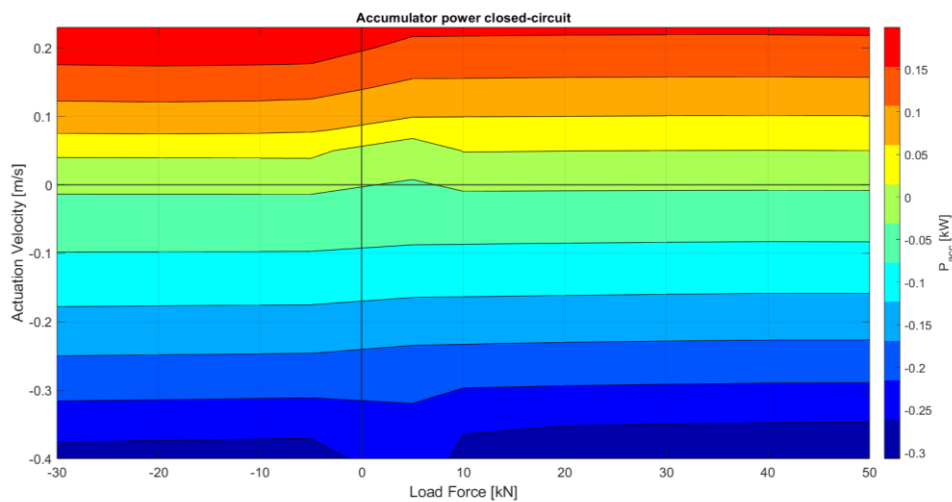
**Figure 6.12: Closed-circuit power flow: resistive extension (a), assistive extension (b), resistive retraction (c), assistive retraction (d)**

Figure 6.13 shows the four-quadrant maps for the electric wall power and the hydraulic system power in the closed-circuit EHA.



**Figure 6.13: Power maps of closed-circuit from simulation**

It can be stated that the power levels are the same observed in the open-circuit architecture. A positive power means that power follows the arrow direction in Figure 6.13 (a). The accumulator power is considered positive during extension motions and, according to the flow rate direction, is also positive during the device's exhaust. The power exchanged by the accumulator in the four-quadrants is shown in Figure 6.14. The power magnitude of the accumulator is ranging between  $-0.3 \text{ kW}$  in assistive and resistive retraction and  $0.2 \text{ kW}$  in assistive and resistive extension. Therefore, it can be noted that the power level exchanged by this device is very low with respect to the power managed by the whole system.



**Figure 6.14: Accumulator power of closed-circuit from simulation**

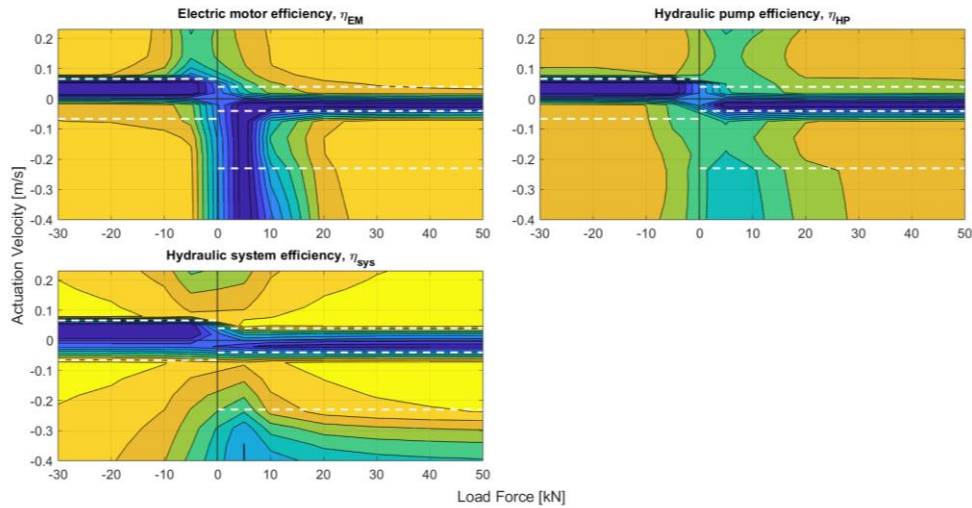
To further explain the performance of the closed-circuit system, Figure 6.15 shows the power flow of the EHA in resistive extension and assistive retraction considering in both cases  $50 \text{ kN}$  as force load and 50% actuation velocity command.



**Figure 6.15: Power flow of closed-circuit EHA: 50% actuation velocity command, 50 kN load force**

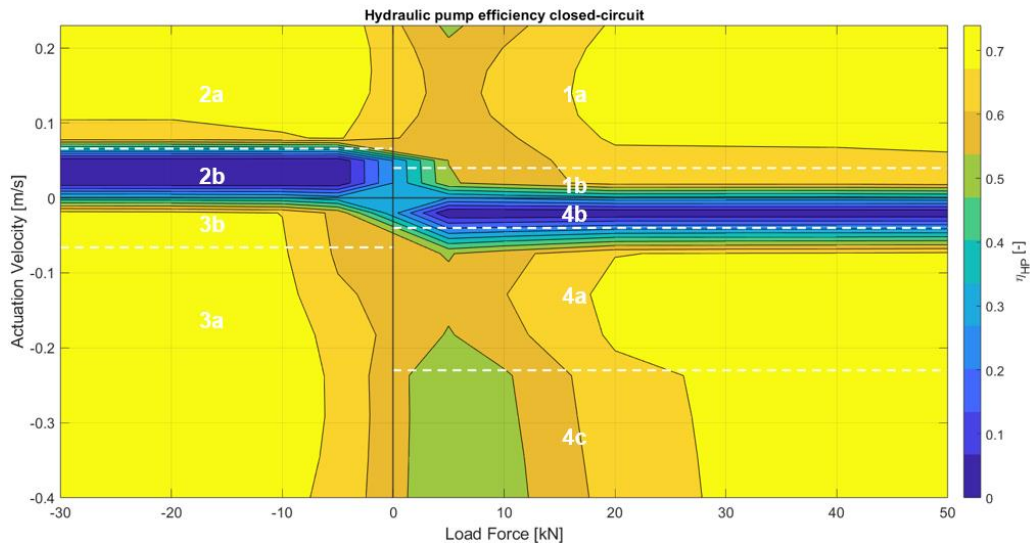
As in the open-circuit, the main source of losses is represented by the hydraulic unit, which in this case is constituted by a four-quadrant pump. The HP demonstrates a solid 78.6% overall efficiency during resistive extension, operating at 1477 rpm and a pressure difference of 131 bar. This efficiency holds steady during assistive retraction, when the HP runs at  $-2569 \text{ rpm}$  and a pressure difference of 123 bar is observed. Notably, the four-quadrant HP shows about 3% greater efficiency compared to the two-quadrant unit used in the open circuit. When working in motor mode, HP is able to regenerate energy with a power of 6.94 kW. Since the EM unit and inverter remain unchanged across both architectures, their efficiencies remain consistent with those observed in the open-circuit configuration, maintaining the same operating conditions. The hydraulic system contribution to power loss is minimal, with the highest observed loss (0.42 kW) occurring during assistive retraction.

The efficiency maps for all the four-quadrants of electric motor, hydraulic pump and hydraulic system are shown in Figure 6.16 using a common colour pattern.



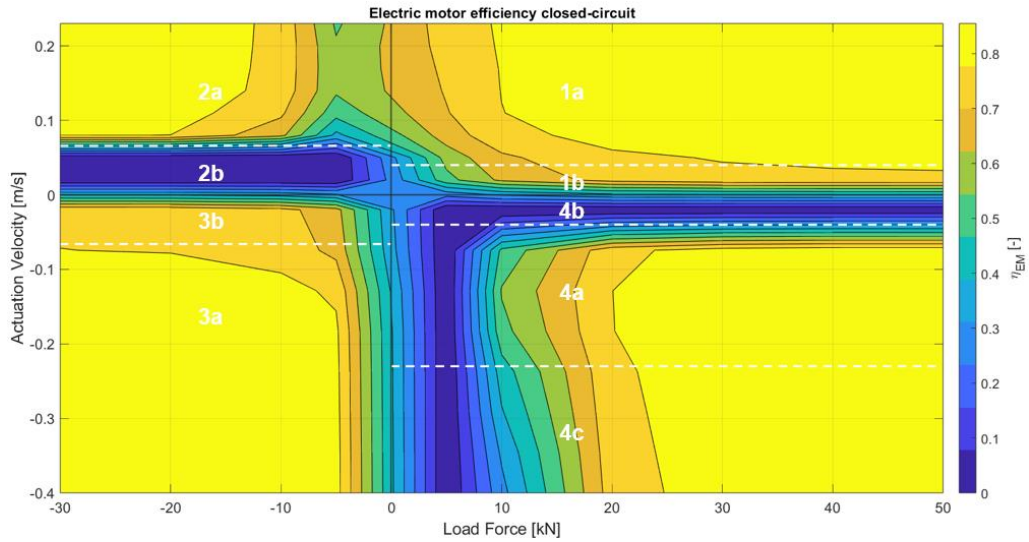
**Figure 6.16: Efficiency maps of the closed-circuit EHA electric motor, hydraulic pump and hydraulic system from simulation**

Figure 6.17 shows that even in the closed-circuit the efficiency is mainly driven by the hydraulic pump, which exhibits around 75% in both pumping and motoring modes. Lower efficiencies (50%) are observed in low power level areas, which means low pressure difference across the device.



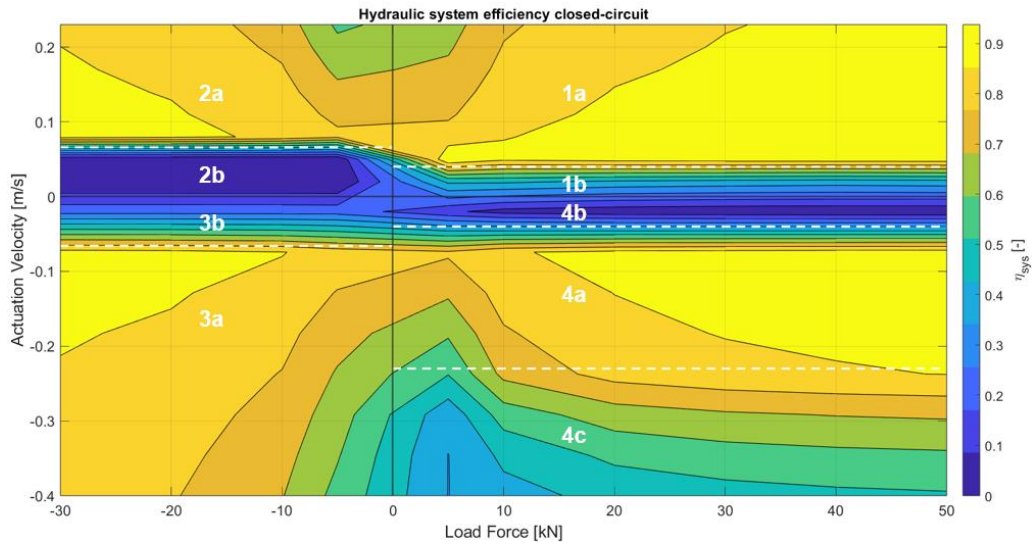
**Figure 6.17: HP efficiency map of the closed-circuit EHA from simulation**

Figure 6.18 presents the efficiency map of the electric motor EM in the closed-circuit architecture. The same considerations apply as in the open-circuit EHA, ensuring consistency in performance analysis across both configurations.



**Figure 6.18: EM efficiency map of the closed-circuit EHA from simulation**

As shown in Figure 6.19, the hydraulic system efficiency is notably higher in the extension modes, consistently exceeding 85%. However, during the retraction modes, efficiency varies, ranging from 90% down to 40%, reflecting the dynamic changes in performance depending on the operating conditions. The simulation model developed for this new architecture offers enhanced accuracy in modelling the valves and filters, which in turn leads to higher losses compared to the open-circuit system. Additionally, at low force levels, the throttling losses in the valves become a significant contributor to the overall power loss. Further details on the power losses across the entire system will be provided in the following pages.



**Figure 6.19: Hydraulic system efficiency map of the closed-circuit EHA from simulation**

The efficiency map of the overall system for the closed-circuit is shown in Figure 6.20.

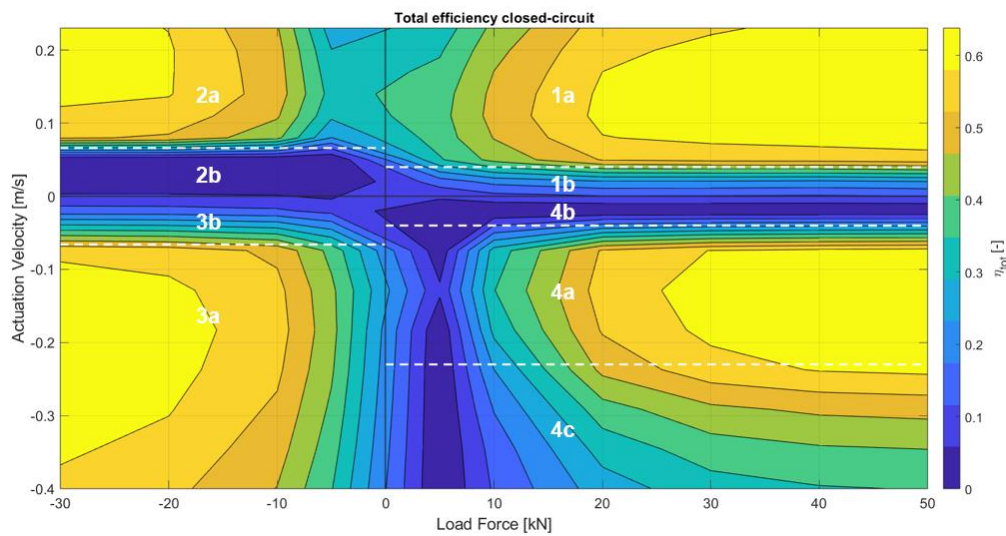


**Figure 6.20: Efficiency map of the closed-circuit EHA from simulation**

As depicted in Figure 6.20, the overall efficiency of the closed-circuit EHA system can peak at 70.15% during assistive retraction. Additionally, the system's efficiency remains between 50% and nearly 70% across most regions of the efficiency map, indicating consistent performance throughout a wide range of operating conditions. In comparison, the average efficiency of mobile hydraulic

applications is approximately 21%, highlighting the significant improvement achieved by implementing the EHA solution.

Efficiency maps are valuable tools for implementing the considered EHA architecture across different applications. For instance, the duty cycles of a compact loader boom may occur in the first and fourth quadrants of the efficiency map, while for the bucket, the cylinder orientations are reversed, placing the duty cycles in the second and third quadrants. Furthermore, efficiency maps can indicate whether the EHA solution operates with high efficiency for specific applications and whether hydraulic components need to be resized to improve energy performance for particular duty cycles.

The power losses in the system are influenced by the operating conditions. A more detailed analysis of these losses can be conducted by examining a general duty cycle, as shown in Figure 6.21. This duty cycle was utilized in previous studies to validate the thermal model developed by Qu [25]. It features nearly constant speeds in both extension ( $1.3 \text{ m/s}$ ) and retraction ( $-0.1 \text{ m/s}$ ), while the applied forces average  $20 \text{ kN}$  in extension and  $5 \text{ kN}$  in retraction. This simulates a loaded boom during the extension phase and an unloaded boom during retraction.

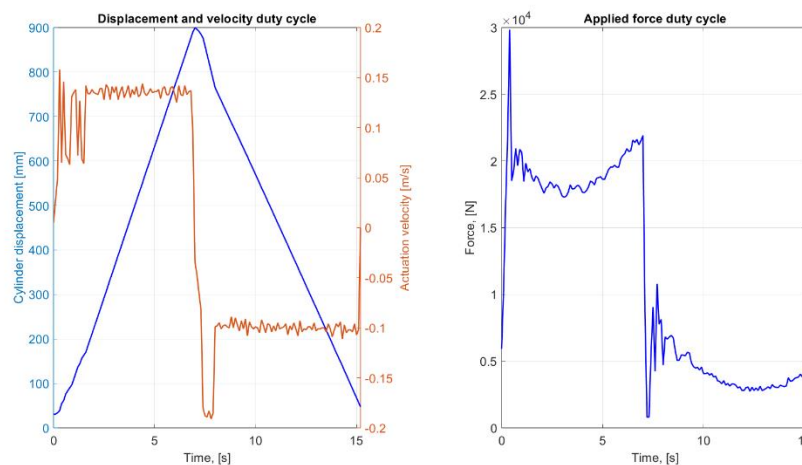


**Figure 6.21: Boom cylinder duty cycle**

By considering the duty cycle outlined above, a scatter plot can be superimposed on the total efficiency map, as shown in Figure 6.22. This allows for a clearer visualization of the system performance across general operating conditions.

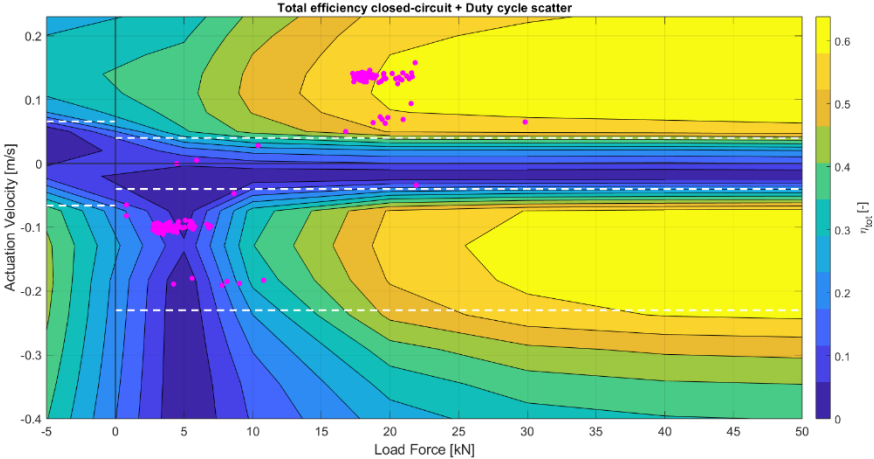


**Figure 6.22: Duty cycle scatter over total efficiency map for the closed-circuit EHA**

The operating point at 20 kN applied force and 0.13 m/s actuation velocity can be considered to study the power loss in the system. The pie chart in Figure 6.23 shows the contribution to the power losses of each element in the EHA system.

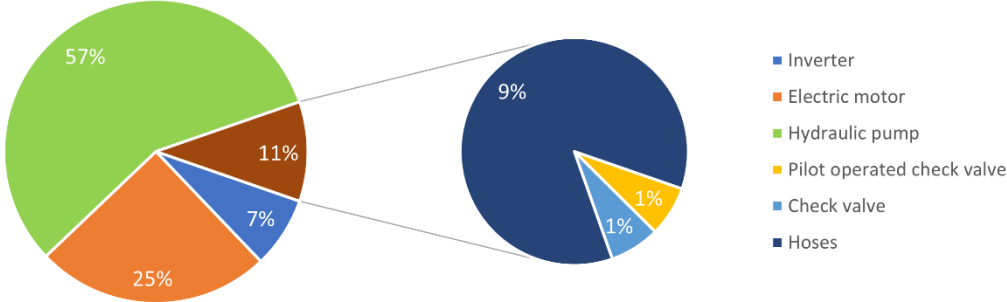


**Figure 6.23: Closed-circuit losses contribution: 20 kN applied force, 0.13 m/s actuation velocity**

The total power loss in the EHA system is 1.32 kW under the given operating conditions, featuring 65% total efficiency. As expected, the primary source of these losses is the hydraulic pump. Additionally, the losses in the hydraulic circuit are mainly attributed to the SAE 8 (12.7 mm) hoses used to connect the cylinder to the manifold section. This choice of hoses was made to ensure the flexibility

required for integrating the EHA system into the reference vehicle. Notably, the valves and the filter in the circuit contribute negligibly to the overall losses. Therefore, it can be concluded that the component selection for the system has been successful.

To justify the decision to implement a closed-circuit EHA rather than an open-circuit EHA, Figure 6.24 is presented to illustrate the efficiency difference between the two systems, where  $\Delta\eta_{tot}$  is defined as follows:

$$\Delta\eta_{tot} = \eta_{tot,closed} - \Delta\eta_{tot,open} \quad (6.24)$$

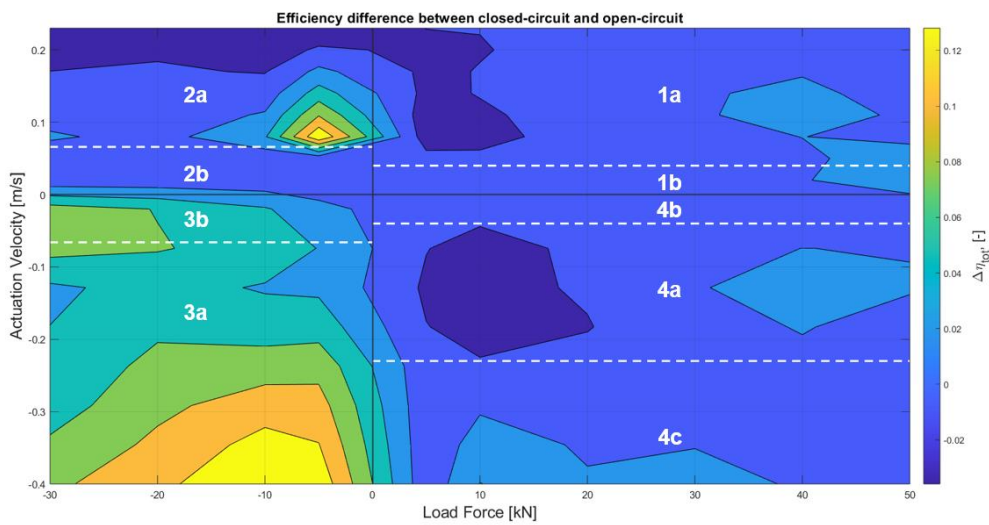


**Figure 6.24: Efficiency difference map from simulation**

When comparing the results of the open-circuit EHA and the closed-circuit EHA, it can be concluded that both architectures exhibit nearly the same efficiency across most regions of the map, including resistive extension, assistive extension, and assistive retraction. However, in resistive retraction, the closed-circuit EHA demonstrates a significant increase in efficiency (up to 15%) at high retraction velocities. This improvement is primarily driven by the hydraulic system efficiency, as the open-circuit EHA is affected by power losses introduced by the 4/3 directional control valve.

Although the closed-circuit EHA was expected to perform worse than the open-circuit version due to the differences in pump design, both units operate efficiently in their respective architectures.

## 6.2 EXPERIMENTAL RESULTS

The experimental results presented in this study were obtained using the setup described in Section 5. In comparison with the simulation results discussed in Section 6.1.2, the tests were conducted with a two-cylinder implementation. Due to the skid-steer actuation system, the actuator velocity is halved, while the maximum permissible load is doubled.

The cylinder configuration for the boom function allows testing in both resistive extension and assistive retraction modes, while the cylinder orientation for the bucket function enables testing in assistive extension and resistive retraction modes. The current tests focus on evaluating the power consumption and efficiency of the electric motor, hydraulic pump, and hydraulic system in the resistive extension mode.

The test procedure involves the following steps:

1. Raise the boom to 10% of its total stroke.
2. Start the test: command the desired speed and begin data acquisition.
3. End the test at 90% of the boom stroke.
4. Average the values from the middle third of the data.

To generate results such as efficiency maps, it is crucial to extract a summary point from each test. This data point is calculated by averaging the values over approximately one-third of the test duration. The data selected for averaging is based on the boom position, with the time interval for averaging that is varying according to the actuator speed. The time bounds are defined by the moments when the boom position is as close as possible to  $0.3\text{ m}$  and  $0.55\text{ m}$ . Consequently, the duration of the data set used for averaging ranges from about 2 to 20 seconds.

All the signals measured during the tests are summarized in Table 6.1. The sources for the pressure and position signals are referenced in Figure 5.9. Rotational speed, torque, and electric power associated with EM are derived from the inverter readings, with the corresponding signal codes provided in the table.

**Table 6.1: Measured signals from tests**

Signal name	Symbol	Source		Units	Frequency [Hz]
Position	$x$	Position transducer	X1	[mm]	10
Bore pressure	$p_A$	Pressure transducer	P2	[bar]	100
Rod pressure	$p_a$		P1		
Pump bore pressure	$p_{P,bore}$		P4		
Pump rod pressure	$p_{P,rod}$		P5		
Accumulator pressure	$p_{acc}$		P3		
Shaft rotational speed	$n$	Inverter	ru08	[rpm]	
Shaft torque	$T$		ru81	[Nm]	
Electric power	$P_{el}$		ru82	[kW]	

All the signals derived from the measurements are summarized in Table 6.2. Due to the two different sampling rates, some derived measurements require down sampling from 100 Hz to 10 Hz.

**Table 6.2: Derived signals from measurements**

Signal name		Equation	Units	Frequency [Hz]
Actuator velocity		$\dot{x} = \frac{x_i - x_{i-1}}{t_i - t_{i-1}}$	[m/s]	10
Actuator force		$F = A_p p_A - A_r p_a$	[N]	100
Cylinder power		$P_{CYL} = F \dot{x}$	[kW]	10
Volumetric flow rate	Resistive extension	$Q = \dot{x} A_p$	[L/min]	
	Assistive retraction			
Volumetric efficiency	Pump mode	$\eta_{v,P} = \frac{Q}{n V_d}$	[-]	
	Motor mode	$\eta_{v,M} = \frac{n V_d}{Q}$		
Cylinder pressure difference		$\Delta p_{cyl} = p_{P,bore} - p_{P,rod}$	[bar]	100
Hydraulic pump pressure difference		$\Delta p_{HP} = p_{P,bore} - p_{P,rod}$		
Hydro-mechanical efficiency	Pump mode	$\eta_{hm,P} = \frac{V_d \Delta p_{HP}}{T}$	[-]	
	Motor mode	$\eta_{hm,M} = \frac{T}{V_d \Delta p_{HP}}$		
Hydraulic pump power		$P_{HP} = \Delta p_{HP} Q$	[kW]	
Electric motor mechanical power		$P_{EM} = n T$		

The experimental results are compared with simulation results obtained from the model shown in Figure 6.25. This model consists of two cylinders and includes sub-models from the 2D mechanical library, designed to replicate the planar model of the CASE TV380. The simulation data are derived using the same procedure outlined for the experimental tests.

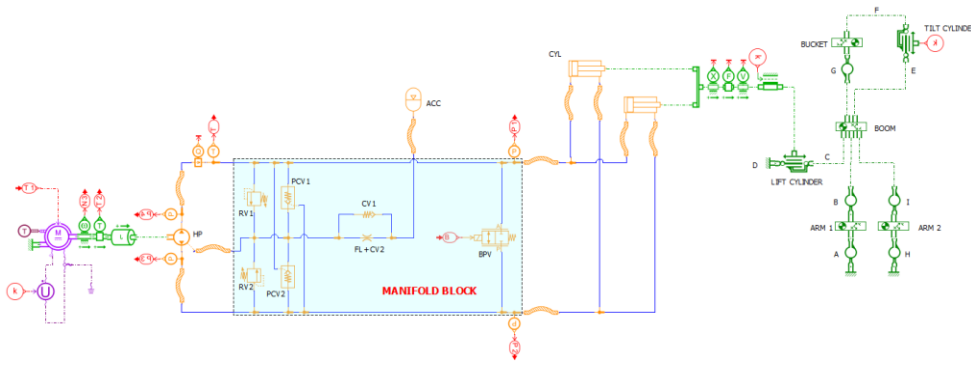


**Figure 6.25: Simulation model of closed-circuit EHA with 2D mechanism**

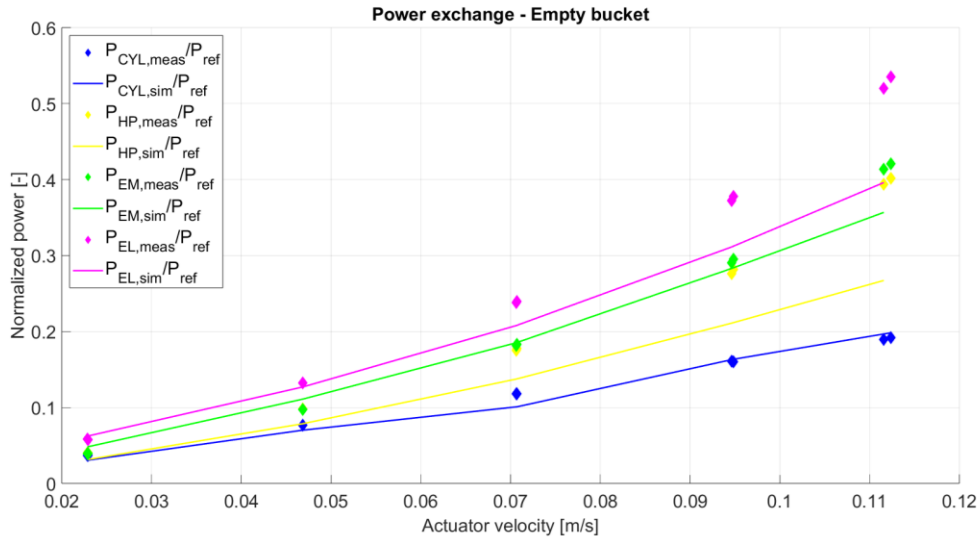
Tests are conducted under three different load conditions: an empty bucket, a load of 1500 *lb* (680.4 *kg*), and a load of 3260 *lb* (1478.7 *kg*). These conditions are chosen to cover a wide range of applied loads, with the empty bucket representing a 25 *kN* load and the maximum mass load corresponding to 75 *kN*. It is important to note that the load is equally distributed between the two cylinders of the boom function. Additionally, five different actuator velocity commands are tested for each load condition, with each measurement being repeated three times to assess the accuracy and reliability of the results. As previously discussed, in the two-cylinder configuration, the actuator velocity is halved compared to the single actuator arrangement, as the flow supplied by HP is equally shared between the cylinders. Therefore, the actuator velocity range tested spans from 0.022 *m/s* to 0.112 *m/s*, compared to the maximum linear speed of 0.23 *m/s* achieved by the actuator in the single-cylinder configuration for resistive extension. Additionally, the low-speed mode is not evaluated in the tests, as the primary focus is on assessing the efficiency of the EHU. In low-speed mode, the actuator velocity is mainly controlled by the opening of the BPV, which is not central to this efficiency evaluation.

Due to the change in orientation of the cylinders during the extension motion, the applied force varies throughout the performed tests. While this variation is expected to be limited to a few *kN*, it introduces some uncertainty into the measured data, as an average value is considered. This same behaviour is replicated in the simulation model, thanks to the use of the 2D mechanical library.

Moreover, averaging these values is necessary to obtain a summary point, which is used to assess the system's performance under steady-state conditions.

The data for both power consumption and efficiencies have been normalized in relation to reference values. However, the data related to the overall efficiency of the closed-circuit EHA has not been normalized.

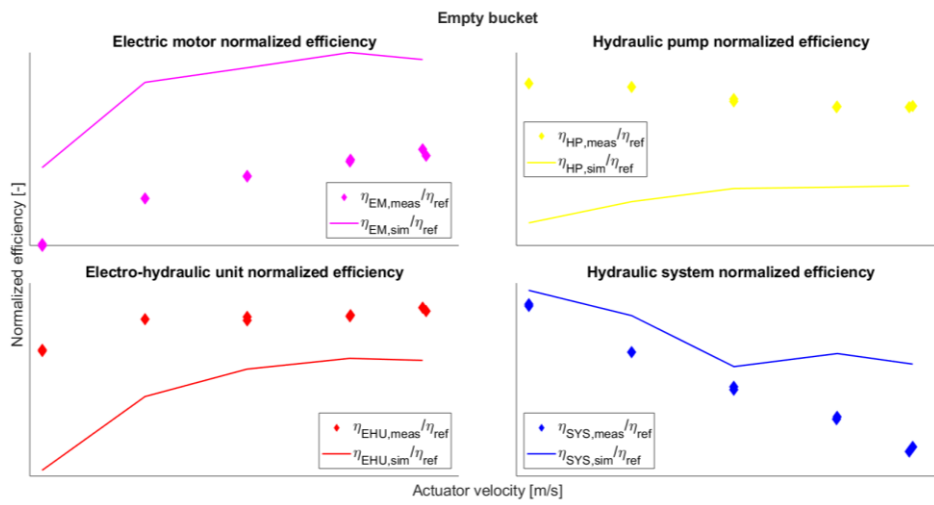
Figure 6.26 shows the normalized power exchange plot for the empty bucket load condition. Measurements are represented by diamond markers, while simulation results are indicated by the continuous line. The electric power is measured at the input of EM (magenta), while the mechanical power transmitted through the shaft between EM and HP (green), the hydraulic power of the HP (yellow), and the power output from CYL (blue) are calculated based on the equations provided in Table 6.2. It can be observed that a good match between experimental and numerical data is achieved at low actuation velocities, while larger discrepancies are noted for the electric power (magenta) and the hydraulic power of HP (yellow) at higher velocities. This behaviour may be attributed to the generic electric model, which does not accurately replicate the real power consumption of the synchronous reluctance motor from Spin. Specifically, a power difference of  $1.98 \text{ kW}$  is observed between the measured and simulated input electric power of EM at the maximum commanded speed, representing an error of 23.89%. Moreover, the consistent increasing trend of power with the rise in commanded velocity is observed in both the measured and simulated data.



**Figure 6.26: Measured and simulated normalized powers for the empty bucketed load condition**

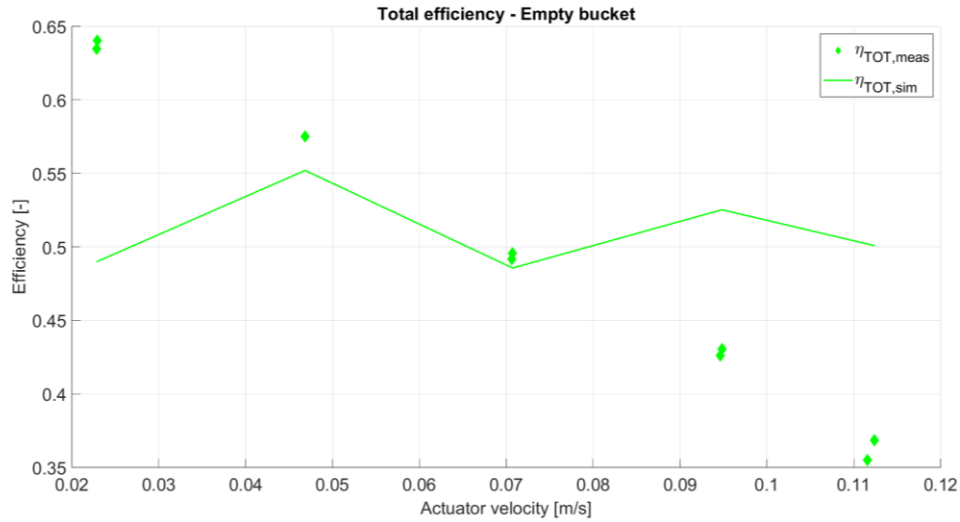
Figure 6.27 shows measured and simulated normalized efficiencies for EM (magenta), HP (yellow), EHU (red) and hydraulic system (blue). The hydraulic unit efficiency at low velocities exceeds one, indicating potential errors in the measurements. Specifically, torque measurements from the inverter may be affected by uncertainty. The normalized efficiency measured for the EM peaks at 80%, which is inconsistent with the efficiency maps provided by the sponsor, and also lower than the simulated data, which reaches up to 91.6%. In contrast, HP demonstrates high efficiency (96% at 0.112 m/s), which is notably higher than the typical overall efficiency of a hydraulic unit. These individual efficiency values for the EM and HP suggest inaccuracies in the mechanical power measurements at the shaft. However, the normalized efficiencies measured for the EHU are reliable, ranging from 69% to 76%, and show a reasonable match with the simulation results, both in trend and error, with a discrepancy of around 7% across a wide range of velocities. Finally, the hydraulic system normalized efficiency is evaluated, showing 93% efficiency at low volumetric flow rates within the system. However, at higher flow rates, the efficiency decreases, reaching 47% when HP supplies a maximum of 55 L/min. Discrepancies are observed at high commanded velocities between measurements and simulation,

which can be attributed to power losses in the hoses that are not accounted for in the simulation model, as it excludes the effects of hose bending and fittings.



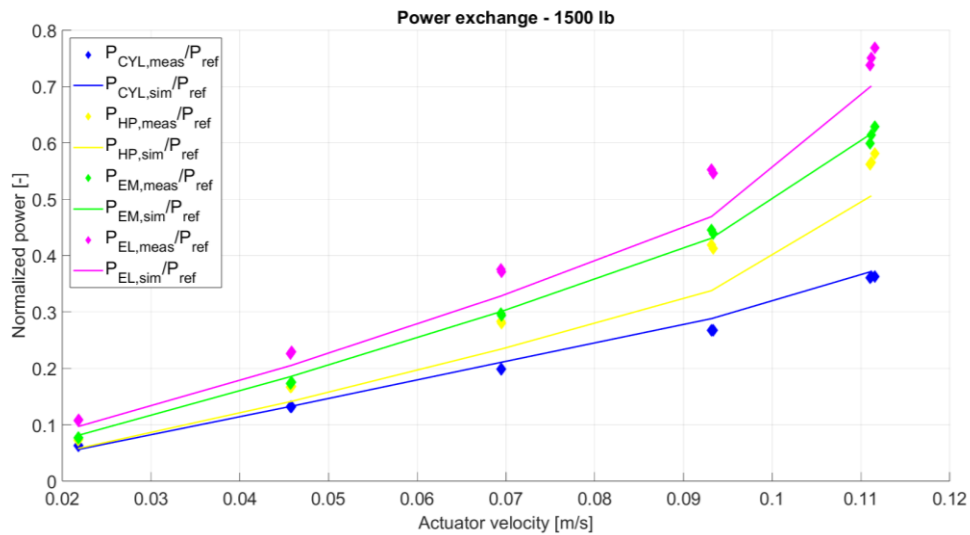
**Figure 6.27: Measured and simulated normalized efficiencies for the empty bucketed load condition**

Figure 6.28 shows measured and simulated total efficiency for the closed-circuit EHA with empty bucket. The overall efficiency of the EHA system in the measurements, which drops to 37%, is strongly affected by inefficiencies in the hydraulic system. This problem could be addressed with improved piping. The decreasing efficiency trend closely follows that of the hydraulic system efficiency. In contrast, the simulated data consistently remain within a narrow range of 50% to 55%.



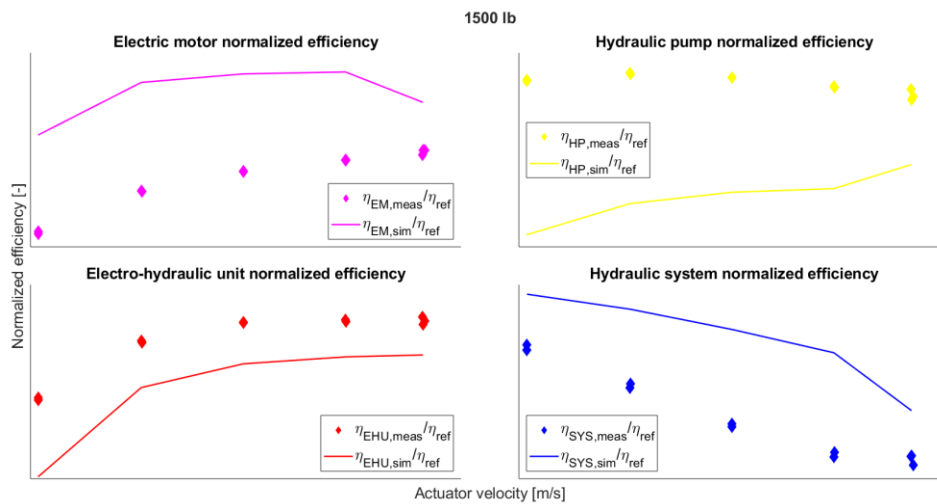
**Figure 6.28: Measured and simulated total efficiency for the empty bucked load condition**

Figure 6.29 shows the normalized power exchange plot for the 1500 *lb* load condition. It can be observed that a better match between experimental and numerical data is achieved across all actuation velocities with respect to the empty bucket load condition. Specifically, a power difference of 0.78 *kW* is observed between the measured and simulated input electric power of the EM at the maximum commanded speed, resulting in an error of 6.57%.



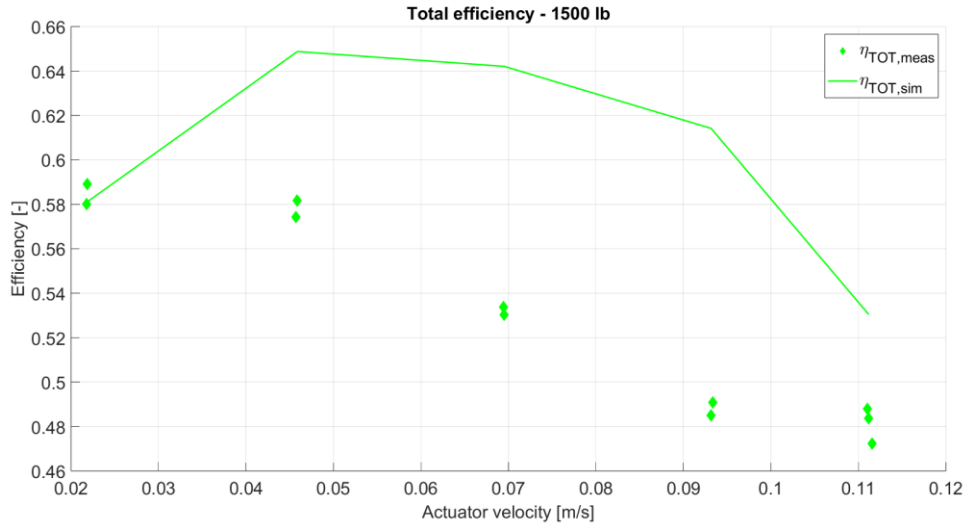
**Figure 6.29: Measured and simulated normalized powers for the 1500 *lb* load condition**

Figure 6.30 shows measured and simulated normalized efficiencies for EM, HP, EHU and hydraulic system. Even for the 1500 *lb* load EM and HP efficiencies result inconsistent with the simulation data due to the shaft power inaccuracy. However, the normalized efficiencies measured for the EHU are reliable, ranging from 68.1% to 76.6%, and exhibit a reasonable match with the simulation results, both in terms of trend and error. The discrepancy between the measured and simulated efficiencies is around 4% across a wide range of velocities.



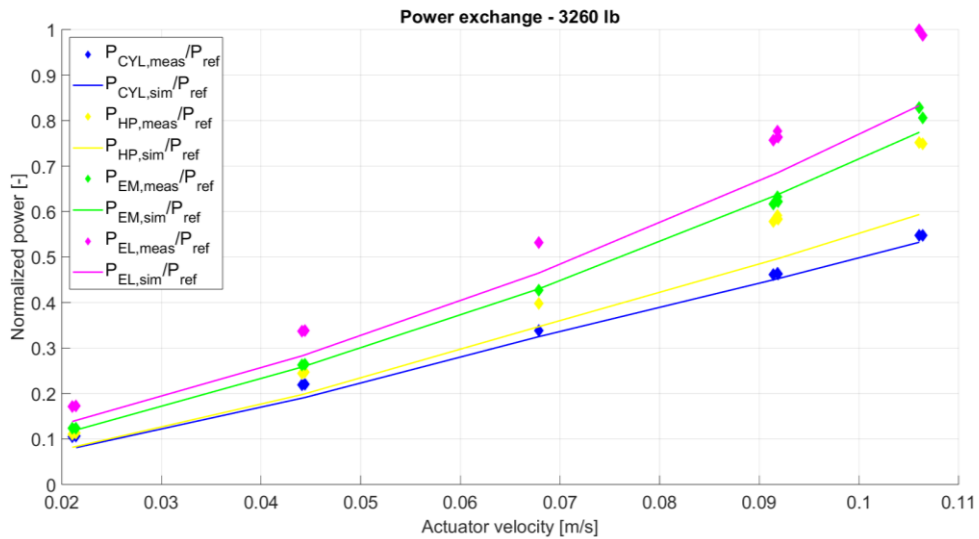
**Figure 6.30: Measured and simulated normalized efficiencies for the 1500 *lb* load condition**

Figure 6.31 shows measured and simulated total efficiency for the closed-circuit EHA with 1500 *lb* as load applied. The overall efficiency of the EHA system in the measurements, which drops to 48%, is less impacted by inefficiencies in the hydraulic system at higher loads. This is because the power level increases with the load, and throttling losses in the pipes and manifold become a less significant portion of the overall power consumption. The decreasing measured efficiency of the EHA in this case aligns with the simulations for medium to high actuation velocities, though a maximum discrepancy of 10% is still observed at 0.069 *m/s*.



**Figure 6.31: Measured and simulated total efficiency for the 1500 lb load condition**

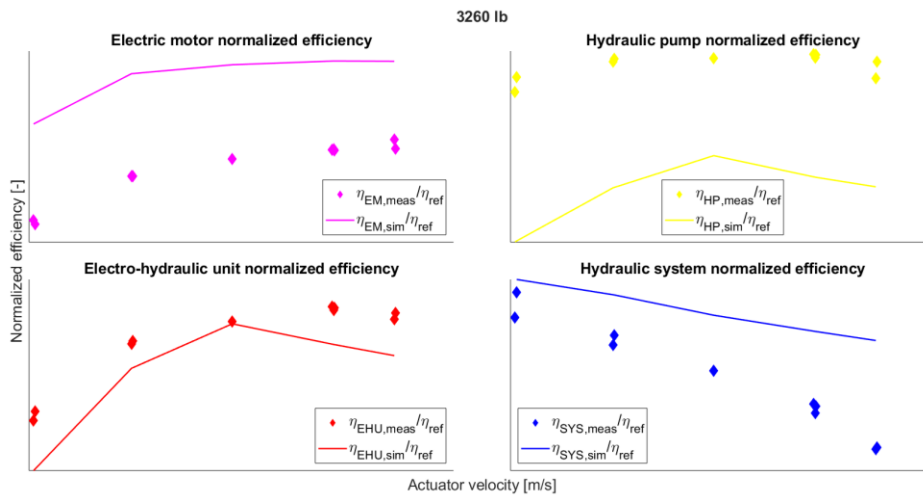
Figure 6.32 shows the normalized power exchange plot for the 3260 lb load condition.



**Figure 6.32: Measured and simulated powers for the 3260 lb load condition**

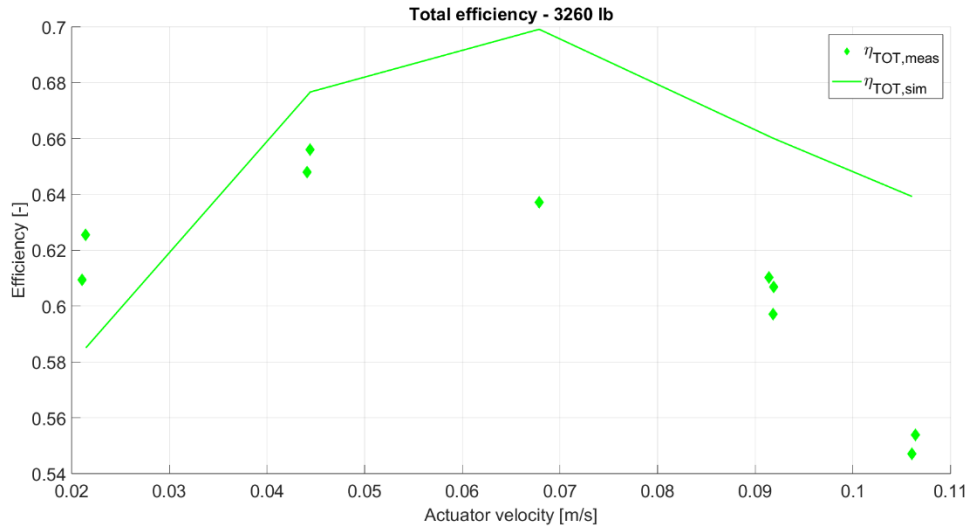
Figure 6.33 shows measured and simulated normalized efficiencies for EM, HP, EHU and hydraulic system considering an applied load of 3260 lb. The normalized efficiencies measured for the EHU range from 64.8% to 77% and show the best match with the simulation results among the three considered loading conditions. The maximum discrepancy between the measured and

simulated efficiencies is approximately 3% across the entire velocity range, with an almost perfect match observed at 0.068 m/s. The efficiency trends for EM and HP are consistent with those observed in previous measurements. Additionally, a noticeable increase in hydraulic system efficiency is observed as the power level of the EHA rises, with a minimum efficiency of 73.4% at high velocities.



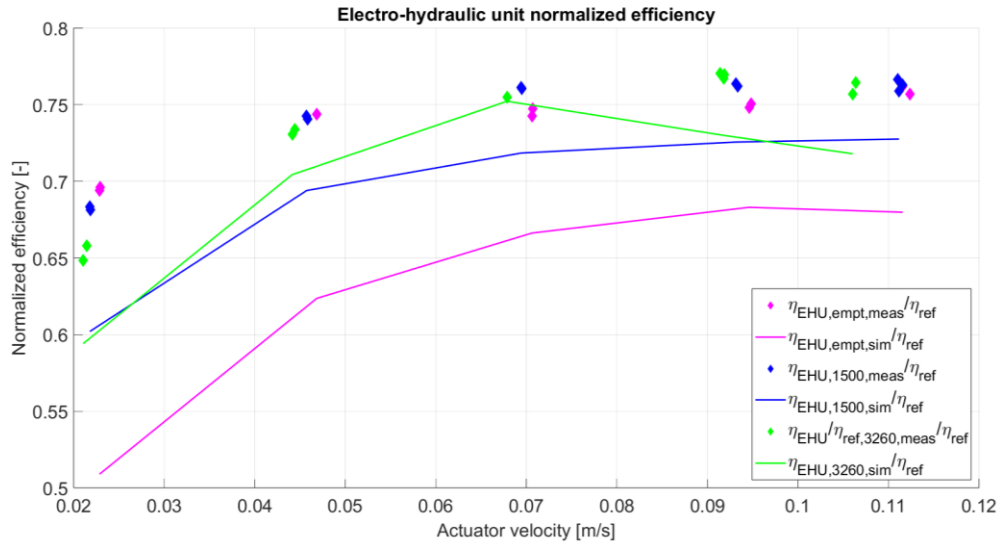
**Figure 6.33: Measured and simulated normalized efficiencies for the 3260 lb load condition**

Figure 6.34 shows measured and simulated total efficiency for the closed-circuit EHA with 3260 lb as load applied. Better overall efficiencies are observed for this loading condition, reaching a maximum of 65% at medium actuation velocities. The EHA efficiency for these operating conditions highlights the potential benefits of implementing this architecture on the reference vehicle.



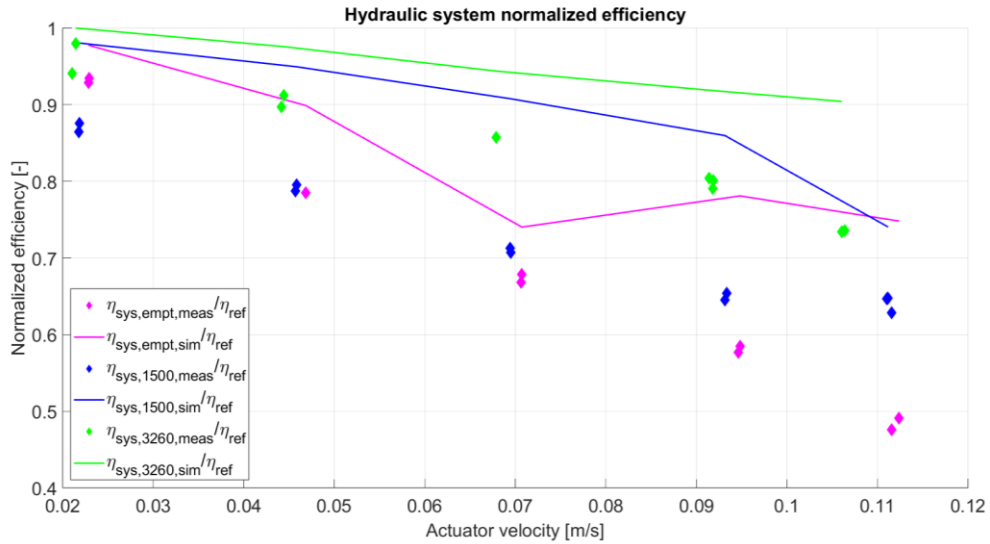
**Figure 6.34: Measured and simulated total efficiency for the 3260 lb load condition**

Figure 6.35 is considered to further evaluate the dependency on the load of the EHU normalized efficiency. As the applied load increases, and consequently the pressure difference across HP, the efficiency of the EHU improves. It is important to note that, while volumetric efficiency typically decreases with pressure due to increased leakage losses, it increases with speed. This is because higher pressure leads to more leakage, while a higher working speed reduces the relative impact of these leakage losses compared to the overall flow. Additionally, hydro-mechanical efficiency improves as the outlet pressure rises. This is because the internal friction of the pump is only slightly influenced by pressure, and becomes less significant as the working pressure increases. However, if the rotational speed is below a certain minimum operating speed, hydro-mechanical efficiency remains very low. As the speed increases, the efficiency reaches a peak, then gradually decays due to fluid shear or churning losses. Regarding the electric motor, its efficiency increases as both the rotational speed, which is related to the commanded velocity, and the applied torque, which is linked to the pressure difference across the hydraulic pump, increase.



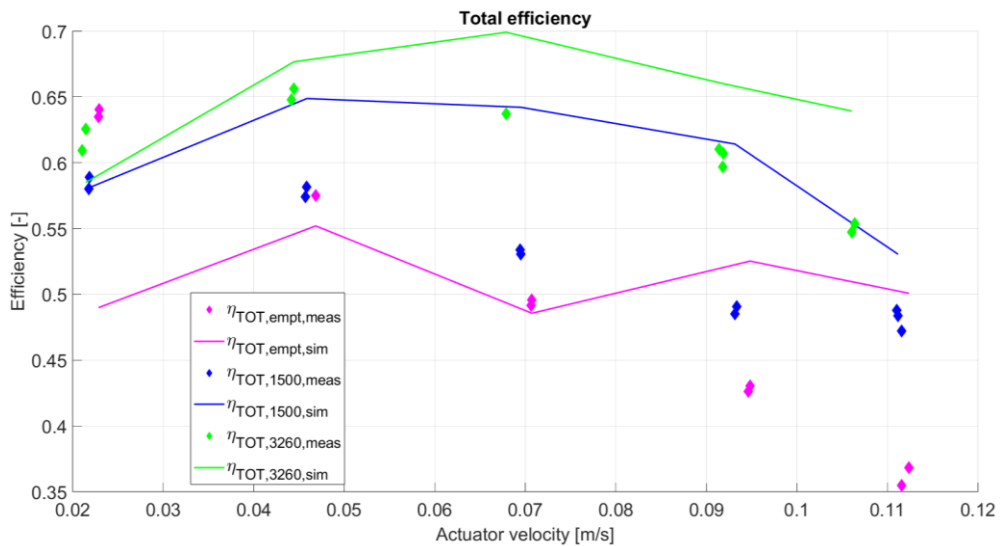
**Figure 6.35: Measured and simulated EHU normalized efficiency under all load conditions**

Figure 6.36 is considered to further evaluate the dependency on the load of the hydraulic system normalized efficiency. Losses in the system due to hoses, fittings, valves, and filters become less significant at higher power levels, which occur when higher loads are applied. As a result, lower system efficiencies are expected in the empty bucket condition, while higher efficiencies are observed when a load of 3260 *lb* is applied. Furthermore, throttling losses are more marked at higher flow rates, which occur when higher actuator velocities are commanded, leading to greater energy losses under these conditions.



**Figure 6.36: Measured and simulated hydraulic system normalized efficiency under all load conditions**

Figure 6.37 is used to further assess the dependence of the EHA total efficiency on the applied load. Consistent with the efficiency trend observed in the EHU and hydraulic system at higher loads, the overall EHA efficiency for the closed-circuit architecture is also higher when 3260 lb are applied to the bucket.



**Figure 6.37: Measured and simulated EHA total efficiency under all load conditions**

# 7. CONCLUSION

## 7.1 SUMMARY

This study presents two architectural designs for an EHA system, both utilizing a fixed-displacement pump and a variable-speed electric motor. The two configurations are an open-circuit system and a closed-circuit system. The system sizing is based on the principle of selecting the prime mover to provide the required flow rate at operating points that offer high efficiency. In line with the concept of decentralized hydraulic systems, the primary goal of the EHA is to minimize throttle losses in the hydraulic circuit. Low- and high-speed operating conditions can be achieved by using a bypass valve, though this introduces some throttle losses as the valve opens. While efficiency is reduced during low-speed operations, such conditions are infrequent in the typical duty cycle of mobile applications, and thus their impact on overall performance is minimal.

The selection of components for the EHA has been carefully optimized, with particular attention given to accumulator sizing, which serves as the basis for selecting valves and filter with precision. The process also places significant emphasis on the hydraulic unit and electric motor, ensuring the creation of a high-efficiency EHU built with commercially available components. Additionally, a custom manifold has been designed to seamlessly integrate the hydraulic components, enabling an efficient configuration for the entire EHA system on the reference vehicle. This design not only simplifies the setup but also minimizes pressure drops, thereby reducing energy losses within the hydraulic circuit.

A simulation model has been developed in Simcenter Amesim environment based on the lumped parameter method. Different libraries are integrated to reproduce in a realistic way the mechatronic systems under study.

This work has thoroughly explored the instrumentation of the reference vehicle with the closed-circuit architecture, focusing on its application in a compact skid steer loader featuring an open-centre hydraulic system. The integration of the EHA required only minimal modifications to the baseline system, ensuring a seamless adaptation. The chosen hydraulic configuration, alongside the implementation of the data acquisition system and power electronics, has been presented as a key aspect of the experimental setup. This approach not only highlights the practical feasibility of incorporating the EHA into existing systems.

The research objectives outlined in Section 1.4 are addressed and elaborated in this thesis:

- Evaluate the performance of a high-efficiency EHA architecture with energy recovery capabilities.
- Reduce the hydraulic system costs by employing a VM-FP configuration as the EHU, ensuring full-speed range operation without requiring the fixed-displacement pump to operate at low speeds.
- Proposing a sizing methodology for a scalable EHA design tailored to mobile applications.
- Developing a simulation model in Simcenter Amesim, which can serve as a design tool for future sizing and optimization efforts.
- Creating efficiency maps for both open- and closed-circuit systems across all four quadrants, to validate performance under various operating conditions of the EHA.
- Implementing the closed-circuit EHA on a reference vehicle without modifying the main mechanical structure, while preserving both baseline and EHA operation modes.
- Analyzing the power management of the EHA system, with particular focus on the commercial EHU that includes a four-quadrant external gear

pump and a synchronous reluctance motor, assessing its potential for power regeneration.

In terms of simulation results, a reference 20 kW application was considered, featuring a differential cylinder with a 0.89 m stroke and a maximum force of 50 kN. The main results are as follows:

- The studied EHA system can achieve efficiencies up to 70% for both open-circuit and closed-circuit architectures. The individualized system works efficiently by decreasing the throttling losses and enabling energy regeneration.
- The low-speed modes exhibit low efficiencies due to the bypass valve being open. Same holds for the fast-assistive retraction mode, where the use of BPV results in high throttling losses, assuming the pump operates at the same maximum speed under both assistive and resistive loads.
- The closed-circuit EHA is 3% to 15% more efficient than the open-circuit system. The small performance difference is mainly due to the fact that the standard two-quadrant pump and the new four-quadrant pump design exhibit similar efficiencies in both pumping and motoring modes. Additionally, the accumulator in the closed-circuit system provides limited energy savings because of the constrained operating pressure required in the drain line.
- Power losses are primarily driven by the hydraulic pump in both EHA architectures. The remaining contributors, in order of importance, are the electric motor, hydraulic circuit, and inverter. Focusing on the main contributors within the hydraulic system, it can be observed that the 4/3 directional valve is the primary source of power losses in the open-circuit system. In the closed-circuit system, however, the power losses are shared equally between the valves and the filter.

In terms of experimental results, the closed-circuit EHA with the commercial EHU was implemented on a CASE TV380 skid steer compact loader and tested.

The boom function was evaluated in resistive extension mode, utilizing two differential cylinders. The main results are as follows:

- The measurement and simulation trends for power exchange in the system are consistent, with relative errors reaching a maximum of 25% for low loads applied to the system. However, for higher loads, the discrepancy between measured and simulated data is reduced to 10%.
- The EHU normalized efficiency reaches a maximum of 77% when high loads are applied, highlighting the high efficiency of the commercial electro-hydraulic unit provided by the sponsor. Additionally, the simulated efficiency aligns with the measured trends, showing a discrepancy ranging between 8% and 4% under high actuation velocities across all loading conditions.
- The hydraulic system efficiency is strongly influenced by the actuation velocity, primarily due to the high pressure drops in the manifold and hoses, which result in significant throttling losses. These losses have less impact as the power level increases with higher loads. At high actuation speeds, the normalized efficiency can reach a minimum of 47% with an empty bucket and a maximum of 73.4% when 3260 *lb* are loaded.
- The total efficiency of the closed-circuit EHA is primarily influenced by hydraulic system losses at high actuation velocities, particularly when low loads are applied. However, the overall measured efficiency can reach up to 65%, demonstrating the advantages of implementing this architecture on the reference vehicle.

The studied system offers a viable solution for integrating EHAs into cost-sensitive applications, such as off-road vehicles in construction and agriculture. This is due to its high energy efficiency and significant potential for energy recuperation during assistive load conditions. Implementing this technology in the aforementioned fluid power machines could potentially increase the energy efficiency of the fluid power actuation system from the 21% documented in the literature to up to 70%, as demonstrated in this study.

## 7.2 FUTURE WORK

Here are some potential research directions for the future, based on the findings presented in this thesis:

- Future tests will focus on investigating the remaining three operational modes: assistive extension, resistive retraction, and assistive retraction.
- The implementation of the EHA on the reference vehicle could be improved by reducing the length of hoses and increasing their diameter. The minor and major losses encountered in the system can cause significant pressure drops between the cylinder and the hydraulic unit, reducing system efficiency. To address this, the use of rigid pipes could be considered as an alternative to the current hoses. However, adopting rigid pipes would necessitate substantial modifications to the baseline hydraulic system to ensure the continued proper functioning of both the open-centre system and the new EHA system.
- A water-cooling system could be implemented to prevent the electric motor from overheating during more demanding drive cycles. Specifically, the inverter controller is designed to shut down the motor when temperatures exceed a specified threshold to prevent damage to the electric motor. The need for a cooling system is even more critical, as the current system relies on maintaining the electric motor at 0 *rpm* during idle phases to hold the load.
- A low-cost, high-performance load-holding function could be integrated into the hydraulic system to reduce power consumption during idle phases. The goal is to minimize the use of costly solenoid valves while also eliminating the need for the electric motor EM to maintain the load. Currently, a passive load-holding strategy based on pilot-operated check valves is being investigated as a potential solution.
- A control logic for the self-levelling of the bucket during boom actuation can be implemented to replicate the function of the pre-existing hydraulic subsystem used in the reference vehicle. In the current case study, two independent hydraulic systems are employed for the boom and bucket

functions. A control strategy, utilizing displacement sensors and taking into account the system kinematics, can be developed to automatically adjust the bucket position, ensuring it remains balanced during both the lifting and lowering phases of the boom.

- This study primarily emphasizes the steady-state performance, such as efficiency. In contrast to traditional valve-controlled hydraulic systems, the EHA controls the actuation velocity by adjusting the speed of the EHU. As a result, investigating the dynamic performance of the EHA system becomes crucial, especially in terms of its response and the design of the controller for mode transitions under varying load conditions.
- A battery system could be sized and implemented to store regenerated energy during assistive modes, optimizing the system for mobile applications compared to the stationary setup used in this study. Furthermore, all power electronics will need to be redesigned and integrated for installation on the CASE TV380 to ensure proper functionality in the mobile environment.
- Comprehensive experiments on the assistive retraction mode of the boom could be conducted. Furthermore, tests could be extended to the bucket function to evaluate the efficiency of the reference vehicle equipped with the implemented closed-circuit EHA in both the assistive extension and resistive retraction quadrants.

## 8. BIBLIOGRAPHY

- [1] A. Vacca and G. Franzoni, Hydraulic Fluid Power: Fundamentals, Applications, and Circuit Design. John Wiley & Sons, 2021
- [2] Boston Dynamics. (2024) Automate your warehouse with Stretch. [Online]. Available: <https://bostondynamics.com/products/stretch>
- [3] Case New Holland. (2024) Compact truck loaders TV380. [Online]. Available: <https://www.casece.com/emea/en-il/products/compact-track-loaders/compact-track-loaders/models/tv380>
- [4] Case New Holland. (2024) Magnum series. [Online]. Available: <https://www.caseih.com/en-us/unitedstates/products/tractors/magnum-series>
- [5] Boeing. (2024) Boeing 787 Dreamliner. [Online]. Available: <https://www.boeing.com/commercial/787#overview>
- [6] Masia A, “Greenhouse Gas Emissions-Off Highway Vehicles Solutions and Future Trends”, Maha Fluid Power Research Center, Lafayette, 2022, Webinar
- [7] Our World in Data. (2022) Annual CO2 Emissions. [Online]. Available: <https://ourworldindata.org/co2-and-greenhouse-gas-emissions#all-charts>
- [8] Our World in Data. (2024) CO2 and Greenhouse Gas Emissions. [Online]. Available: <https://ourworldindata.org/co2-and-greenhouse-gas-emissions?insight=human-greenhouse-gas-emissions-have-increased-global-average-temperatures#key-insights>
- [9] United States Environmental Protection Agency. (2024) Why We Need to Decarbonize Transportation. [Online]. Available: [https://www.epa.gov/greenvehicles/why-we-need-decarbonize-transportation#:~:text=The%20U.S.%20National%20Blueprint%20for%20Transportation%20Decarbonization%20\(Blueprint\)%20is](https://www.epa.gov/greenvehicles/why-we-need-decarbonize-transportation#:~:text=The%20U.S.%20National%20Blueprint%20for%20Transportation%20Decarbonization%20(Blueprint)%20is)

- [10]National Fluid Power Association (NFPA). (2023) NFPA Roadmap Committee: Meeting Report on Customer Drivers. [Online]. Available: <https://www.nfpa.com/NFPA/NFPARoadmapCommitteeMeetingReport-CustomerDrivers1.pdf>
- [11]Love L, Lanke E, Alles P. Estimating the Impact (Energy, Emissions and Economics) of the US Fluid Power Industry. 2012, NREL
- [12]Zimmerman JD, Pelosi M, Williamson CA, Ivantysynova M. Energy consumption of an LS excavator hydraulic system. In ASME international mechanical engineering congress and exposition 2007 Jan 1 (Vol. 42983, pp. 117-126).
- [13]Vacca, Andrea. "Energy efficiency and controllability of fluid power systems." *Energies* 11.5 (2018): 1169.
- [14]Patel T. " Flow Sharing Energy Recovery (FSER) Systems: Single Actuator Testing and Diesel Excavator Testing". 2024, International Maha Fluid Power Conference
- [15]Beltrami D, Iora P, Tribioli L, Uberti S. Electrification of compact off-highway vehicles—overview of the current state of the art and trends. *Energies*. 2021 Sep 6;14(17):5565.
- [16]Qu S, Fassbender D, Vacca A, Busquets E. A cost-effective electro-hydraulic actuator solution with open circuit architecture. *International Journal of Fluid Power*. 2021 May 31;22(2).
- [17]Qu S, Vacca A, Fassbender D, Busquets E, Rexroth B. Formulation, design and experimental verification of an open circuit electro-hydraulic actuator. In *Proceedings of the 2020 IEEE Global Fluid Power Society PhD Symposium (GFPS)*, Online 2020 Oct 19 (pp. 19-21).
- [18]Qu S, Fassbender D, Vacca A, Busquets E, Neumann U. A closed circuit electro-hydraulic actuator with energy recuperation capability.
- [19]Qu S, Fassbender D, Vacca A, Busquets E. A high-efficient solution for electro-hydraulic actuators with energy regeneration capability. *Energy*. 2021 Feb 1;216:119291.

- [20]Zappaterra F, Vacca A, Sudhoff SD. A compact design for an electric driven hydraulic gear machine capable of multiple quadrant operation. *Mechanism and Machine Theory*. 2022 Nov 1;177:105024.
- [21]Zappaterra F, Pan D, Ransegnola T, Vacca A, Sudhoff SD, Busquets E. A novel electro-hydraulic unit design based on a shaftless integration of an internal gear machine and a permanent magnet electric machine. *Energy Conversion and Management*. 2024 Jun 15;310:118432.
- [22]Qu S, Zappaterra F, Vacca A, Liu Z, Busquets E. Experimental verification of an electro-hydraulic actuation system driven by an integrated electro-hydraulic unit. *International Journal of Fluid Power*. 2023 May 3:327-60.
- [23]Qu S, Zappaterra F, Vacca A, Liu Z, Busquets E. Design and Verification of an Open-Circuit Electro-Hydraulic Actuator System with an Integrated Electro-Hydraulic Unit. *Purdue Univ., West Lafayette, IN (United States)*; 2022 Jun 13.
- [24]Qu S, Zappaterra F, Vacca A, Busquets E. An electrified boom actuation system with energy regeneration capability driven by a novel electro-hydraulic unit. *Energy Conversion and Management*. 2023 Oct 1;293:117443.
- [25]Qu S, Fassbender D, Vacca A, Busquets E. Development of a lumped-parameter thermal model for electro-hydraulic actuators. *Purdue Univ., West Lafayette, IN (United States)*; 2021 Apr 13.
- [26]Ivantysyn J, Ivantysynova M. *Hydrostatic pumps and motors: principles, design, performance, modelling, analysis, control and testing*. (No Title). 2003.
- [27]Wikipedia. (2024) Electric motor. [Online]. Available: [https://en.wikipedia.org/wiki/Electric\\_motor#Types](https://en.wikipedia.org/wiki/Electric_motor#Types)
- [28]Cao Z, Mahmoudi A, Kahourzade S, Soong WL. An overview of electric motors for electric vehicles. In *2021 31st Australasian Universities power engineering conference (AUPEC) 2021 Sep 26 (pp. 1-6)*. IEEE.
- [29]Heidari H, Rassölkin A, Kallaste A, Vaimann T, Andriushchenko E, Belahcen A, Lukichev DV. A review of synchronous reluctance motor-drive advancements. *Sustainability*. 2021 Jan 13;13(2):729.

- [30]Boglietti A, Pastorelli M. Induction and synchronous reluctance motors comparison. In2008 34th annual conference of IEEE industrial electronics 2008 Nov 10 (pp. 2041-2044). IEEE.
- [31]Donaghy-Spargo CM. Synchronous reluctance motor technology: opportunities, challenges and future direction. Engineering & technology reference. 2016 May 7.
- [32]Heidari H, Andriushchenko E, Rassõlkin A, Kallaste A, Vaimann T, Demidova GL. Comparison of synchronous reluctance machine and permanent magnet-assisted synchronous reluctance machine performance characteristics. In2020 27th International Workshop on Electric Drives: MPEI Department of Electric Drives 90th Anniversary (IWED) 2020 Jan 27 (pp. 1-5). IEEE.
- [33]Heybroek K, Palmberg JO. Evaluating a pump controlled open circuit solution.
- [34]Settima. (2024) Continuum. [Online]. Available:  
<https://www.settima.it/products/continuum-pumps/continuum.html>
- [35]Hydac. (2024) Bladder accumulators. [Online]. Available:  
[https://www.hydac.com.au/pub/media/productattach/e/\\_/e.3.201.28.03.16.pdf#:~:text=HYDAC%20high%20flow%20bladder%20accumulators%20type%20SB330%20are%20high%20performance](https://www.hydac.com.au/pub/media/productattach/e/_/e.3.201.28.03.16.pdf#:~:text=HYDAC%20high%20flow%20bladder%20accumulators%20type%20SB330%20are%20high%20performance)
- [36]Sun Hydraulics. (2024) CKGBXAN. [Online]. Available:  
<https://www.sunhydraulics.com/model/CKGB/XAN>
- [37]Sun Hydraulics. (2024) CXFAXAN. [Online]. Available:  
<https://www.sunhydraulics.com/model/CXFA/XAN>
- [38]Sun Hydraulics. (2024) RDDALAN. [Online]. Available:  
<https://www.sunhydraulics.com/model/RDDA/LAN>
- [39]Sun Hydraulics. (2024) FLHAXDN. [Online]. Available:  
<https://www.sunhydraulics.com/model/FLHA>

- [40]Rexroth. (2024) PROPORTIONAL DIRECTIONAL VALVE KKDSR1NB/HCG12N0K4V. [Online]. Available: [https://store.boschrexroth.com/Hydraulics/Valves/Cartridge-valves/Electro-proportional/PROPORTIONAL-DIRECTIONAL-VALVE\\_R901024009?cclcl=en\\_AU](https://store.boschrexroth.com/Hydraulics/Valves/Cartridge-valves/Electro-proportional/PROPORTIONAL-DIRECTIONAL-VALVE_R901024009?cclcl=en_AU)
- [41]Fitch EC, Hong IT. Hydraulic component design and selection. Stillwater, OK, USA: BarDyne; 1998.
- [42]Kuriyama of America, Inc. (2024) Hydraulic Hose Sizing Nomogram. [Online]. Available: <https://products.kuriyama.com/Asset/H%20SizingNomogram.pdf>
- [43]Rexroth. (2024) SCREW-IN CARTRIDGE VALVE 0431250027A0000. [Online]. Available: [https://store.boschrexroth.com/SCREW-IN-CARTRIDGE-VALVE\\_R930004414?cclcl=en\\_US](https://store.boschrexroth.com/SCREW-IN-CARTRIDGE-VALVE_R930004414?cclcl=en_US)
- [44]Rexroth. (2024) PRESSURE RELIEF VALVE DBDS 6 K1X/315. [Online]. Available: [https://store.boschrexroth.com/PRESSURE-RELIEF-VALVE\\_R900423725?categoryId=a0KTr000003PZnGMAW](https://store.boschrexroth.com/PRESSURE-RELIEF-VALVE_R900423725?categoryId=a0KTr000003PZnGMAW)
- [45]Rexroth. (2024) DIRECTIONAL SPOOL VALVE 4WE10G5X/EG12N9K4/M. [Online]. Available: [https://store.boschrexroth.com/ccrz\\_\\_ProductDetails?sku=R901278796&cclcl=en\\_AE](https://store.boschrexroth.com/ccrz__ProductDetails?sku=R901278796&cclcl=en_AE)
- [46]Rexroth. (2024) In line filter with filter element according to DIN 24550. [Online]. Available: [https://airlinemedia.airlinehyd.com/Literature/Manufacturer\\_Catalogs/Bosch%20Rexroth/InLine\\_Filter\\_DIN24550\\_RE51447\\_2011-10.pdf](https://airlinemedia.airlinehyd.com/Literature/Manufacturer_Catalogs/Bosch%20Rexroth/InLine_Filter_DIN24550_RE51447_2011-10.pdf)
- [47]Siemens. (2024) Simcenter Amesim Software. [Online]. Available: <https://plm.sw.siemens.com/en-US/simcenter/systems-simulation/amesim/>
- [48]CASE Construction. (2024) CASE TV380. [Online]. Available: <https://assets.cnhindustrial.com/casece/nafta/assets/Brochures/Products/Compact-Track-Loaders/TV380/CTL-TV380-Specs-201812.pdf>

## **9. APPENDIX A – VALVES AND FILTER SELECTION ACCORDING TO ACCUMULATOR SIZING FOR THE CLOSED-CIRCUIT EHA**

The components selected in this section are the best in terms of pressure drops measured for maximum flow rates for the closed-circuit EHA.

Considering the different operating conditions, the flow across the components can vary depending on the charge or discharge of the accumulator. Therefore, also the pressure drops across the valves and the filter are not fixed. The pressure drops reported in the following tables between brackets are the one representing the discharge phase.

The pressure drops are related to the maximum volumetric flow rates passing through the valve or filter. The maximum flow can be computed according to equations reported in Section 2. These  $\Delta p$  are derived by the characteristic curves (pressure drop vs. volumetric flow rate) of each device. The 18 cc/rev 4Q Continuum pump from Settima Meccanica is considered for the sizing of the components.

Different brands are considered during the selection of the components. In particular valves and filters from the catalogues of Sun Hydraulics, Parker Hannifin, Bosh Rexroth and Hydac are considered.

The components selected from Sun Hydraulics are reported in Table 9.1. All the components required for the closed-circuit EHA can be found in their catalogue with a relatively small pressure drop at the maximum flow. The filter selected

from Sun Hydraulics is of the cartridge type, hence it can be screwed into the manifold reducing the number of hoses.

**Table 9.1: Selected components from Sun Hydraulics**

Type	Code	Maximum pressure [bar]	Maximum flow rate [L/min]	Nominal flow rate [L/min]	Pressure drops at nominal flow [bar]	Cracking pressure [bar]	Relief pressure [bar]	Maximum adjustable pressure [bar]	Cavity code
Pilot operated check valve	CKGBXAN	344.74	227.125	37.9 (22)	2.76 (2)	0.28	-	-	T-17A
Check valve	CXFAXAN	344.74	151.416	40 (22)	0.84 (0.42)	0.28	-	-	T-5A
Relief valve	RDDALAN	344.74	94.63	54	-	-	210	206.84	T-10A
Type	Code	Maximum flow rate [L/min]	Maximum operating pressure [bar]	Nominal flow rate [L/min]	Pressure drops [bar]	Filter rating [µm]	Weight [kg]	Maximum temperature [°C]	Cavity code
Filter	FLHAXDN	151.42	344.74	37.9	0.5	40	0.53	-	T-16A

The components selected from Parker Hannifin are reported in Table 9.2. No filter is selected for this brand because of the too high pressure drops.

**Table 9.2: Selected components from Parker Hannifin**

Type	Code	Maximum pressure [bar]	Maximum flow rate [L/min]	Nominal flow rate [L/min]	Pressure drops at nominal flow [bar]	Cracking pressure [bar]	Relief pressure [bar]	Maximum adjustable pressure [bar]	Cavity code
Pilot operated check valve	CPH124P N	350	75	37.9 (22)	2.7 (2.1)	1.7	-	-	C12-3
Check valve	D04B2-0.2 N	420	160	40 (22)	2 (0.9)	0.2	-	-	C10-2
Relief valve	PRH102 S 30	380	56.3	54	-	-	210	207	C10-3

The components selected from Bosh Rexroth are reported in Table 9.3. Even in this case no filter is selected. Moreover, the 2/2 bidirectional, proportional, control valve used in the architecture is introduced.

**Table 9.3: Selected components from Bosh Rexroth**

Type	Code	Maximum pressure [bar]	Maximum flow rate [L/min]	Nominal flow rate [L/min]	Pressure drops at nominal flow [bar]	Cracking pressure [bar]	Relief pressure [bar]	Maximum adjustable pressure [bar]	Cavity code
Pilot operated check valve	04.33.08 10 27 00	350	200	37.9 (22)	1.5 (2.5)	1.5	-	-	CA-16A-3C
Check valve	04.31.23.00 85 00	350	80	40 (22)	2.5 (1.25)	0.5	-	-	CA-10A-2N
Relief valve	04.15.23 03 85 35 00	350	120	54	-	-	210	350	CA-10A-2N
Bypass valve	KKDSR1N B/HCG24N 0K4V	350	38 (34 opposite direction)	37	-	-	-	-	R/T-13A

The components selected from Hydac are reported in Table 9.4. In this case only the filter is selected to complete the architecture with Parker and Rexroth components. The filter is of the low-pressure, inline type. It cannot be screwed into the manifold, but requires hoses connections to this last device.

**Table 9.4: Selected components from Hydac**

Type	Code	Maximum flow rate [L/min]	Maximum operating pressure [bar]	Pressure drops [bar]	Filter rating [ $\mu$ m]	Weight [kg]	Maximum temperature [°C]	Connection
Filter	RFON60DC10A1.X/12	60	25	0.1	10	0.9	100	3/4" Threaded - ISO 228

The filter from Hydac represents the best option in terms of pressure drops, 0.1 bar with respect to 0.5 bar for the Sun Hydraulics filter. Moreover, Sun Hydraulics filter FLHAXDN is of the high-pressure type, when the maximum pressure expected in the drain line of the circuit cannot be greater than 10 bar. Even if Hydac filter suits better the requirements for the closed-circuit EHA, it is better to purchase the remaining valves from only one company for logistic reasons.

The choice of the accumulator can be finalized only after that the remaining valves and filter are selected. The pressure drops are a very important parameter for the sizing of the accumulator. Due to the big sizes and high weights of these components a big focus should be given to their dimensioning. Even slightly

bigger pressure drops can cause to increase the size of the accumulator to the next possible one according to the available catalogs.

The parameters used to size the accumulator are computed according to equations from Section 3.1.3. The most demanding function from the reference vehicle is represented by the boom due to the bigger stroke of the considered cylinders from CNH.

Table 9.5 shows the parameters of the accumulator if Sun Hydraulic components are chosen for the implementation. The smaller accumulator size from Hydac catalogue [35] to meet the drain requirements is 10 L.

**Table 9.5: Accumulator parameters using Sun Hydraulics components**

<b>Parameter</b>	<b>Symbol</b>	<b>Value</b>	<b>Unit</b>
Effective gas volume	$V_0$	7	L
Minimum pressure	$p_1$	3.42	bar
Maximum pressure	$p_2$	8.66	bar
Estimated maximum pressure	$p_{2,est}$	8.63	bar
Pre-charge pressure	$p_0$	3.08	bar
Maximum gas volume	$V_1$	6.60	L
Minimum gas volume	$V_2$	3.79	L
Minimum rest volume	$V_{rest}$	0.39	L

Table 9.6 shows the parameters of the accumulator if Parker Hannifin valves and Hydac filter are chosen for the implementation. The smaller accumulator size from Hydac catalogue [35] to meet the drain requirements is 10 L.

**Table 9.6: Accumulator parameters using Parker Hannifin valves and Hydac filter**

Parameter	Symbol	Value	Unit
Effective gas volume	$V_0$	9	$L$
Minimum pressure	$p_1$	4	$bar$
Maximum pressure	$p_2$	7.9	$bar$
Estimated maximum pressure	$p_{2,est}$	7.81	$bar$
Pre-charge pressure	$p_0$	3.6	$bar$
Maximum gas volume	$V_1$	8.48	$L$
Minimum gas volume	$V_2$	5.66	$L$
Minimum rest volume	$V_{rest}$	0.52	$L$

Table 9.7 shows the parameters of the accumulator if Bosh Rexroth valves and Hydac filter are chosen for the implementation. The smaller accumulator size from Hydac catalogue [35] to meet the drain requirements is 20  $L$ . Hence, the Bosh Rexroth components are not suitable for the current EHA since a bigger accumulator is needed.

**Table 9.7: Accumulator parameters using Bosh Rexroth valves and Hydac filter**

Parameter	Symbol	Value	Unit
Effective gas volume	$V_0$	13	$L$
Minimum pressure	$p_1$	4.75	$bar$
Maximum pressure	$p_2$	7.40	$bar$
Estimated maximum pressure	$p_{2,est}$	7.30	$bar$
Pre-charge pressure	$p_0$	4.27	$bar$
Maximum gas volume	$V_1$	12.22	$L$
Minimum gas volume	$V_2$	9.40	$L$
Minimum rest volume	$V_{rest}$	0.78	$L$

Implementing the Sun Hydraulics components, a bigger margin in terms of accumulator volume (7  $L$ ) is obtained with respect to Parker Hannifin (9  $L$ ). Considering the actual effective gas volume of the accumulator from catalogue, the accumulator parameters for the Sun Hydraulics implementation can be listed in Table 9.8.

**Table 9.8: Final accumulator parameters**

Parameter	Symbol	Value	Unit
Effective gas volume	$V_0$	9.3	<i>L</i>
Minimum pressure	$p_1$	3.42	<i>bar</i>
Maximum pressure	$p_2$	8.66	<i>bar</i>
Estimated maximum pressure	$p_{2,est}$	6.60	<i>bar</i>
Pre-charge pressure	$p_0$	3.08	<i>bar</i>
Maximum gas volume	$V_1$	8.78	<i>L</i>
Minimum gas volume	$V_2$	5.96	<i>L</i>
Minimum rest volume	$V_{rest}$	0.52	<i>L</i>

This last selection is also able to implement an 22 *cc/rev* hydraulic unit without increasing the size of the accumulator. The new pressure drops according to the increased flow rates for the Sun hydraulic components are shown in Table 9.9.

**Table 9.9: Pressure drop in Sun Hydraulic components with 22 *cc/rev* HP**

Type	Code	Maximum flow rate [L/min]	Nominal flow rate [L/min]	Pressure drops at nominal flow [bar]
Pilot operated check valve	CKGBXAN	227.125	46.8 (27.4)	2.76 (2)
Check valve	CXFAXAN	151.416	49.3 (27.4)	0.84 (0.42)
Relief valve	RDDALAN	94.63	66	-
Filter	FLHAXDN	344.74	49.3	1

The accumulator parameters considering the new pump size and maintaining the 10 *L* accumulator are shown in Table 9.10.

**Table 9.10: Final accumulator parameters with 22 *cc/rev* pump**

Parameter	Symbol	Value	Unit
Effective gas volume	$V_0$	9.3	<i>L</i>
Minimum pressure	$p_1$	4.09	<i>bar</i>
Maximum pressure	$p_2$	7.97	<i>bar</i>
Estimated maximum pressure	$p_{2,est}$	7.77	<i>bar</i>
Pre-charge pressure	$p_0$	3.68	<i>bar</i>
Maximum gas volume	$V_1$	8.76	<i>L</i>
Minimum gas volume	$V_2$	5.94	<i>L</i>
Minimum rest volume	$V_{rest}$	0.54	<i>L</i>

Table 9.11 lists the final results of the components selection in terms of accumulator size for both 18 *cc/rev* and 22 *cc/rev* hydraulic units.

**Table 9.11: Accumulator size based on components selection and HP volumetric displacement**

<b>Brand</b>	<b>HP volumetric displacement [cc/rev]</b>	<b>Required effective gas volume [L]</b>	<b>Accumulator volume from catalogue [L]</b>
Sun Hydraulics	18	7	10
Parker Hannifin + Hydac		9	10
Bosh Rexroth + Hydac		13	20
Sun Hydraulics	22	9	10
Parker Hannifin + Hydac		15	20
Bosh Rexroth + Hydac		35	42

# ACKNOWLEDGMENTS

Arrivato alla fine di questo percorso, desidero ringraziare tutte le persone che mi sono state vicine e che mi hanno fatto sentire tutto il loro sostegno. Anticipo con un po' di rammarico che, probabilmente, non riuscirò a trasmettervi, tramite queste righe, tutto l'apprezzamento che provo nei vostri confronti. Non credo questo sia un limite dell'ingegnere per antonomasia, ma sono certo che, se avessi avuto eccellenti capacità di scrittura, avrei sbagliato facoltà.

Un sentito ringraziamento va ai miei relatori. Al Professore Mazza, per avermi proposto la tesi negli Stati Uniti, un'esperienza che ha ampliato i miei orizzonti e che mi ha permesso di crescere non solo dal punto di vista accademico, ma anche umano. Al Professore Vacca, per la guida, il supporto e la disponibilità dimostrati durante tutto il percorso di ricerca. La sua esperienza è stata fondamentale per la realizzazione di questo lavoro.

I would like to express my heartfelt thanks to each member of the Maha Fluid Power Research Center. Upon my arrival in the United States, I was warmly welcomed into a well-organized lab, filled with a lively atmosphere and excitement for the research. Your dedication and passion for fluid power have been truly inspiring, and I have learned so much from all of you. As I return to Italy, I carry with me a deepened interest in this vast field, one that I hope will continue to shape my academic and professional journey. Special thanks to Nathan and Seshan for their exceptional support.

Desidero anche ringraziare Filippo Boiardi, che mi ha offerto l'opportunità di collaborare con Settima Meccanica nel completamento del loro progetto con la Purdue University. Spero che le nostre strade possano incrociarsi nuovamente in futuro.

Un pensiero speciale va alla mia famiglia tutta, che mi ha sempre sostenuto con amore e pazienza. Ai miei genitori, per aver creduto in me più di quanto io stesso non facessi e per avermi dato la possibilità di intraprendere esperienze che, da solo, non avrei mai potuto neanche sognare. Questa tesi la dedico a voi. A mia sorella Ludovica, per il supporto emotivo e per la leggerezza che mi ha dato nel percorso universitario. Ai miei nonni Carmine, Giovanna e Vittoria, per la gioia con cui hanno affrontato il superamento di ogni mio singolo esame. A mio nonno Aldo, che avrei tanto voluto potesse partecipare a questo secondo traguardo. A mia zia Donatella, per l'interesse che ha sempre mostrato verso ciò che studio e per gli inestimabili consigli che mi ha dato. Un grazie di cuore va anche ai miei zii e cugini, per il loro affetto e il continuo supporto che mi hanno dato durante questo percorso. Ad Hera, per la sua capacità di tranquillizzare il mio animo con un semplice battito di coda.

Un sentito ringraziamento va ai miei 'Soci': Gabriele, Carmen, Tiziano, Salma, Daniele e Francesco. Ho avuto la fortuna di incontrare delle persone fantastiche con cui ho condiviso giornate di studio e serate di divertimento indimenticabili (A heartfelt thank you to my 'Soci': Gabriele, Carmen, Tiziano, Salma, Daniele, and Francesco. I consider myself lucky to have met such wonderful people with whom I shared unforgettable study sessions in the morning and fun-filled evenings). Ad Annibale, il mio primo vero punto di riferimento a Torino, non solo un amico, ma una presenza costante e fondamentale nella mia vita sin dai tempi del liceo. Ad Alessandro, che con grande sorpresa ho ritrovato nella mia prima lezione al Politecnico e che considero un vero tutor in questa esperienza. A Giusy, per il sostegno e la complicità che mi ha dato durante il percorso della magistrale.